Modelling of Inhomogeneous Magnetic Fields in Electromagnetic Devices

A thesis submitted in fulfilment of the requirements for the degree of Master of Engineering

Braden John Kidd

Master of Energy Systems, University of Melbourne

School of Engineering

College of Science, Engineering and Health

RMIT University

October 2018

Thesis Declaration

I certify that except where due acknowledgement has been made, the work is that of the author alone; the work has not been submitted previously, in whole or in part, to qualify for any other academic award; the content of the thesis is the result of work which has been carried out since the official commencement date of the approved research program; any editorial work, paid or unpaid, carried out by a third party is acknowledged; and, ethics procedures and guidelines have been followed.

I acknowledge the support I have received for this research through the provision of an Australian Government Research Training Program Scholarship.

<div align="center">

Braden John Kidd 1ˢᵗ October 2018

</div>

Table of Contents

Contents

List of Figures

List of Symbols

- $\mathcal{R}$ — Magnetic circuit reluctance
- i — Electrical circuit current
- n — Number of electrical current windings
- Φ — Net magnetic flux
- μ_0 — Magnetic permeability of free space
- μ_r — Materials relative magnetic permeability
- l — Length variable
- A_{csa} — Cross sectional area of magnetic material
- B — Magnetic flux density
- H — Magnetic field strength
- R_t — Torus major radius
- r_t — Torus minor radius
- B_{max} — Maximum magnetic flux density
- B_{min} — Minimum magnetic flux density
- U — Total magnetic flux energy
- V — Volume
- t — Time
- φ — Application specific angle variable
- ε — Fill grade modulation index
- v — Voltage variable
- $P_{\text{magnetic\_field}}$ — Power transfer to the magnetic field
- $P_{\text{reluctance}}$ — Power transfer due to change in reluctance
- x — Local displacement variable
- A — Solenoid length variable
- a — Local length integration variable
- r — Local radius integration variable
- $(r_1, .., r_5)$ — Solenoid radius variables
- F — Force
- ω — Rotational frequency
- φ — Phase variable
- Φ_r — Magnetic flux induced from rotor currents
- Φ_s — Magnetic flux induced from stator currents
- ω_f — Synchronous frequency
- ω_s — Slip frequency
- ω_r — Rotational frequency
- P_{stator_s} — Power transfer to the stator from the stators frame of reference
- P_{rotor_s} — Power transfer to the rotor from the stators frame of reference
- P_{rotor_r} — Power transfer to the rotor from the rotors frame of reference
- T_r — Rotor torque
- P_r — Power transfer due to rotor torque
- K_i — Conversion constant to convert stator current to stator flux
- K_v — Conversion constant to convert stator voltage to magnetic flux derivative

- V_s *Stator winding voltage amplitude*
- i_s *Stator winding current amplitude*
- σ *Local angle variable*
- R_{loop} *Electrical resistance of circuit incorporating two opposite rotor bars*
- R_r *Rotor resistance in ohm radians*
- r_i *Rotor inner radius*
- r_o *Rotor outer radius*
- s_i *Stator inner radius*
- s_m *Stator slot region outer radius*
- s_b *Stator backplane radius*
- C_r *Rotor bar cross sectional area ratio*
- C_s *Stator slot cross sectional area ratio*
- λ *Angle between stator and net magnetic flux vector*
- θ *Angle between stator voltage vector and net magnetic flux vector*
- R_s *Stator winding resistance*
- L *Stator winding stray inductance*
- ρ *Change in stator voltage vector due to winding resistance and stray inductance*
- P_{supply} *Power supplied from external source to the motor*
- P_{sm} *Power loss due to stator eddy current losses*
- P_{rm} *Power loss due to rotor eddy current losses*
- M_{se} *Coefficient of stator eddy current losses*
- M_{re} *Coefficient of rotor eddy current losses*
- P_{re} *Power loss due to currents in rotor bars*
- P_r *Inductive power transfer to the rotor*
- P_τ *Inductive rotor power transfer to kinetic energy*

Abstract

Modelling complex electromagnetic devices incorporating inhomogeneous magnetic fields typically requires computationally intensive solutions based on numerical methods. Simple magnetic path problems are often solved using less computationally intensive analytical techniques such as equivalent circuit approximations. Deciding upon which model to use depends on device complexity and involves a tradeoff between accuracy and computational efficiency.

By expanding upon existing magnetic circuit theory, considering stored magnetic energy and vector analysis, it is possible to use magnetic circuit analysis to accurately model complex electromagnetic devices. The focus on energy facilitates the ability to incorporate inhomogeneous magnetic fields into magnetic circuit analysis that would traditionally require the use of numerical methods. This thesis derives closed form equations to describe electromagnetic device characteristics for a toroid, solenoid and a case study induction machine. By considering stored magnetic field energy, this approach allows the relationship between electrical, magnetic and kinetic energy to be quantified and analyzed in ways that allows improved accuracy compared with conventional magnetic circuit modeling methods. This thesis also provides insights into how geometric parameters impact energy transfer and operational characteristics of electromagnetic devices.

Chapter 1

1 Introduction

1.1 Introduction

Choosing a modeling technique to predict the operational characteristics of electromagnetic devices often involves a tradeoff between computational complexity and required accuracy. High level abstract models such as electrical and magnetic equivalent circuits require relatively minimal computational time as they can be solved using closed form equations. When modelling complex electromagnetic interactions or when a high level of accuracy is required, more computationally intensive techniques such as numerical methods are commonly used.

One significant factor in the discrepancy between computational efficiency of different modelling techniques is the ability to derive closed form equations. Closed form equations such as those used by equivalent circuits can be solved with considerably less computations than arrays of linear or differential equations such as those used by numerical methods. Due to this, much of the current electromagnetic device modelling research involves achieving an optimum balance between accuracy and computational efficiency.

The research presented in this thesis considers derivation of magnetic circuit parameters for non-homogenous magnetic field distributions in complex geometries. Magnetic circuit analysis focused on stored energy is used to describe the operational characteristics of electromagnetic devices without the need for empirically derived parameters. This also allows electromagnetic devices incorporating spatially varying material properties, complex magnetic field distributions and constituent motion to be modelled without computationally intensive numerical methods.

Vector applications of energy based magnetic circuit equations are used to model electromagnetic devices incorporating circular motion. This allows magnetic flux-based models to be developed that describe the relationships between electrical, magnetic and mechanical parameters of electromagnetic devices incorporating circular motion.

1.2 Literature review

The research presented in this thesis covers areas of electromagnetic theory relating to modelling the characteristics of electromagnetic devices. Considerable research has been conducted in these fields over for over a century resulting in a vast body of knowledge upon which the analytical techniques are developed in this thesis.

1.2.1 Electrical Equivalent Circuits

Equivalent models provide a simple and intuitive technique to analyze the operation of an electromagnetic device. One common equivalent circuit technique involves electrical circuit equivalents comprised of networks of linear passive elements such as resistors, inductors and ideal transformers. Simple electromagnetic devices such as inductors and transformers can be effectively modeled using these techniques that account for their non-ideal characteristics. Electromagnetic devices incorporating constituent motion such as linear actuators and rotating machines can also be modeled using electrical equivalent circuits. This is achieved by making component parameters a function of the position and velocity of individual components.

Electrical equivalent circuit are often used to model electrical motors. This allows for simple implementation of control using either open loop or closed loop control algorithms. The simplest electrical equivalent model assumes that the motor is series parallel L and R circuit representing magnetization, copper losses, core losses and a Back Electro-Motive Force (Back-EMF) [1]. A common application of this technique is for simple open loop voltage frequency control of an induction motor [2].

A more comprehensive circuit equivalent model for the induction motor is the Steinmetz equivalent circuit model. This model was first proposed by Charles Proteus Steinmetz in 1897 by analyzing an induction motor as a rotating transformer [3]. Since then, this model, also called the T equivalent circuit, has become such a common model in textbooks that it is referred to as the 'Universal Induction Motor Model' [4]. The circuit consists of resistive and inductive elements with the resistor *RL* in figure 1.1 being a function of the rotor speed and synchronous frequency.
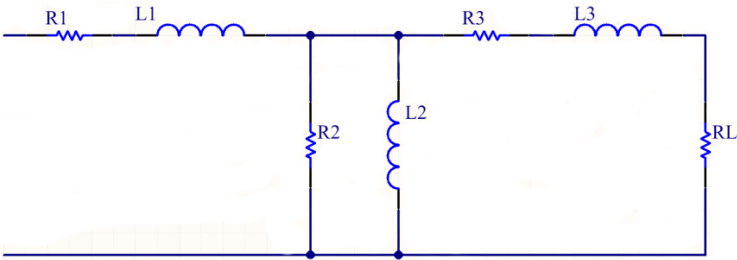
Figure 1.1, A Steinmetz equivalent circuit of an induction motor

This circuit with appropriately chosen parameters can be used to plot the characteristic speed torque curve of an induction motor with sufficient accuracy to enable basic control and simulation [5]. It is also possible to add additional capacitors and resistors into this circuit to improve its accuracy at higher frequencies [4]. However, it oversimplifies the operation of the induction motor and can be improved upon using more complicated equivalent circuits. To achieve this more complex networks of electrical components are used with more complex component parameters [6].

1.2.2 Magnetic Equivalent Circuits

Magnetic equivalent circuits are the oldest technique used to analyze electromagnetic devices. The foundations for this analytical technique date back to June 1828 when Joseph Henry demonstrated that there was a relationship between the magnetic field strength of an electromagnet and the number of electrical turns [7]. This discovery paved the way for the practical invention of the telegraph. In 1885 John Hopkinson in his article "Magnetization of Iron" published by the Royal Society demonstrated the relationship between current and magnetic flux in an electromagnet [8]. This allowed the development of a simple linear model called Hopkinson's law linking the Magneto Motive Force (MMF) to magnetic flux. The value used to scale the magnetic flux as a function of MMF was first referred to as reluctance by Oliver Heaviside [9].

This linear model between MMF, reluctance and magnetic flux offers a simple method to analyze magnetic path problems in a technique that is analogous to using Ohm's law for electrical circuits. For example, consider the simple magnetic circuit path problem as shown in figure 1.2.
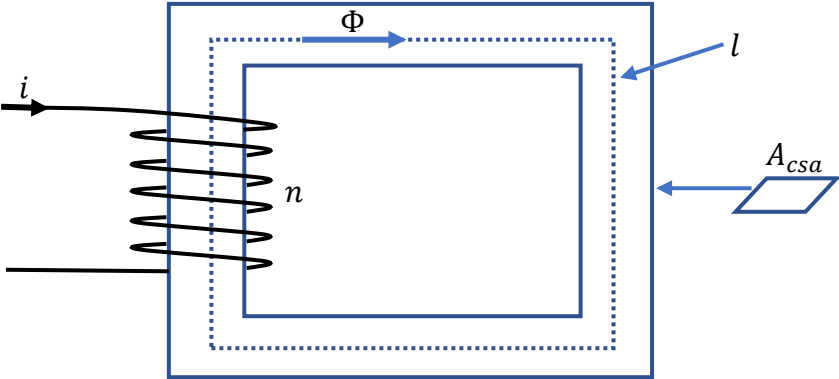
Figure 1.2, A simple magnetic circuit path

In figure 1.2, the MMF will be the product of winding current i and the number of turns N. The magnetic path reluctance $\mathcal{R}$ can be calculated to be equation (1.1) where l is the average path

length and A_{csa} is the cross-sectional area of the magnetically permeable material and μ_r is the relative permeability of the magnetic material.

$$\mathcal{R} = \frac{l}{\mu_0 \mu_r \times A_{csa}}$$ *(1.1)*

The equation (1.1) value of reluctance can be substituted into Hopkinson's law to calculate the relationship between the electric current i and the magnetic flux Φ.

$$in = \mathcal{R}\Phi$$ *(1.2)*

Magnetic equivalent circuits are useful for analyzing simple magnetic path problems as shown in figure 1.2. This linear model is only an approximation as it does not account for the non-linear magnetization properties of the material and it assumes a uniform magnetic flux distribution throughout the material. Despite these limitations, the simplicity and relative accuracy in simple magnetic path problems has kept this model relevant [10].

1.2.3 Equivalent Models for Rotating Fields

Alternating Current (AC) motors operate on the underlying principle of a rotating magnetic field. Mathematically describing the properties of a rotating magnetic field is therefore an important factor in describing the operations of AC machines. Scientific study into rotating magnetic fields first started in 1824 when Francois Arago demonstrated that a rotating copper disc could have a magnetizing effect on a magnetized needle [11]. This effect would cause the needle to rotate in the same direction as the copper disc when placed near the spinning copper disc. Although there were many theories proposed to explain this motion, it was eventually shown by Michael Faraday in 1831 to be caused by eddy currents in the copper disc caused by electromagnetic induction [11]. Despite the interest of the academic community, rotating magnetic fields caused by electromagnetic induction had no practical applications at the time and therefore no significant research was undertaken for the next few decades.

The first workable rotating magnetic field was demonstrated to the physical society of London on 28th June 1879 by Walter Baily. In his paper "A mode of producing Arago's rotation" he demonstrated how to use two batteries and a hand cranked communicator to produce a rotating magnetic field that could cause a copper disc to rotate [12]. This model was improved upon by Galileo Ferraris who in 1885 used two alternating currents energizing two separate coils with an angular displacement of 90° to generate a rotating magnetic field capable of rotating a copper disc [13]. Ultimately it was Nicola Tesla's design of producing a rotating magnetic field using alternating current, patented in 1888 that was commercially successful [14].

Although Tesla described the induction motor and rotating magnetic fields in detail in his patent, his analysis was more descriptive than mathematical. It was no until 1929 that Robert H Park first

described how to analyze a rotating magnetic field caused by a poly phase induction motor that a mathematical description of a rotating magnetic field was derived [15]. Park used a rotating frame of reference to view the magnetic field that allows a complicated AC circuit to be analyzed like a DC circuit of reduced complexity. The Clarke transformations (also known as Alpha – beta transformations) as first described by Edith Clarke can also be used to model a rotating magnetic field albeit from a stationary frame of reference.

A combination of the Park and Clarke transformation are used to implement a model called the Direct Quadrate (D-Q) model for analyzing rotating magnetic fields. The D-Q allows an AC motor incorporating a rotating magnetic field to be analyzed using a similar technique to that used for Direct Current (DC) motor analysis.

There are two specific parameters required to be measured using the D-Q model. These are flux producing currents and torque producing currents. Flux producing currents are referred to as direct and are at in phase with the stator flux. Torque producing currents are referred to as quadrate and are at right angles to the stator flux [16].

To control a motor using the D-Q model, the required torque and flux needs to be calculated. Then, either Field Oriented Control or Direct Torque Control can be used to adjust the motor voltage and frequency. Measuring the stator voltage, current and rotor speed then allows the controller to estimate the actual magnetic flux and torque. This is compared to the pre-set values and the output voltage can be adjusted to minimize the error between the required and measured values of flux and torque. Independent equivalent circuits made up of resistors, inductors and voltages sources are used to calculate the torque and flux based on output measurements [17].

1.2.4 Lumped Parameter Model

Numerical methods involve dividing the geometry of the electromagnetic device into many discrete elements. One common technique used to achieve this is the Lumped Parameter Model (LPM). LPMs involve representing a physical system as an interconnected spatially distributed mesh of discrete elements that approximate the behavior of each individual elemental component. When applied to the analysis of electromagnetic devices, LPM typically involves using many sources of MMF and reluctance elements distributed within the geometry of the device to form an interconnected mesh.

LPM is a natural progression of basic magnetic circuit analysis as it allows more complex magnetic field distributions to be modeled using the underlying concepts of reluctance, magnetic flux and MMF. This reduces the approximations and assumptions inherent to the application of basic magnetic circuit analysis to practical situations that inevitably incorporate complex geometries and non-uniform magnetic flux density distributions

LPM has seen many variations in its application to modelling electromagnetic devices. Common LPM techniques used today include Reluctance Mesh Modelling (RMM) [18] and Magnetic Equivalent Circuits (MEC) [19]. Both techniques involve analyzing the electromagnetic device as being comprised of many interconnected reluctance components and sources of MMF. Basic implementations of LPM can only model linear behavior of magnetic fields. However, variations of RMM and MEC can be used to simulate and detect faults in rotating machines [20] and account for the nonlinear behavior of magnetic fields under specific circumstances [21].

As with all LPM models, they require detailed knowledge of the construction of the individual motor being controlled and are more computationally intensive that electrical equivalent circuits. The underlying assumptions of LPM make it inherently difficult to model complex magnetic field behavior such as saturation, leakage and skewing effects [19]. Therefore, simulation results obtained using other modelling techniques or from direct measurements are required to accurately simulate complex electromagnetic devices.

1.2.5 Finite Element Modelling

Finite Element Modelling (FEM) is a numerical method that involves directly solving Maxwell's equations as partial differential equations at the boundaries of each elemental component. As such, it is similar to LPM in that the electromagnetic device is represented as an interconnected mesh of elementary components. However, FEM does not require the use of linear modelling approximations to calculate the state of each elementary component as is the case for LPM. This results in a highly accurate model capable of modelling magnetic fields in complex geometries and accommodating a wide range of magnetic field behaviors.

FEM as a mathematical analysis technique was first proposed by Richard Courant in 1943 for solving engineering problems [22]. Due to the computational complexity required to solve engineering problems, it was not until the late 1950's that computers became fast enough to make this technique viable. In 1965 Alan Winslow was the first to apply FEM to simulating magnetic fields within a magnetically permeable material [23]. This paved the way for greater uptake of FEM to analyze electromagnetic devices during the 1970's [24]. Due to the computational power of modern computers and many CAD implementations, FEM is considered the industry standard magnetic field modelling technique used today [19].

Although FEM is usually considered the most accurate magnetic field modelling technique available, it still has some limitations. The major limiting constraint preventing the universal uptake of this model is its computational complexity [25]. This primarily restricts it use to design purposes only, as solving the complete FEM model for real time control of a device is not practical with available computing power. To apply FEM for use in real time control applications typically involves combining it with other modelling techniques or using a partial or low-resolution implementation [26].

Another observed limitation of FEM is its accuracy when modelling force and magnetic losses [19]. These limitations mean that an FEM simulation cannot be used to definitively prove the behavior of a magnetic field without experimental evidence to confirm its predictions. Despite these limitations, the overall high level of accuracy of this model makes it a useful benchmark when assessing the accuracy of other modelling techniques such as that which is presented in this thesis.

1.2.6 Research Gap

The electromagnetic device modelling techniques described thus far can be broadly classified as either numerical methods based, or closed form equation based. Generally, numerical methods-based models will result in high accuracy at the expense of high computational intensity relative to closed form equations. Deriving a model that has a high level of accuracy with moderate or low levels of mathematical computations is a desirable goal of current electromagnetic research due to the applications of such models to real time control and optimization.

Numerical methods are often used instead of reduced complexity models when an electromagnetic device incorporates in-homogeneous magnetic flux distributions and time varying reluctances. The research presented in this thesis demonstrates how existing magnetic circuit theory can be extended using energy and vector-based equations to derive closed form solutions for these situations. In doing so it is possible to calculate the dynamic behavior of electromagnetic devices that would typically require the use of numerical methods.

The analytical technique presented in the thesis will also be applied to electromagnetic devices incorporating rotating magnetic fields. Magnetic flux-based models, such as the D-Q model seek to achieve an optimal balance between accuracy and computational intensity. Despite the D-Q model incorporating greater detail than simple magnetic circuit path models, it is still requires a high level of abstraction. This is due to the requirement to convert AC parameters to their DC equivalent where only selected currents either produce flux or experience torque.

The proposed magnetic circuit modelling technique uses vector-based relationships between rotating magnetic fields to simplify their analysis. This simplifies the analysis of an induction motor without the need for converting AC circuit parameters to their DC equivalent such as occurs with the D-Q model. Using these vector-based relationships also allows for magnetic flux based models of rotating magnetic fields to be derived where all electric currents contribute to the magnetic flux and experience torque.

1.3 Research Questions

1.3.1 Research Question 1. How does magnetic circuit modelling of a stationary magnetic device consisting of an inhomogeneous magnetic field distribution compare to Finite Element Modelling?

Traditional applications of magnetic circuit theory to electromagnetic devices assume a uniform magnetic flux density and uniform material permeability. In simple magnetic path problems this can yield satisfactory results. However, as magnetic field distributions and material magnetic properties become more varied these assumptions result in reduction in accuracy.

Accounting for variations in magnetic flux density and relative permeability when deriving magnetic circuit parameters results in improved accuracy. It also allows magnetic circuit equations to more accurately describe the relationship between electric current and magnetic fields over a wide range of geometric parameter variations. This increase in accuracy can be achieved without incurring any significant increase in computation times.

In this thesis, magnetic circuit equations that model dynamically stored energy will be used to calculate the magnetic reluctance of a simple electromagnetic device accounting for the non-uniform distribution of the magnetic field and inhomogeneous material properties. FEM simulations are then used as a benchmark to assess the accuracy of results obtained with and without accounting for inhomogeneous field distributions.

1.3.2 Research Question 2. How can magnetic circuit modelling be applied to the transient analysis of variable reluctance devices incorporating inhomogeneous magnetic field distributions?

Magnetic circuit analysis in its basic implementation is usually applied to simple magnetic path problems. Deriving transient electrical, magnetic and mechanical electromagnetic device behavior usually requires more complex modelling techniques such as LPM. An example of such a situation involves the transient modelling of a linear actuator such as a solenoid.

Existing magnetic circuit analysis can be used to calculate force experienced by the armature as a function of armature position and winding current for simple solenoid configurations. However, practical solenoids incorporate diverging magnetic fields and complex B-H field relationships that can be difficult to model using conventional magnetic circuit modelling techniques. Due to this, computationally intensive FEM is usually required for real world transient simulation of a solenoids electric and magnetic characteristics.

A compromise between accuracy and computational intensity can be achieved by considering dynamic stored energy in the magnetic circuit to model solenoid transient behavior. This is because energy based magnetic circuit equations can account for changes in reluctance and the effect of non-aligned B-H fields on magnetic field energy.

To assess the accuracy of energy based magnetic circuit modelling, a FEM simulation of a solenoid will be used to establish a benchmark against which predictions can be assessed for their accuracy. An effective MMF and reluctance can be calculated by analyzing the contribution of each segment of the solenoid to their respective parameter. This analytical technique allows for a single source of MMF and reluctance to be used to derive transient equations to describe electric current, magnetic flux and force as a function of winding voltage.

1.3.3 Research Question 3. How can magnetic circuit modelling be applied to the analysis of rotating magnetic fields incorporating inhomogeneous magnetic field distributions?

Electromagnetic devices incorporating rotating magnetic fields are inherently difficult to describe using simple modelling techniques. This is because these devices comprise of multiple materials with different electrical and magnetic properties that form complex geometries. When electrical equivalent circuits are used to model electromagnetic devices incorporating rotating magnetic fields such as that in an induction machine, parameters are either derived using numerical methods such as the finite element model or via direct measurements. One reason for this is that electrical circuit elements were originally derived to describe electrical components with no internal motion. It is therefore necessary to make the properties of these electrical components a function of a motors electromagnetic structure.

An alternative to this technique is to describe the operation of an induction motor using a vector-based application of magnetic circuit theory. Electrical currents in both the rotor and stator induce a magnetic field that can be represented in vector form. By representing the net magnetic flux and its time derivative as rotating vectors, it is possible to relate all electrical currents and induced voltages to these quantities. This allows operational parameters such as efficiency, torque, power factor and supply current to be calculated.

The main advantage of this technique is that closed form equations can be derived to model the operation of the induction motor. Closed form equations are known to result in reduced computation times relative to numerical method techniques. Such an advantage is necessary when using a model for real time calculations. Existing commonly used models for real time control include the Steinmetz model and the Direct Quadrate model. The Steinmetz model is an inherently abstract model as it is comprised of equivalent electrical circuit components. Even though the Direct Quadrate model is more detailed than the Steinmetz model, it still incorporates a high-level

of abstraction as it assumes that only some currents contribute to magnetic flux while others contribute to torque.

Predictions made by the proposed vector based magnetic circuit model are benchmarked against those derived using FEM. As FEM is usually considered the most accurate simulation model of magnetic fields, this comparison will provide useful insights into the accuracy of vector based magnetic circuits.

1.4 Contribution of Research

The research presented in this thesis contributes to the analysis of electromagnetic devices by providing an alternative analytical technique that aims to achieve an optimal balance between computational efficiency and accuracy. This contribution is summarized in the following dot points.

- **Modelling of electromagnetic devices incorporating non-uniform magnetic flux distributions.**

  Traditional magnetic circuit analysis assumes uniform magnetic flux densities for simple magnetic path applications. More complex field distributions typically require the use of numerical methods such as lumped parameter models. The analytical technique presented in this thesis demonstrates how energy based magnetic circuit analysis can be used to calculate magnetic circuit parameters for complex field distributions.

- **Using magnetic circuit analysis to calculate electrical, magnetic and mechanical properties of a time varying reluctance device.**

  Calculating the time varying characteristics of electromagnetic devices incorporating constituent motion is usually achieved using numerical methods. This is due to the inherent difficulties encountered when modelling complex field distributions and time varying reluctances. The research in this thesis presents an analytical technique using energy based magnetic circuit equations that allows closed form equations to be derived for time varying electrical, magnetic and mechanical parameters.

- **Describing the properties of rotating magnetic fields using vector based magnetic circuit analysis.**

  Modeling rotating magnetic is commonly achieved using high level equivalent circuits or with computationally intensive numerical methods. An alternative analytical technique can be achieved using vector applications of magnetic circuit equations. This allows for simulation parameters to be derived directly from the unique geometry of the rotating machine without the need for numerical methods. In doing so, it is possible to derive closed form equations without the need for empirical data or correction factors.

1.5 Basis of the Research

In this thesis magnetic circuit analysis focusing on stored energy will be used to derive closed form equations that describe the operational characteristics of electromagnetic devices. This analytical technique can be used to apply magnetic circuit analysis to non-uniform magnetic field distributions in geometrically complex devices. To demonstrate the advantages of energy based magnetic circuit analysis, this technique will be applied to three separate situations. These involve electromagnetic devices with both constant and time varying reluctances including circular motion.

To achieve the stated outcomes for this thesis, the energy based magnetic circuit equations used must be expressed in vector form. These equations can be derived by analyzing the geometry of a torus. A torus is the volume enclosed by a circle that is swept around an axis. The distance between the center of the swept circle and the axis is known as the major radius R_t while the radius of the swept circle is the minor radius r_t. Figure 1.3 shows an example of torus made of a magnetically permeable material with electric current carrying conductors passing through its center.
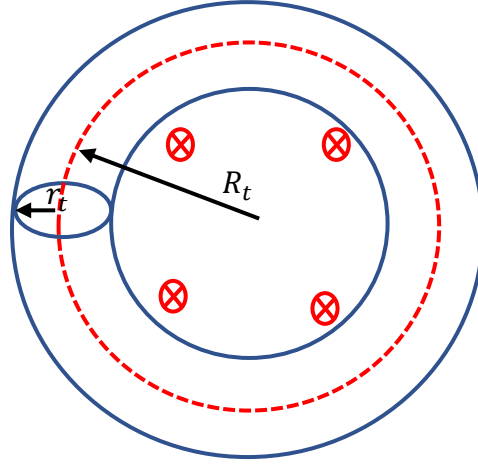
Figure 1.3. Torus geometry

The magnetic flux density at the major radius R_t can be calculated using Amperes law to be equation (1.3) by solving Ampere's law for the red dotted line as shown in figure 1.3. In equation (1.3), i is the winding current, n is the number of current turns and μ_r is the relative permeability of the material.

$$\oint B.dl = \mu_0 \mu_r in$$

$$B = \frac{\mu_0 \mu_r in}{2\pi R_t} \tag{1.3}$$

Multiplying the magnetic flux density at the major radius by the area of the radial cross section of the torus allows the approximate value of the magnetic flux Φ to be calculated.

$$\Phi \approx \frac{\mu_0 \mu_r in r_t^2}{2R_t} \tag{1.4}$$

Hopkinson's law relates the Magneto Motive Force (MMF) which is defined to be the winding current multiplied by the number of turns, with the magnetic flux. For this application, Hopkinson's law can be expressed as shown in equation (1.5).

$$ni = \mathcal{R}\Phi \tag{1.5}$$

Substituting the equation (1.4) value of magnetic flux into Hopkinson's law as stated to be equation (1.5) allows the approximate value of magnetic reluctance to be calculated.

12

$$ni \approx \mathcal{R} \frac{\mu_0 \mu_r i n r_t^2}{2 R_t}$$

$$\mathcal{R} \approx \frac{2 R_t}{\mu_0 \mu_r r_t^2} \qquad (1.6)$$

Equation (1.6) is only an approximation as the magnetic flux density within the torus was assumed to be constant to derive equation (1.4). However, the magnetic flux density within the torus as described by equation (1.3) decreases with radial distance. The difference between the maximum and minimum magnetic flux density within the torus as shown in figure 1.3 can be calculated using Ampere's law to be equation (1.7).

$$B_{max} - B_{min} = \frac{\mu_0 \mu_r i n r_t}{\pi \left(R_t^2 - r_t^2 \right)} \qquad (1.7)$$

The difference between the maximum and minimum magnetic flux densities as described by equation (1.7) only becomes zero when the minor radius r_t becomes zero. Therefore, the equation (1.6) value of magnetic reluctance that was derived based on the assumption on uniform magnetic flux density only becomes exact when the minor radius r_t becomes zero. This can be expressed mathematically as shown in equation (1.8).

$$\mathcal{R} = \lim_{r_t \to 0} \frac{2 R_t}{\mu_0 \mu_r r_t^2} \qquad (1.8)$$

Equation (1.8) cannot be directly evaluated as setting the minor radius to zero results in an infinite value of reluctance. This problem can be overcome by describing the energy stored in the torus as the minor radius approaches zero. The magnetic field energy within the torus can be described by integrating the known formula for magnetic field energy density in terms of the magnetic flux density B and the magnetic field strength H over the volume of the torus.

$$U = \frac{1}{2} \iiint B \cdot H \, dV \qquad (1.9)$$

As the minor radius approaches zero, the magnetic flux density becomes constant allowing equation (1.9) to be solved by simply multiplying the magnetic field energy density by the volume of the torus. The magnetic field strength H can also be expressed in terms of the magnetic flux density B using the relationship $B = \mu_0 \mu_r H$. This allows the energy within the torus to be calculated to be equation (1.10).

$$U = \lim_{r_t \to 0} \frac{\pi^2 R_t r_t^2}{\mu_0 \mu_r} (B \cdot B) \tag{1.10}$$

Magnetic circuit equations are usually expressed in terms of the magnetic flux as opposed to the magnetic flux density as shown in equation (1.10). The magnetic flux flowing through the torus Φ can be calculated by multiplying the magnetic flux density B by the cross-sectional area of the torus.

$$\Phi = B\pi r_t^2 \tag{1.11}$$

Substituting equation (1.11) into equation (1.10) allows equation (1.12) to be derived.

$$U = \lim_{r_t \to 0} \frac{R_t}{\mu_0 \mu_r r_t^2} (\Phi \cdot \Phi) \tag{1.12}$$

Equation (1.8) and equation (1.12) both contain a r_t^2 term. Therefore, it is possible to express equation (1.8) in terms of r_t^2 and substitute the result into equation (1.12) thereby eliminating the dependence on both the minor radius r_t and the major radius R_t. This allows the all geometric specific parameters of the magnetic circuit in equation (1.12) to be eliminated resulting in the generic magnetic circuit equation (1.13).

$$U = \frac{1}{2} \mathcal{R} (\Phi \cdot \Phi) \tag{1.13}$$

In equation (1.13), the magnetic flux is represented as a vector quantity while the magnetic reluctance is a scalar quantity. Differentiating energy with respect to time allows an expression for power as represented by the variable P to be derived. This is achieved by assuming both magnetic reluctance and magnetic flux are implicit functions of time and using the product rule for vector quantities.

$$P = \frac{1}{2} \left(\frac{d\mathcal{R}}{dt} (\Phi \cdot \Phi) + \mathcal{R} \left(\frac{\partial}{\partial t} (\Phi \cdot \Phi) \right) \right)$$

$$P = \mathcal{R} \left(\Phi \cdot \frac{\partial \Phi}{\partial t} \right) + \frac{1}{2} \frac{d\mathcal{R}}{dt} (\Phi \cdot \Phi) \tag{1.14}$$

Equation (1.14) allows the rate energy is transferred to a magnetic circuit to be calculated due to changes in magnetic reluctance and flux. Another relationship that can be derived from the equation (1.13) value of magnetic circuit energy is its implications for magnetic reluctance. Magnetic reluctance is defined to be the value magnetic flux must be scaled by to equal the MMF. To understand the implications this has on magnetic circuit analysis, consider the simple magnetic

circuit as shown in figure 1.4 where l is the length of the enclosed volume and A_{csa} is the area when represented in vector form is parallel to the direction of the magnetic flux density.
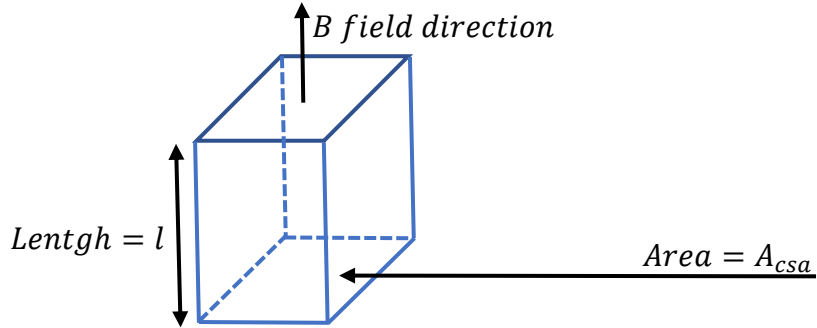
Figure 1.4. Simple magnetic circuit geometry

Applying the conventional definition of magnetic reluctance to the analysis of the enclosed volume in figure 1.4 that has a constant magnetic flux density and magnetic permeability results in the equation (1.15) value of reluctance.

$$\mathcal{R} = \frac{l}{\mu_0 \mu_r A_{csa}} \qquad (1.15)$$

Equation (1.15) is the commonly used definition of magnetic reluctance as applied to magnetic circuit analysis. This definition as is usually mentioned in textbooks, is derived using Hopkinson's law and Ampere's law. The reluctance of a magnetic circuit can thus be calculated by breaking it down into individual components and solving equation (1.15) for each elemental component. This technique is often applied to the derivation of lumped parameter models. Although this works in some situations, it is inaccurate where the H and B fields are non-aligned. This can be demonstrated by equating the equation (1.9) value of magnetic circuit energy to the derived magnetic circuit energy equation (1.13).

$$\frac{1}{2}\mathcal{R}(\Phi \cdot \Phi) = \frac{1}{2}\iiint B \cdot H \, dV$$

$$\mathcal{R} = \frac{\iiint B \cdot H \, dV}{\Phi \cdot \Phi} \qquad (1.16)$$

By evaluating the total magnetic circuit energy, it is possible to calculate the value of reluctance. An alternative way to view equation (1.16) it to describe the contribution each volumetric element dV contributes to the total reluctance as shown by equation (1.17).

$$\frac{d\mathcal{R}}{dV} = \frac{B \cdot H}{\Phi \cdot \Phi} \qquad (1.17)$$

Integrating equation (1.17) over the entire volume will allow the reluctance to be calculated. In a situation where the magnetic flux is not known or is difficult to calculate, the MMF can be used for the reluctance calculation instead. This is achieved by substituting Ampere's law for the MMF term in Hopkinson's law as shown in equation (1.18).

$$\oint H \cdot dl = \mathcal{R}\Phi \qquad (1.18)$$

Equation (1.18) can be substituted into equation (1.16) to eliminate its dependence on the magnetic flux. Performing this substitution results in equation (1.19):

$$\mathcal{R} = \frac{\left(\oint H \cdot dl\right)^2}{\iiint B \cdot H \, dV} \qquad (1.19)$$

The contour integral of the H field along a path that encloses all current loops as shown in equation (1.19) represents the net motion of charge within the system. Therefore, equation (1.19) states that magnetic reluctance is the ratio of the square of the net motion of charge to the resulting energy caused by this motion. Defining magnetic reluctance this way has implications for how magnetic circuit analysis can be interpreted relative to the laws of physics describing motion and electromagnetic interactions.

The following chapter demonstrates how the equations derived in this chapter and the underlying principals can be applied to magnetic circuit analysis. This is achieved by first applying these equations to the analysis of a static magnetic field. It is also necessary to demonstrate that this form of analysis is compatible with existing magnetic circuit analysis. This will be achieved in the next chapter by modelling a toroid to demonstrates the implications of inhomogeneous magnetic field distribution on magnetic reluctance calculations.

2 Modelling Magnetic Circuits with Fixed Reluctance

To demonstrate the ability of magnetic circuits to describe the operation of electromagnetic devices incorporating inhomogeneous magnetic flux densities, the magneto static properties of a torus will be analyzed in this chapter.

2.1 Calculation of Reluctance of a torus with consideration of inhomogeneous magnetic fields

A torus is the volume enclosed by a circle that is swept around an axis. The distance between the center of the swept circle and the axis is known as the major radius R_t while the radius of the swept circle is the minor radius r_t. This geometry was chosen due to its ease of mathematical modelling and FE simulation.

In the previous chapter, the reluctance of a torus was calculated for the case where the minor radius was much less than the major radius.
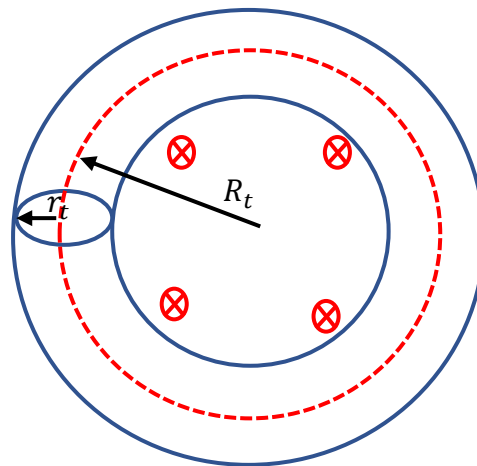
Figure 2.1. Torus geometry

The approximate value of the torus reluctance based on the assumption of homogeneous cross section magnetic flux density as calculated in the preceding chapter was calculated to be equation (2.1).

$$\mathcal{R} \approx \frac{2R_t}{\mu_0 \mu_r r_t{}^2} \qquad (2.1)$$

To determine the a more accurate value of magnetic reluctance, the non-uniform nature of the magnetic flux needs to be accounted for. This can be calculated by considering the cross section of the torus as shown in figure 2.2. In figure 2.2, a small rectangular cross section of the torus is shown in red at a distance of r from the central axis with a width of dr.
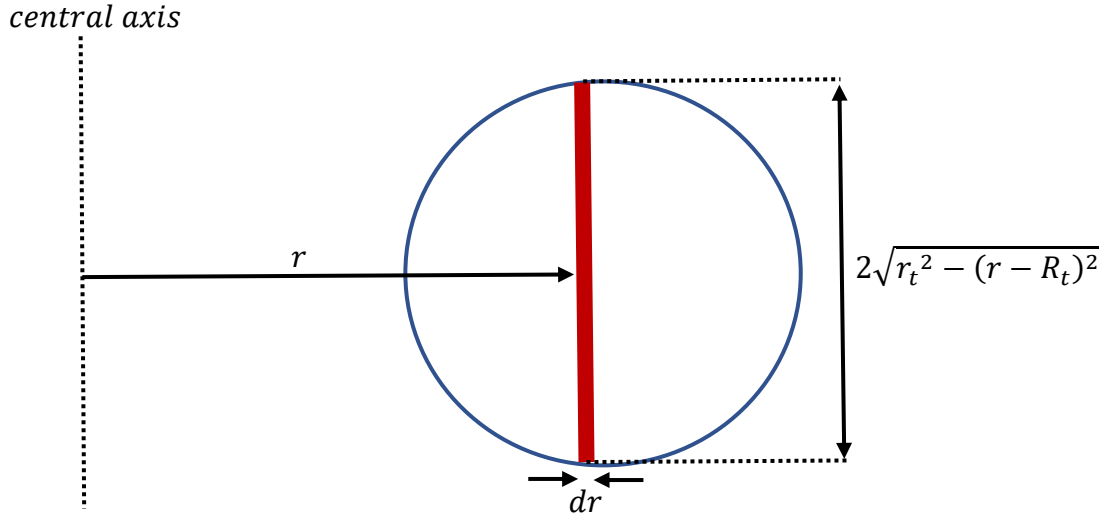
Figure 2.2. Torus cross section

The magnetic flux density was calculated in the preceding chapter to be equation (1.3) using Ampere's law. This was a function of the distance from the central axis which is represented in figure 2.2 with the variable r. Using the dimensions shown in figure 2.2, the value of the magnetic flux density within the torus becomes equation (2.2).

$$B = \frac{\mu_0 \mu_r i n}{2\pi r}$$

(2.2)

Multiplying the magnetic flux density by the area shown in figure 2.2 allows the magnetic flux for this region of constant magnetic flux density to be calculated. Integrating this value over the entire cross section of the torus as shown in figure 2.2 allows the total magnetic flux to be calculated.

$$\Phi = \int_{R_t - r_t}^{R_t + r_t} \frac{\mu_0 \mu_r i n}{\pi r} \sqrt{r_t^2 - (r - R_t)^2} \, dr$$

$$\Phi = \mu_0 \mu_r i n \left(R_t - \sqrt{R_t^2 - r_t^2} \right)$$

(2.3)

Hopkinson's law can be used to calculate the torus reluctance by divining the MMF by the equation (2.3) value of magnetic flux.

$$\mathcal{R} = \frac{ni}{\Phi}$$

$$\mathcal{R} = \frac{1}{\mu_0\mu_r\left(R_t - \sqrt{R_t{}^2 - r_t{}^2}\right)} \qquad (2.4)$$

It is also possible to derive this same reluctance value by calculating energy stored in the magnetic circuit. Consider a small volume of the torus enclosed by the area depicted in figure 2.3 at a distance of r from the central axis, swept around a small angular rotation of $d\varphi$.
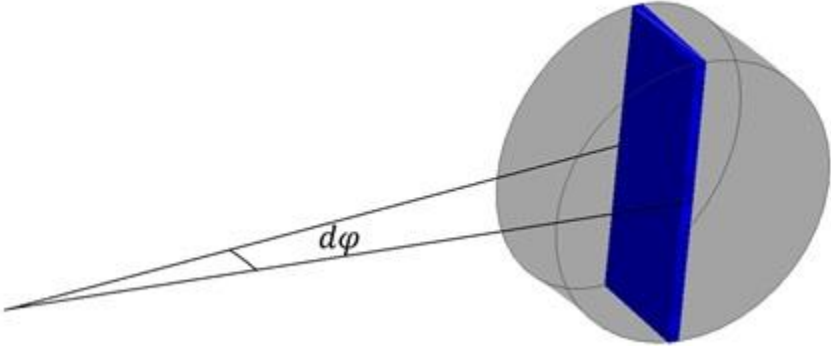
Figure 2.3. Small volume inside torus with constant magnetic flux density

The dimensions of the small enclosed volume from figure 2.3 are shown in figure 2.4.
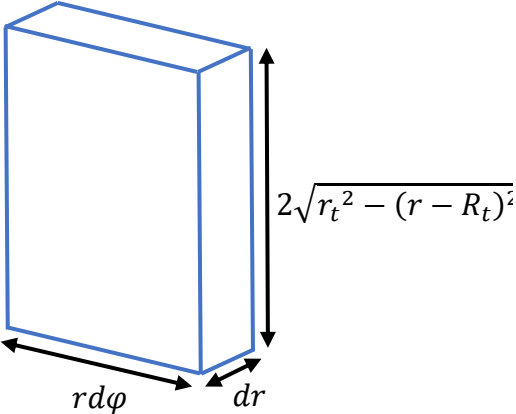
Figure 2.4. Dimensions of small volume inside torus with constant magnetic flux density

19

The stored energy within this small volume as represented by the differential equation term dU can be calculated by substituting the equation (2.2) value of magnetic flux density into the equation for magnetic field energy density for a small volume dV.

$$dU = \frac{B^2}{2\mu_0\mu_r} dV$$

$$dU = \frac{\mu_0\mu_r(in)^2}{8\pi^2 r^2} dV \tag{2.5}$$

Substituting the volume of constant magnetic flux density from figure 2.4 into equation (2.5) and integrating over the volume of the torus allows the total magnetic field energy to be calculated.

$$dU = \frac{\mu_0\mu_r(in)^2}{4\pi^2 r} \sqrt{r_t^2 - (r - R_t)^2}\, d\varphi\, dr$$

$$U = \int_{R_t-r_t}^{R_t+r_t} \int_0^{2\pi} \frac{\mu_0\mu_r(in)^2}{4\pi^2 r} \sqrt{r_t^2 - (r - R_t)^2}\, d\varphi\, dr$$

$$U = \frac{\mu_0\mu_r(in)^2}{2} \left(R_t - \sqrt{R_t^2 - r_t^2} \right) \tag{2.6}$$

Magnetic reluctance can be calculated using magnetic circuit stored energy by substituting the equation (2.6) value of energy and the equation (2.3) value of magnetic flux into equation (1.13). As the magnetic flux vector is parallel to itself, the dot product from equation (1.13) can be replaced with multiplication. Performing these operations allows the equation (2.7) value of magnetic reluctance to be calculated.

$$\mathcal{R} = \frac{2U}{\Phi^2}$$

$$\mathcal{R} = \frac{1}{\mu_0\mu_r \left(R_t - \sqrt{R_t^2 - r_t^2} \right)} \tag{2.7}$$

The magnetic reluctance of a torus calculated using both the conventional approach and the stored energy method results in the same equation as demonstrated by equation (2.4) and (2.7).

2.2 Simulation study on modelling inhomogeneous magnetic fields in a torus with uniform permeability

The advantages of accounting for the non-uniform distribution of the magnetic flux density when using magnetic circuit analysis can be demonstrated by comparing predictions made using magnetic circuit analysis with those obtained using FEM. This can be demonstrated using a FEM simulation of a torus to calculate its magnetic reluctance and then comparing the results to predictions made by equation (2.4) and equation (2.7). The FEM simulated torus has the following parameters.

- Relative Permeability $\mu_r = 4000$

- Major Radius $R_t = 45\text{mm}$

- Minor Radius $r_t = 15\text{mm}$

- $MMF = 10\text{At}$

A cross section of the simulated torus is shown in figure 2.5 with the magnetic material shown in grey and the path for the current shown in light brown.
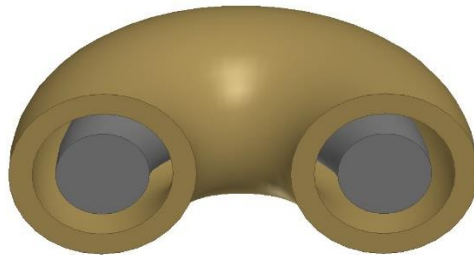
Figure 2.5. FEM simulated torus cross section

Performing the simulation using the parameters listed above allows the non-uniform distribution of the magnetic flux density to be measured. The magnetic flux density for a cross section of the magnetic material of the torus is shown in figure 2.6.
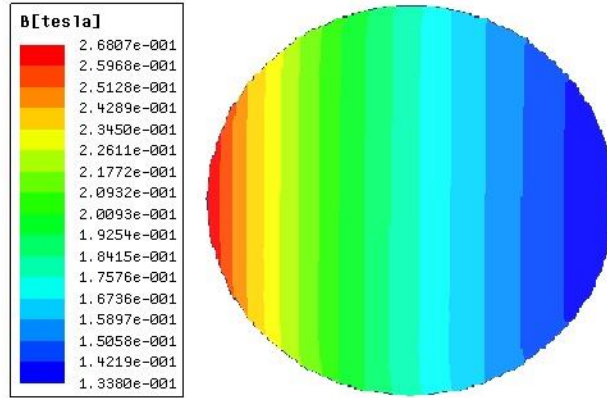
Figure 2.6. FEM simulated magnetic flux density within cross section of torus

It can be observed from figure 2.6 that the magnetic flux density varies as a function of distance from the central axis. Accounting for this effect should result in a more accurate value of magnetic reluctance. This difference in accuracy was calculated by using the FEM simulation as a benchmark against which the reluctance values obtained using a constant and variable magnetic flux density were measured. Figure 2.7 shows the results of the FEM simulated torus reluctance compared to the equation (2.1) reluctance equation derived assuming a constant magnetic flux density and the equation (2.7) reluctance equation assuming non-uniform magnetic flux density.

The simulated and predicted results were compared for different values of the minor radius. The MMF, major radius and relative permeability we the same values used for the figure 2.5 torus while the minor radius was varied over a range of 37.5mm to 11.25mm. To plot these results, the torus aspect ratio is used which is the major radius R_t divided by the minor radius r_t.

22
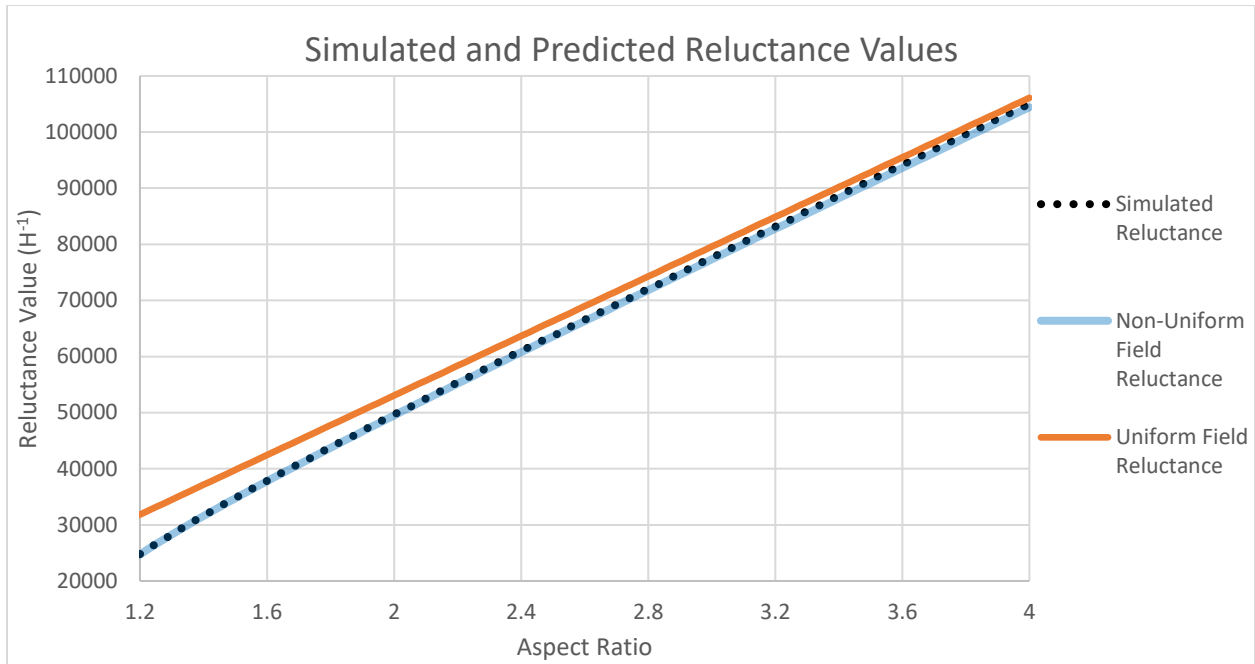
Figure 2.7. Simulated and predicted reluctance values

The percentage difference between the FEM simulated reluctance and reluctance values obtained using a fixed and variable magnetic flux density is shown in figure 2.8 for different aspect ratios.
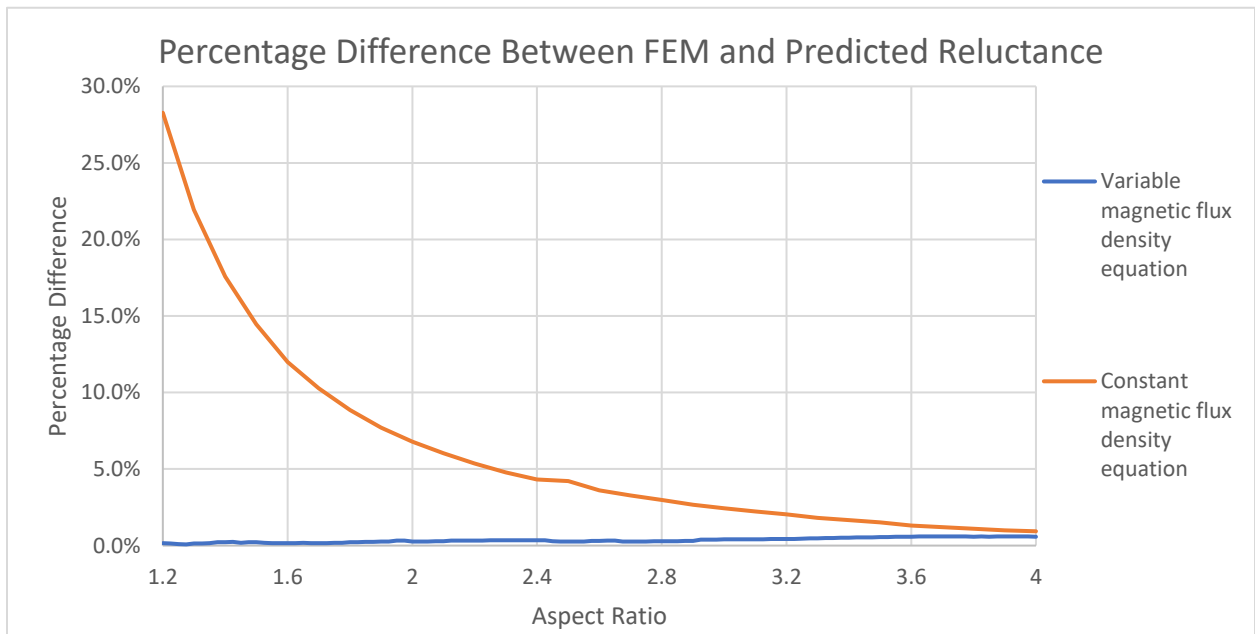
Figure 2.8. Percentage difference between the predicted reluctance and the FEM simulated reluctance

23

Figure 2.8 demonstrates that when the minor radius is large relative to the major radius, as represented by a low aspect ratio, not accounting for the variable distribution of the magnetic flux density results in significant errors in calculating reluctance. This error is reduced relative to the FEM predicted reluctance value as the minor radius is decreased relative to the major radius. The reluctance value calculated by accounting for variations in magnetic flux density remains within 0.5% of the FEM simulated value for all aspect ratios simulated.

The advantages of factoring in the effect of non-homogenous magnetic field distributions for a torus with a low aspect ratio can be quantitively compared in table 2.1. Table 2.1 lists the FEM simulated reluctance of the torus and the predicted values using both a homogeneous and non-homogenous field distribution. The percentage difference between the predicted reluctance values and FEM simulated values are also shown.

Torus Aspect Ratio	FEM Simulated Reluctance (H^{-1})	Homogeneous Magnetic Field Reluctance		Non-Homogeneous Magnetic Field Reluctance	
		Value (H^{-1})	% Difference	Value (H^{-1})	% Difference
1.1	20,651	20,667	0.08%	29,178	41.29%
1.2	24,814	24,713	0.41%	31,831	28.28%
1.3	28,277	28,259	0.07%	34,484	21.95%
1.4	31,588	31,563	0.08%	37,136	17.57%
1.5	34,760	34,723	0.11%	39,789	14.47%
1.6	37,895	37,786	0.29%	42,441	12.00%
1.7	40,894	40,780	0.28%	45,094	10.27%
1.8	43,865	43,723	0.32%	47,746	8.85%
1.9	46,790	46,626	0.35%	50,399	7.71%
2.0	49,676	49,498	0.36%	53,052	6.80%

Table 2.1. Simulated and predicted reluctance values

It can be observed from table 2.1 that reluctance values calculated using a non-homogenous field distribution becomes closer to the FEM simulated value the larger the aspect ratio becomes. This is because the difference between the largest and smallest magnetic flux density decreases as the aspect ratio increases. Reluctance values calculated accounting for the non-homogenous nature of

the magnetic field remain closely aligned with the FEM simulated value even for small aspect ratios.

Although this example has demonstrated that using energy based magnetic circuit analysis is a valid analytical technique, it also required more calculations to derive the reluctance of the torus compared to only using Hopkinson's law based on the magnetic flux. For more complex magnetic path problems such as those that incorporate materials with varying magnetic permeability this is not the case.

2.3 Simulation study on modelling inhomogeneous magnetic fields in a torus with permeability that varies axially

To demonstrate the modelling of materials with varying magnetic permeability, consider a torus with an angular dependent relative permeability that varies axially. This can be achieved by varying the fill grade of the material. Figure 2.9 shows a cross section cut perpendicular to the central axis of such a torus, where increased relative permeability of the material is shown as a darker region within the torus.
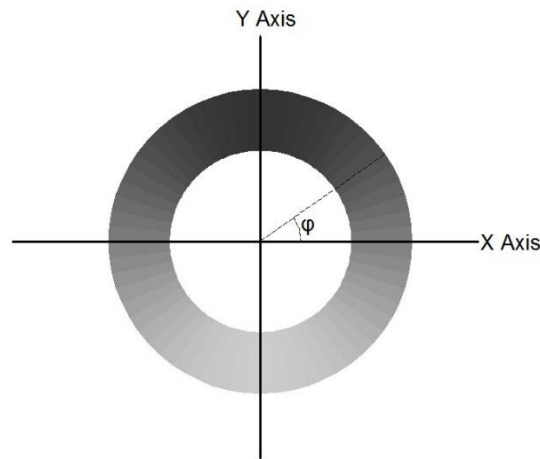
Figure 2.9. Cross section of a variable fill grade torus cut perpendicular to the central axis

The magnetic permeability of the torus is a function of the angle φ as shown in figure 2.8 and defined by equation (2.8).

$$\text{Magnetic permeability} = \mu_0 \mu_r (1 + \varepsilon \sin(\varphi)) \qquad (2.8)$$

In equation (2.8), μ_r is the average relative permeability and ε is the fill grade modulation index which is a number between 0 and 1. If the fill grade modulation index is 0 then the material

permeability will be a constant. As the fill grade modulation index increases, so does the axial variations in material permeability.

To calculate the magnetic reluctance of the torus using the same geometric parameters as shown in figure 2.1, the relationship between the B and H field must be defined as stated in equation (2.9).

$$B = \mu_{eq} H \tag{2.9}$$

Equation (2.9) will be true for the variable fill grade torus as the B field will still be assumed to be linearly proportional to the H field for magnetic circuit analysis. Amperes law can be used to calculate the H field value at a distance of r from the central axis using the figure 2.1 torus geometry. This value of the H field can be substituted into equation (2.9) to calculate the magnetic flux density at a distance of r from the central axis inside the torus to be equation (2.10).

$$B = \frac{\mu_{eq} i n}{2\pi r} \tag{2.10}$$

Integrating the equation (2.10) value of magnetic flux density over the radial cross section of the torus as shown in figure 2.2 allows the magnetic flux to be calculated to be equation (2.11).

$$\Phi = \int_{R_t - r_t}^{R_t + r_t} \frac{\mu_{eq} i n}{\pi r} \sqrt{r_t{}^2 - (r - R_t)^2} \, dr$$

$$\Phi = \mu_{eq} i n \left(R_t - \sqrt{R_t{}^2 - r_t{}^2} \right) \tag{2.11}$$

Hopkinson's law cannot be used to calculate the reluctance of the torus using only the magnetic flux in this case as the value of μ_{eq} is unknown. One way to find the value of μ_{eq} is to calculate the total energy within the torus caused by magnetic flux. The energy of a small segment of the torus dU with a volume of dV can be calculated using the equation for magnetic field energy density.

$$dU = \frac{B^2}{2\mu_0 \mu_r (1 + \varepsilon \sin(\varphi))} dV \tag{2.12}$$

Inserting the equation (2.10) value of magnetic flux density into equation (2.12) and integrating over the volume of the torus allows the total magnetic field energy to be calculated.

$$dU = \frac{\left(\mu_{eq} i n \right)^2 \sqrt{r_t{}^2 - (r - R_t)^2}}{4\pi^2 \mu_0 \mu_r r (1 + \varepsilon \sin(\varphi))} \, dr \, d\varphi$$

26

$$U = \int\limits_{0}^{2\pi} \int\limits_{R_t - r_t}^{R_t + r_t} \frac{\left(\mu_{eq} in\right)^2 \sqrt{r_t^2 - (r - R_t)^2}}{4\pi^2 \mu_0 \mu_r r (1 + \varepsilon \sin(\varphi))} \, dr \, d\varphi$$

$$U = \frac{\left(\mu_{eq} in\right)^2 \left(R_t - \sqrt{R_t^2 - r_t^2}\right)}{2\mu_0 \mu_r \sqrt{1 - \varepsilon^2}} \tag{2.13}$$

Substituting the equation (2.13) value of energy and the equation (2.11) value of magnetic flux into the equation for magnetic circuit energy allows the magnetic circuit reluctance to be calculated.

$$\mathcal{R} = \frac{2U}{\Phi^2}$$

$$\mathcal{R} = \frac{1}{2\mu_0 \mu_r \sqrt{1 - \varepsilon^2} \left(R_t - \sqrt{R_t^2 - r_t^2}\right)} \tag{2.14}$$

Hopkinson's law can now be used to calculate the equivalent permeability value μ_{eq} using the equation (2.11) value of magnetic flux and the equation (2.14) value of magnetic circuit reluctance.

$$\mu_{eq} = \mu_0 \mu_r \sqrt{1 - \varepsilon^2} \tag{2.15}$$

Equation (2.14) can be verified by comparing its reluctance predictions to those calculated using a FEM simulation of a torus with a variable material permeability as defined by equation (2.8). To simulate this situation, a torus was divided into 100 segments with material permeability defined by equation (2.8). The resulting torus as rendered by the FEM simulation software is shown in figure 2.10.
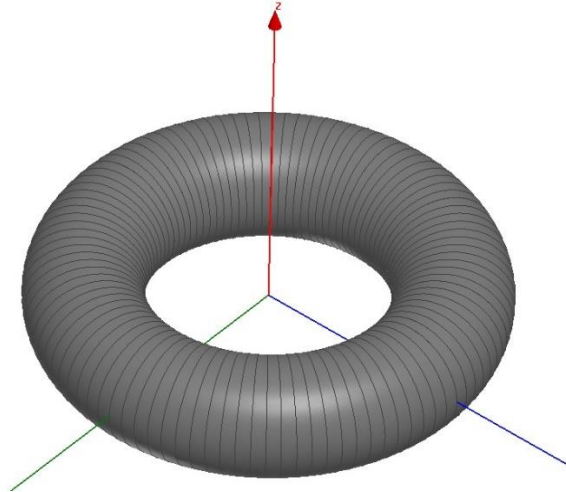
Figure 2.10 - Simulated torus with angular variation of permeability

For this simulation the magnetic and geometric following parameters were used.

- Major Radius $R_t = 45\text{mm}$

- Minor Radius $r_t = 15\text{mm}$

- Magneto Motive Force $= 10\text{At}$

- Average relative permeability $\mu_r = 2500$

- Fill grade modulation index $0 \leq \varepsilon \leq 0.6$

By setting the average relative permeability to 2500 and the maximum fill grade modulation index ε to 0.6, the maximum simulated relative permeability will be 4000 and its minimum value will be 1000. This keeps the relative permeability to within realistic values, thereby ensuring the simulated data is limited to describing practical situations. Based on these values, the fill grade modulation index of the torus from figure 2.10 was simulated over a range of values between 0 and 0.6. The simulated reluctance values and those predicted using equation (2.14) are shown in figure 2.11.
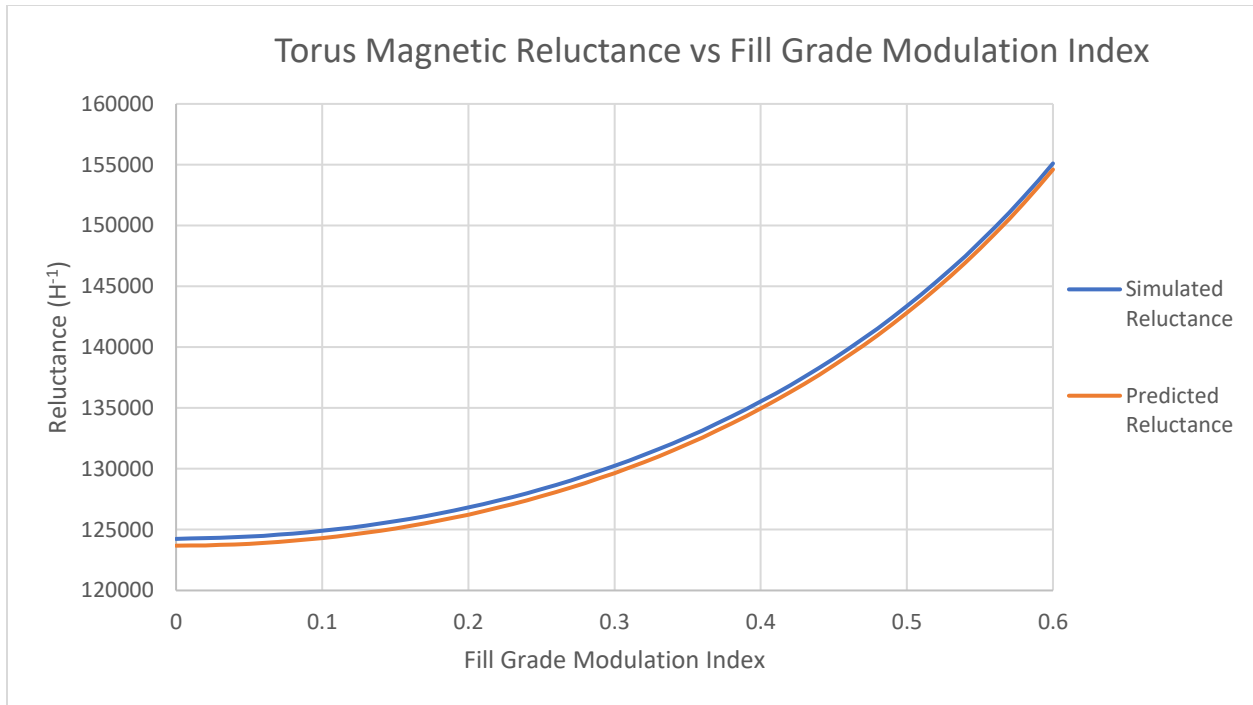
Figure 2.11 - Simulated and predicted torus reluctance as a function of fill grade modulation index

The simulated and predicted reluctance values are within 0.5% of each other for the range of fill grade modulation index values simulated. This demonstrates that the equation (2.14) value of magnetic reluctance yields results comparable to that obtained using FEM simulation.

2.4 Conclusion

In this chapter of this thesis, it has been demonstrated how stored energy-based analysis of magnetic field can be used to model inhomogeneous magnetic field distribution in devices such as a toroid. Although due to the simple geometric nature of the torus being analyzed, there was no significant advantage of using stored energy-based analysis compared to conventional methods.

Further advantages of energy based magnetic circuit analysis can be observed when analyzing more complex magnetic field distributions with nonaligned B and H fields. In a torus, the B and H fields are aligned throughout the entire volume resulting in the same outcome using conventional and energy based magnetic circuit analysis. In the next chapter, a more geometrically complex situation will be considered involving time varying reluctance and nonaligned B and H fields to demonstrate advantages of using energy based magnetic circuit analysis compared to conventional techniques.

3 Modelling Magnetic Circuits with Variable Reluctance and Inhomogeneous Magnetic Field Distribution

In this chapter, stored magnetic energy-based analysis is applied to a case that exhibits inhomogeneous magnetic field distributions and variable reluctance. A solenoid is an example of a time varying reluctance magnetic circuit as the magnetic reluctance will be a function of armature displacement. Although a simple solenoid can be analyzed using magnetic circuit analysis, the transient analysis of a more complex solenoid would typically require the use of LPM or FEM. In this chapter, a transient analysis of a solenoid incorporating diverging magnetic fields will be analyzed and the modelling results compared to those obtained using FEM.

3.1 Mathematical Analysis of Magnetic Circuits with Variable Reluctance

For a transient analysis of a variable reluctance magnetic circuit, it is necessary to define the rate of energy transfer to a magnetic circuit as a function of reluctance and magnetic flux. The magnetic circuit energy and the rate of energy transfer to the magnetic circuit was derived in the introduction (equations (1.13) and (1.14)). For the case of a solenoid, the magnetic flux of the magnetic circuit will not change its orientation during operation. As the magnetic flux does not rotate, the magnetic flux and its time derivative will be parallel to each other. Therefore, the dot product of the magnetic flux with its partial time derivative can be replaced with the multiplications of the magnetic flux with its time derivative and the dot product of the magnetic flux with itself can be replaced by the square of the magnetic flux. Applying these simplifications to the vector equations (1.13) and (1.14) results in the equation (3.1) for energy and the equation (3.2) for power as:

$$U = \frac{1}{2}\mathcal{R}\Phi^2 \tag{3.1}$$

$$P = \mathcal{R}\Phi\frac{d\Phi}{dt} + \frac{1}{2}\Phi^2\frac{d\mathcal{R}}{dt} \tag{3.2}$$

Equation (3.2) consists of two product terms. The first term describes the rate of energy transfer to the magnetic field and the second term describes that converted into kinetic energy. This statement can be verified by considering a tightly wound conductive helix with n turns. Faraday's law of induction can be used to calculate the change in magnetic flux caused by an externally applied voltage v:

$$v = n\frac{d\Phi}{dt} \tag{3.3}$$

Multiplying both sides of this equation by the current flowing in the coil i, the power transferred to the magnetic field to be calculated as:

$$vi = ni\frac{d\Phi}{dt} \tag{3.4}$$

Using Hopkins law to replace the MMF term ni from equation (3.4) and replacing the product of voltage and current with power $P_{magnetic\_field}$ allows the calculation of the rate of energy transfer to the magnetic field as:

$$P_{\text{magnetic\_field}} = \mathcal{R}\Phi\frac{d\Phi}{dt} \tag{3.5}$$

Since no electrical losses were considered, all the energy transfer as described by equation (3.5) must be transferred to the magnetic field, thereby identifying the power transfer described by the first product term of equation (3.2).

To determine the function of the second product term from equation (3.2), it is necessary to consider a magnetic circuit in motion. If the magnetic reluctance is path dependent, a change in position will result in a change in reluctance. This will impact the energy stored in the magnetic field. To calculate the change in energy caused by a change in position, consider the derivative of the equation (3.1) value of energy with respect to reluctance while keeping the magnetic flux constant.

$$U = \frac{1}{2}\mathcal{R}\Phi^2$$

$$\frac{dU}{d\mathcal{R}} = \frac{1}{2}\Phi^2 \tag{3.6}$$

Assuming reluctance is a continuous function of displacement, there will be a defined derivative of reluctance as a function of position. Multiplying both sides of equation (3.6) by the derivative of reluctance with respect to position allows the chain rule to be used to calculate the derivative of energy with respect to position:

$$\frac{dU}{dx} = \frac{1}{2}\Phi^2\frac{d\mathcal{R}}{dx} \tag{3.7}$$

31

where the displacement is represented by the variable x. Equation (3.7) describes the derivative of energy with respect to position. This is the definition of force. Therefore, equation (3.7) can be used to calculate changes in motion. If the magnetic circuit is in motion, the change in kinetic energy can be calculated by multiplying the force by velocity. This allows equation (3.8) to be derived by multiplying equation (3.7) by velocity, as represented by the time derivative of the magnetic circuit's position.

$$\frac{dU}{dx} \times \frac{dx}{dt} = \frac{1}{2}\Phi^2 \frac{d\mathcal{R}}{dx} \times \frac{dx}{dt}$$

$$P_{\text{reluctance}} = \frac{1}{2}\Phi^2 \frac{d\mathcal{R}}{dt} \qquad (3.8)$$

As the power transfer described by equation (3.8) was calculated by only accounting for changes in position, it can be concluded that it describes energy transferred into kinetic energy.

3.2 Modelling of a Solenoid with inhomogeneous magnetic fields and variable reluctance

A solenoid consists of a moving rod called the armature and a stationary frame for the return magnetic flux called the yoke. Both the armature and yoke will form a cylindrical shape around a central axis in this example as this will result in a non-uniform magnetic flux within the yoke and the air gap between the armature and yoke. A cross section of this solenoid as it appears above the central axis that has not been drawn to scale is shown in figure 3.1 showing relevant dimensions from the central axis.
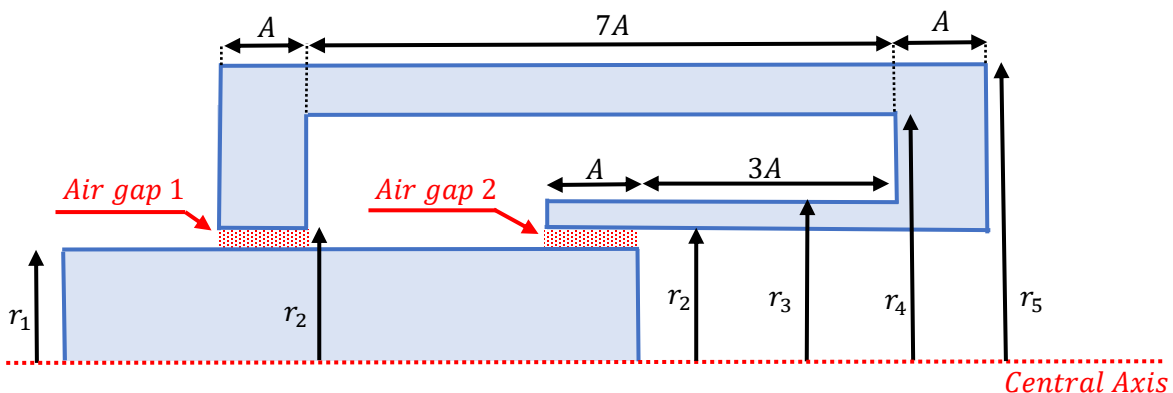
Figure 3.1 – Solenoid cross section

In figure 3.1, the blue lines represent the boundaries of the yoke and armature and the black arrows define the dimensions used. Magnetic flux will travel through the armature and form a closed loop by returning through the yoke. To complete this path, the magnetic flux will need to pass through

two air gaps. The left air gap in figure 3.1 will be referred to as air gap 1 and the right air gap as air gap 2.

The armature forms a cylindrical shape and is shown in figure 3.2 in its left most position. In this position, air gaps 1 and 2 have the same depth of *A*. When the solenoid is energized, the armature will move to the right for a maximum distance of 4*A* resulting in the length of air gap 2 to be 5*A*. The armature is long enough to ensure that air gap 1 has a constant length. This motion will result in a reduction in magnetic path reluctance caused by air gap 2 resulting in a magnetic circuit with an armature position dependent reluctance.

Magnetic circuit analysis will be used to analyze this solenoid with the results being compared to a FEM based computer simulation. The cross section of this solenoid is shown in figure 3.2 that will be used to for FEM simulations.
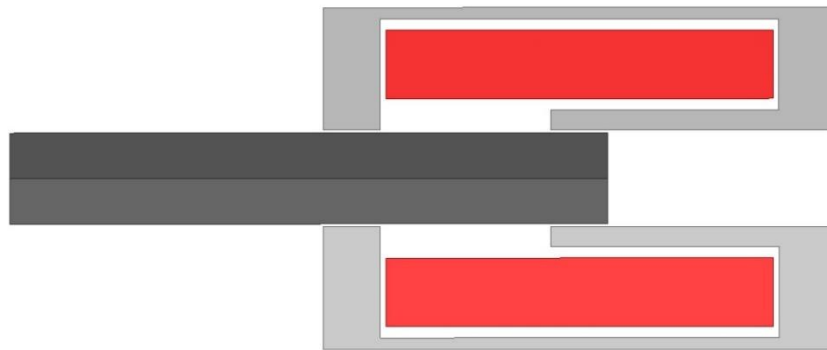
Figure 3.2 – Computer rendered cross section of solenoid

In figure 3.2, the red area is the solenoid windings, the dark grey area is the armature and the light grey area is the yoke. Rotating this geometry around the central axis results in a cylindrical shaped solenoid as shown in figure 3.3.
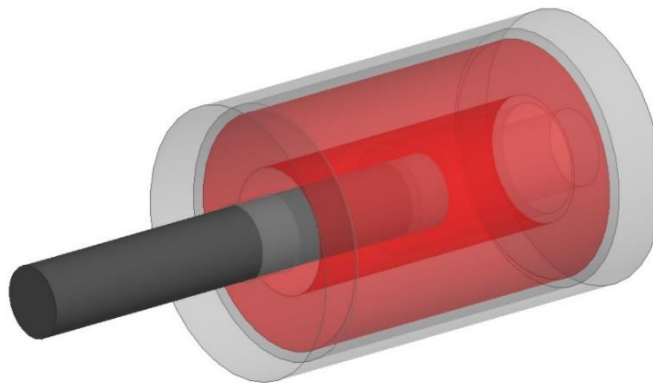
Figure 3.3 – 3D Computer rendered image of solenoid

This solenoid can be modelled as a magnetic circuit comprising of a source of MMF and the series connection of reluctances due to the yoke, armature and two air gaps. To calculate the reluctance of the armature, it is necessary to break it into 3 segments as shown in figure 3.4.
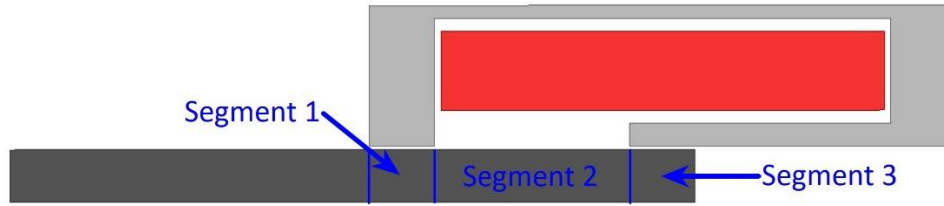
Figure 3.4 – Solenoid armature divided into segments

3.2.1 Stored energy in armature segment-1

The first segment is the section of the armature parallel to air gap 1. The magnetic flux density in this section is not a constant as magnetic flux is leaving the armature and flowing into the yoke. Assuming the magnetic flux leaving the armature in this section has a constant magnetic flux density, the integration variables can be shown as depicted in figure 3.5.
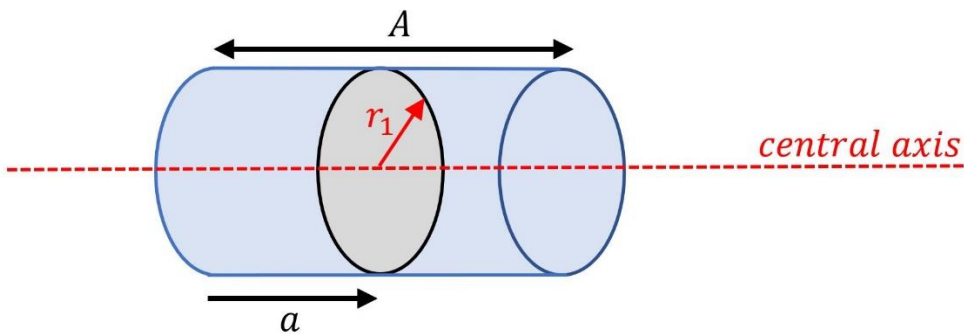
Figure 3.5 – Cross section of armature segment 1

Magnetic flux remaining in this segment will be linearly proportional to the depth a. The magnetic flux density within segment 1 of the armature at a depth of a will be equation (3.9).

$$\text{Magnetic flux at depth } a := \Phi \frac{a}{A} \tag{3.9}$$

Equation (3.9) can be used to calculate the magnetic flux present in the armature segment at a distance of a as shown in figure 3.5. Assuming the magnetic flux is not a function of radial distance from the central axis, the magnetic flux density can be calculated by dividing the equation (3.9) value of magnetic flux by the grey cross-sectional area shown in figure 3.5. This results in the equation (3.10) value of magnetic flux density.

$$\text{Magnetic flux density} = \frac{a\Phi}{\pi r_1{}^2 A} \tag{3.10}$$

The energy due to the equation (3.10) value of magnetic flux density can be calculated using the magnetic flux energy density as:

$$dU = \frac{B^2}{2\mu_0\mu_r} dV$$

$$dU = \frac{(a\Phi)^2}{2\mu_0\mu_r(\pi r_1{}^2 A)^2} dV \tag{3.11}$$

Integrating the equation (3.11) value of energy over the volume of segment 1 allows its total energy to be calculated. To perform this integration, cylindrical coordinates will be used where r is the radial distance from the axis, a is the distance parallel to the axis as per figure 3.5 and θ is the rotational angle around the axis. The region enclosed by a small change in these three variables is the volume enclosed by solid blue lines shown in figure 3.6.
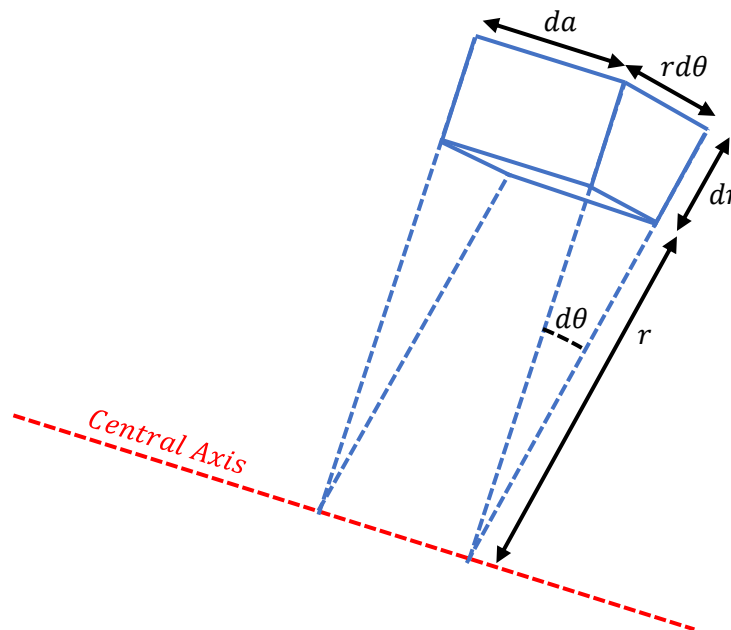
Figure 3.6 – Integration volume used for cylindrical coordinates integration

Integrating the equation (3.11) value of energy over the entire volume of armature segment 1 using the integration variables as shown in figure 3.6 allows the total armature segment 1 energy to be calculated as:

35

$$\text{Armature segment 1 energy} = \int_0^A \int_0^{r_1} \int_0^{2\pi} \frac{(a\Phi)^2}{2\mu_0\mu_r(\pi r_1^2 A)^2} \, r \, d\theta \, dr \, da$$

$$\text{Armature segment 1 energy} = \frac{A\Phi^2}{6\mu_0\mu_r\pi r_1^2} \tag{3.12}$$

3.2.2 Stored energy in armature segment-2

Segment 2 of the armature as shown in figure 3.4 has a constant radius and depth. No magnetic flux enters of leaves this segment resulting in a constant magnetic flux density throughout the segment. Therefore, the energy of this segment can be calculated by multiplying the magnetic field energy density by the segment volume.
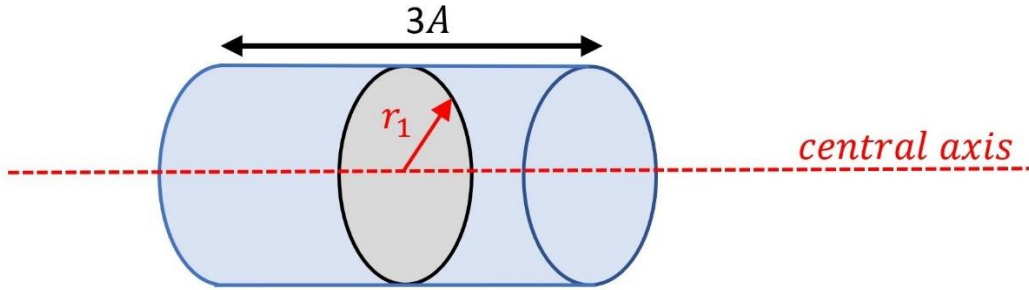
Figure 3.7 – Cross section of armature segment 2

The magnetic flux density in the armature segment 2 is the magnetic flux Φ divided by the cross-sectional area of the armature as shown in grey in figure 3.7.

$$\text{Magnetic flux density} = \frac{\Phi}{\pi r_1^2} \tag{3.13}$$

The energy density can be calculated using the equation (3.13) value of magnetic flux density and the magnetic field energy density equation.

$$dU = \frac{B^2}{2\mu_0\mu_r} \, dV$$

$$dU = \frac{\Phi^2}{2\mu_0\mu_r(\pi r_1^2)^2} \, dV \tag{3.14}$$

Multiplying the energy density of segment 2 of the armature by its volume allows its total energy to be calculated.

$$\text{Armature segment 2 volume} = 3A\pi r_1{}^2$$

$$\text{Armature segment 2 energy} = \frac{3A\Phi^2}{2\mu_0\mu_r\pi r_1{}^2} \qquad (3.15)$$

3.2.3 Stored energy in armature segment-3

The third segment of the armature is a cylindrical shape where the magnetic flux is transferred from the armature to the yoke. The depth of this segment is initially A and increases by the distance the armature is moved to the right x. Figure 2.16 shows this segment of the armature with the integration variables.
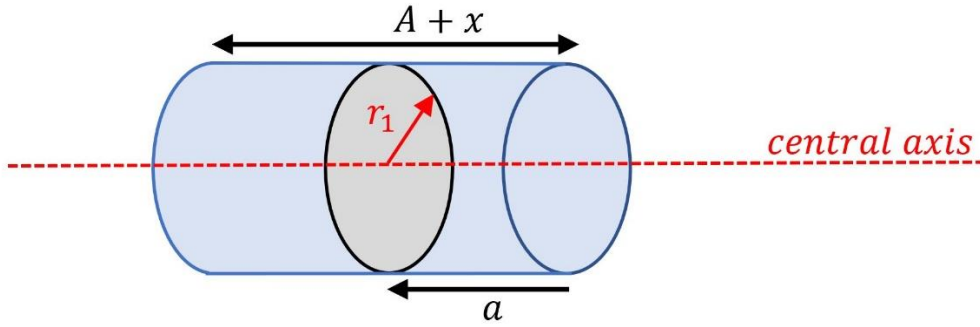
Figure 3.8 – Cross section of armature segment 3

It will be assumed that the magnetic flux density of air gap 2 is constant as the gap between the armature and yoke is constant. Therefore, the magnetic flux remaining in the armature will decrease linearly with depth, reducing to zero by the end of the armature. Based on this assumption, the magnetic flux passing through the armature at a depth of a as shown in figure 3.8 can be calculated as:

$$\text{Armature segment 3 magnetic flux} = \Phi\frac{a}{A+x} \qquad (3.16)$$

The magnetic flux density at a depth of a within segment 3 can be calculated by dividing the equation (3.16) value of magnetic flux by the cross-sectional area of the armature.

$$\text{Magnetic flux density} = \frac{a\Phi}{\pi r_1{}^2(A+x)} \qquad (3.17)$$

The energy density due to the equation (3.17) value of magnetic flux density within this segment of the armature can be calculated using the magnetic field energy density equation.

$$dU = \frac{B^2}{2\mu_0\mu_r} dV$$

$$dU = \frac{(a\Phi)^2}{2\mu_0\mu_r(\pi r_1{}^2)^2(A + x)^2} dV \qquad (3.18)$$

Integrating the equation (3.18) value of energy density over the entire volume of the armature segment 3 as shown in figure 3.8 allows the total energy of this segment to be calculated. This integration is performed using cylindrical coordinates as shown in figure 3.6.

$$\text{Armature segment 3 energy} = \int_0^{A+x} \int_0^{r_1} \int_0^{2\pi} \frac{(a\Phi)^2}{2\mu_0\mu_r(\pi r_1{}^2)^2(A + x)^2} r\, d\theta\, dr\, da$$

$$\text{Armature segment 3 energy} = \frac{(A + x)\Phi^2}{6\mu_0\mu_r\pi r_1{}^2} \qquad (3.19)$$

Magnetic energy within the yoke can also be calculated using a similar process by dividing the yoke into segments. These five segments are shown in figure 2.17.
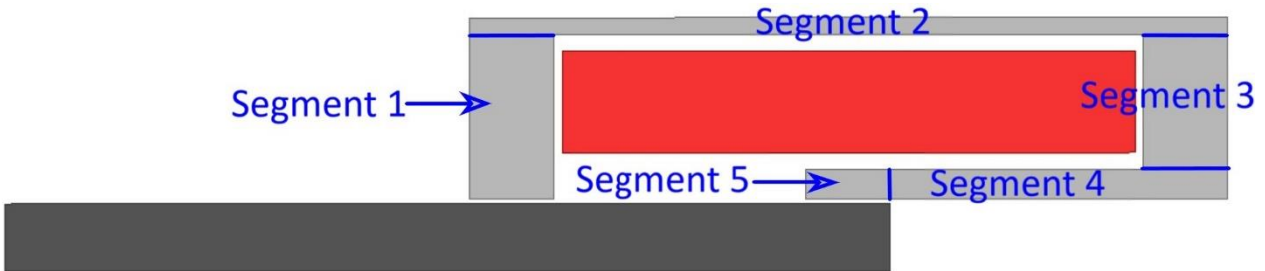
Figure 3.9 – Cross section of yoke with labeled segments

3.2.4 Stored energy in yoke segment-1

In segment 1 of the yoke, magnetic flux will enter via the armature with a uniform magnetic flux density. As the magnetic flux travels outward and towards segment 2, the area it flows through increase thereby reducing the magnetic flux density. While it is possible to model this using lumped parameter approximations, the reluctance of this segment with diverging fields can be calculated simply using energy based magnetic circuit equations. To quantify these values, consider the labeled dimensions in figure 3.10 which will be used for integration.
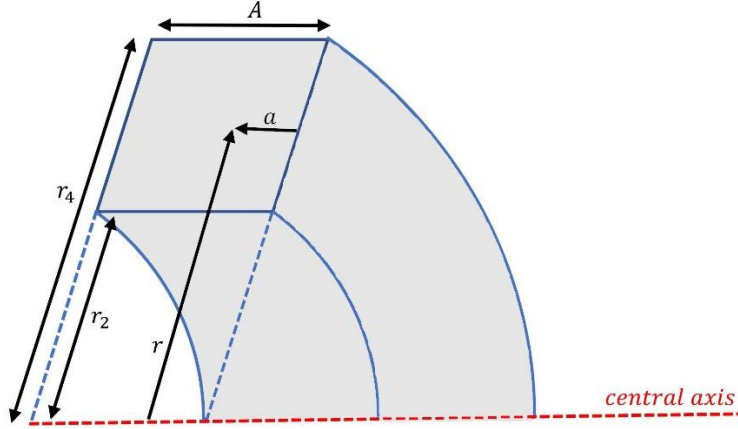
Figure 3.10 – Cross section of yoke segment 1

In segment 1 of the yoke, the magnetic flux will enter at the radial distance of r_2 and travel uniformly outwards towards segment 2. As such, the magnetic flux density will only be a function of the distance from the central axis as represented by the variable r in figure 3.10. Magnetic flux density will not be a function of the distance parallel to the central axis as represented by the variable a in figure 3.10. This means the magnetic flux density as a distance of r from the central axis in figure 3.10 ca be calculated to be equation (3.20).

$$\text{Segment 1 Magnetic flux density} = \frac{\Phi}{2\pi rA} \tag{3.20}$$

The magnetic field energy due to the equation (3.20) magnetic flux density can be calculated using the magnetic field energy density formula.

$$dU = \frac{B^2}{2\mu_0\mu_r}dV$$

$$dU = \frac{\Phi^2}{2\mu_0\mu_r(2\pi rA)^2}dV \tag{3.21}$$

Integrating the magnetic field energy over the volume of segment 1 allows its total energy to be calculated. This integration is performed using a cylindrical coordinate system as shown in figure 3.6.

$$\text{Segment 1 energy} = \int_{r_2}^{r_4}\int_{0}^{A}\int_{0}^{2\pi} \frac{\Phi^2}{2\mu_0\mu_r(2\pi rA)^2}\, r\, d\theta\, da\, dr$$

$$\text{Segment 1 energy} = \frac{\Phi^2}{4\mu_0\mu_r\pi A}\log_e\left(\frac{r_4}{r_2}\right) \tag{3.22}$$

39

3.2.5 Stored energy in yoke segment-2

When calculating the magnetic field energy within segment 2 it will be assumed that the magnetic flux density is constant. This means that only the volume of segment 2 is required to be known. To calculate this volume, consider the cross section of segment 2 as shown in figure 3.11.
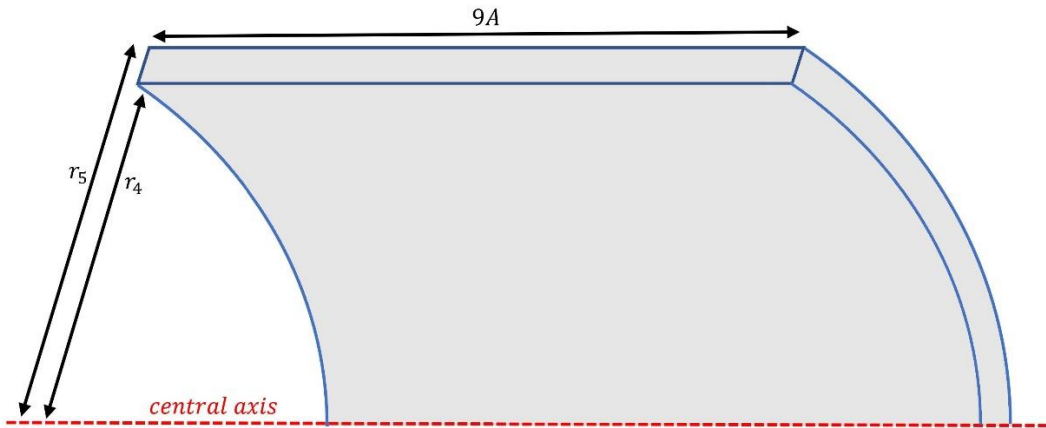
Figure 3.11 – Cross section of yoke segment 2

The volume of segment 2 is given by:

$$\text{Segment 2 volume} = 9\pi A(r_5{}^2 - r_4{}^2) \qquad (3.23)$$

To calculate the magnetic flux density inside segment 2 of the yoke, consider a cross section of the yoke as viewed along the central axis as shown in figure 3.12.
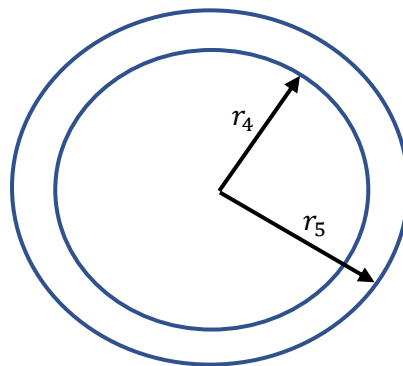
Figure 3.12 – Cross section of yoke segment 2 as viewed along the central axis

Assuming the magnetic flux density is constant within this segment, the magnetic flux density can be calculated by dividing the magnetic flux by the cross-sectional area of the yoke as shown in figure 3.12.

40

$$\text{Segment 2 magnetic flux density} = \frac{\Phi}{\pi(r_5{}^2 - r_4{}^2)} \qquad (3.24)$$

The segment 2 magnetic field energy density can be calculated using the equation (3.24) magnetic flux density and the formula for magnetic field energy density.

$$dU = \frac{B^2}{2\mu_0\mu_r} dV$$

$$\text{Segment 2 energy density} = \frac{\Phi^2}{2\mu_0\mu_r\pi^2(r_5{}^2 - r_4{}^2)^2} \qquad (3.25)$$

Multiplying the equation (3.25) value of magnetic field energy density by the volume of segment 2 allows the total energy of segment 2 to be calculated.

$$\text{Segment 2 energy} = \frac{9A\Phi^2}{2\mu_0\mu_r\pi(r_5{}^2 - r_4{}^2)} \qquad (3.26)$$

3.2.6 Stored energy in yoke segment-3

Segment 3 of the yoke has a similar geometry to segment 1. The only difference is that it has a minimum radius of r_3 instead of r_2. This means the energy of segment 3 can be calculated to be equation (3.27).

$$\text{Segment 3 energy} = \frac{\Phi^2}{4\mu_0\mu_r\pi A} \log_e\left(\frac{r_4}{r_3}\right) \qquad (3.27)$$

3.2.7 Stored energy in yoke segment-4

Segment 4 of the yoke will have a constant magnetic flux density. Its energy can therefore be calculated similarly to segment 2. The only significant difference is that the length of segment 4 depends on the position of the armature. This is shown in the cross section of segment 4 in figure 2.21.
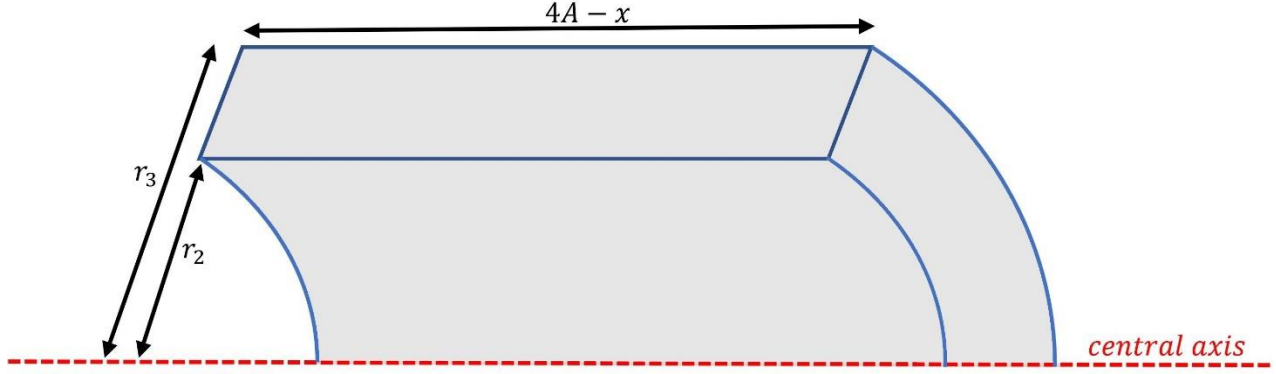
Figure 3.13 – Cross section of yoke segment 4

The volume of segment 4 can be calculated using Pappus centroid theorem to be equation (3.28).

$$\text{Segment 4 volume} = \pi(4A - x)(r_3^2 - r_2^2) \qquad (3.28)$$

The magnetic flux density can be calculated to be equation (3.29) by dividing the magnetic flux by the cross-sectional area of segment 4 perpendicular to the direction of the magnetic flux.

$$\text{Segment 4 magnetic flux density} = \frac{\Phi}{\pi(r_3^2 - r_2^2)} \qquad (3.29)$$

The segment 4 energy density can be calculated using the equation (3.29) value of magnetic flux density and the magnetic field energy density equation.

$$dU = \frac{B^2}{2\mu_0\mu_r} dV$$

$$dU = \frac{\Phi^2}{2\mu_0\mu_r\pi^2(r_3^2 - r_2^2)^2} dV \qquad (3.30)$$

Multiplying the equation (3.30) energy density by the volume of segment 4 allows its total energy to be calculated.

$$\text{Segment 4 energy} = \frac{(4A - x)\Phi^2}{2\mu_0\mu_r\pi(r_3^2 - r_2^2)} \qquad (3.31)$$

3.2.8 Stored energy in yoke segment-5

Segment 5 of the yoke is the segment where magnetic flux is transferred between the yoke and armature. The dimensions of this segment are shown in figure 3.14.
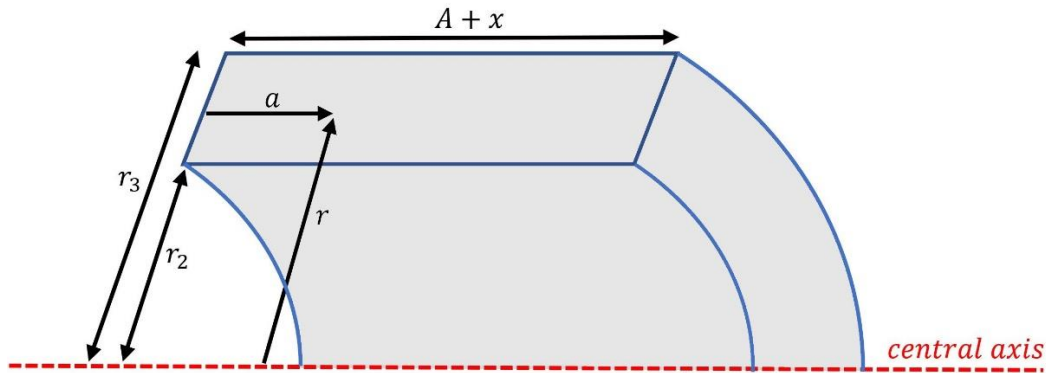
Figure 3.14 – Cross section of yoke segment 5

Assuming the magnetic flux leaving the armature is uniformly distributed along the air gap, the magnetic flux in segment 5 will increase linearly with depth. Therefore, the magnetic flux within segment 5 at a depth of a as shown in figure 3.14 can be calculated to be equation (3.32).

$$\text{Segment 5 magnetic flux} = \Phi \frac{a}{A + x} \tag{3.32}$$

Dividing the magnetic flux by the cross-sectional area of segment 5 perpendicular to the direction of the magnetic flux allows the magnetic flux density to be calculated.

$$\text{Segment 5 magnetic flux density} = \frac{a\Phi}{\pi(A + x)(r_3{}^2 - r_2{}^2)} \tag{3.33}$$

The magnetic field energy density due to the equation (3.33) value of magnetic flux density can be calculated to be equation (3.34).

$$dU = \frac{B^2}{2\mu_0\mu_r} dV$$

$$dU = \frac{(a\Phi)^2}{2\mu_0\mu_r\pi^2(A + x)^2(r_3{}^2 - r_2{}^2)^2} dV \tag{3.34}$$

Integrating energy density due to the magnetic flux density defined by equation (3.34) over the volume of segment 5 using the cylindrical coordinates defined in figure 3.6 allows the total segment 5 magnetic field energy to be calculated.

$$\text{Segment 5 energy} = \int_{r_2}^{r_3} \int_0^{A+x} \int_0^{2\pi} \frac{(a\Phi)^2}{2\mu_0\mu_r\pi^2(A+x)^2(r_3{}^2 - r_2{}^2)^2} \, r \, d\theta \, da \, dr$$

$$\text{Segment 5 energy} = \frac{(A+x)\Phi^2}{6\mu_0\mu_r\pi(r_3{}^2 - r_2{}^2)} \tag{3.35}$$

3.2.9 Stored energy in Air gap-1

The energy in air gap 1 and 2 is more complicated to calculate due to the magnetic flux lines not being parallel to the H field caused by current in the windings. Using energy-based analysis allows this effect to be accounted easily.

To demonstrate this, consider the reluctance of air gap 1 as shown in figure 3.15 where the blue shaded areas are the yoke and armature and the red dotted region is the air gap.
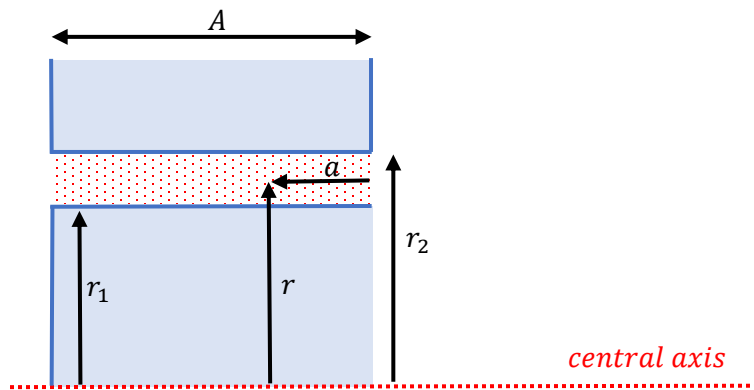
Figure 3.15 – Cross section of air gap 1

The air gap is narrow compared to the armature and yoke, it will have a much greater reluctance due to the absence of high magnetic permeable material. Therefore, magnetic flux will use the shortest possible route to travel through this gap resulting in magnetic field lines at an angle to the central axis. Magnetic flux will travel radially outward from the armature with magnetic flux density only being a function of distance from the central axis. As such, the magnetic flux density at a distance of r from the central axis can be calculated to be equation (3.36).

$$\text{Air gap 1 magnetic flux density} = \frac{\Phi}{2\pi r A} \tag{3.36}$$

Integrating the energy due to this magnetic flux using the scalar magnetic field energy density formula results in the equation (3.37) value of energy in air gap 1.

$$dU = \frac{B^2}{2\mu_0} dV$$

$$\text{Air gap 1 energy} = \int_{r_1}^{r_2} \int_0^A \int_0^{2\pi} \frac{\Phi^2}{8\mu_0\pi^2 r A^2} \, d\theta \, da \, dr$$

$$\text{Air gap 1 energy} = \frac{\Phi^2}{4\pi\mu_0 A} \log_e\left(\frac{r_2}{r_1}\right) \qquad\qquad (3.37)$$

Equation (3.37) can be used to calculate reluctance using the relationship between energy and reluctance.

$$\mathcal{R} = \frac{2U}{\Phi^2}$$

$$\text{Air gap 1 reluctance} = \frac{1}{2\pi\mu_0 A} \log_e\left(\frac{r_2}{r_1}\right) \qquad\qquad (3.38)$$

Due to the position of the windings, the H field at this point will be close to parallel with the central axis. As there is no material in the gap containing magnetic dipoles that can be aligned with the magnetic flux, the only magnetic energy within this region can be calculated using the vector-based energy density equation shown in equation (3.39).

$$dU = \frac{1}{2} B.H \, dV \qquad\qquad (3.39)$$

The maximum amount of energy within the field would occur when the B and H fields are parallel. This cannot happen as no magnetic flux could be transferred between the yoke and stator if the B field was parallel to the central axis. Perpendicular B and H fields results in no energy within the air gap. A good approximation for the average magnetic flux angle (angle of 45°) in the air gap and will be used to for calculating air gap energy for the remainder of this analysis.

Assuming the angle between the B and H fields is 45°, the energy calculated to be equation (3.40) needs to be divided by $\sqrt{2}$ to factor in the effect of nonaligned B and H fields:

$$\text{Air gap 1 energy} = \frac{\Phi^2}{4\sqrt{2}\pi\mu_0 A} \log_e\left(\frac{r_2}{r_1}\right) \qquad\qquad (3.40)$$

The energy in air gap 2 can be calculated using a similar process as that considered for air gap 1. Air gap 2 is a function of the distance the armature has moved to the right as represented by the variable x. Figure 3.16 shows the dimensions of air gap 2 used in integration.

45
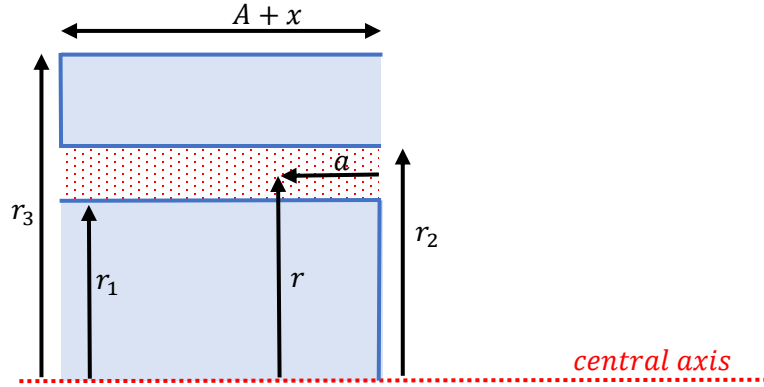
Figure 3.16 – Cross section of air gap 2

The length of this air gap will increase with position of the armature. Taking this into account, the magnetic flux in air gap 2 as a function of distance from the central axis as:

$$\text{Air gap 2 magnetic flux density} = \frac{\Phi}{2\pi r(A + x + r_2 - r_1)} \qquad (3.41)$$

The energy density within air gap 2 can be calculated to be equation (3.42) taking into account the 45° angle between the B and H fields.

$$\text{Air gap 2 energy density} = \frac{\Phi^2}{8\sqrt{2}\mu_0\pi^2 r^2(A + x + r_2 - r_1)^2} \qquad (3.42)$$

Integrating the equation (3.42) value of energy over the volume of air gap 2 results in the equation (3.43) value of energy.

$$\text{Air gap 2 energy} = \int_{r_1}^{r_2} \int_0^{A+x+r_2-r_1} \int_0^{2\pi} \frac{\Phi^2}{8\sqrt{2}\mu_0\pi^2 r^2(A + x + r_2 - r_1)^2} r \, d\theta \, da \, dr$$

$$\text{Air gap 2 energy} = \frac{\Phi^2}{4\sqrt{2}\mu_0\pi(A + x + r_2 - r_1)} \log_e\left(\frac{r_2}{r_1}\right) \qquad (3.43)$$

The reluctance of each component of the solenoid can be calculated using equation (3.1) to calculate reluctance based on energy and magnetic flux. This results in a total armature reluctance of equation (3.44).

$$\text{Armature reluctance} = \frac{13A + x}{3\mu_0\mu_r\pi r_1^2} \qquad (3.44)$$

The total yoke reluctance can be calculated to be equation (3.45).

$$\text{Yoke reluctance} = \frac{1}{\mu_0 \mu_r \pi} \left(\frac{1}{2A} \log_e \left(\frac{r_4{}^2}{r_2 r_3} \right) + \frac{9A}{(r_5{}^2 - r_4{}^2)} + \frac{13A - 2x}{3(r_3{}^2 - r_2{}^2)} \right) \qquad (3.45)$$

The total air gap reluctance can be calculated to be equation (3.46).

$$\text{Total Air gap reluctance} = \frac{1}{2\sqrt{2}\pi\mu_0} \log_e \left(\frac{r_2}{r_1} \right) \left(\frac{1}{A} + \frac{1}{A + x + r_2 - r_1} \right) \qquad (3.46)$$

The total reluctance of the solenoid magnetic circuit can be calculated by summing together the reluctance of the armature, yoke and air gaps.

3.3 Validation of the model using finite element results

To assess the accuracy of these magnetic circuit equations, a FEM simulation was performed of a solenoid to determine the magnetic circuit reluctance. This creates a benchmark against which these proposed magnetic circuit equations can be measured. For this simulation, the following parameters of the geometric variables have been used.

$$r_1 = 0.008 \text{ m}$$

$$r_2 = 0.0085 \text{ m}$$

$$r_3 = 0.012 \text{ m}$$

$$r_4 = 0.28 \text{ m}$$

$$r_5 = 0.03 \text{ m}$$

$$A = 0.01 \text{ m}$$

A computer rendering of both the B and H fields is shown in figures 3.17 and 3.18 using the above-mentioned geometric parameters.
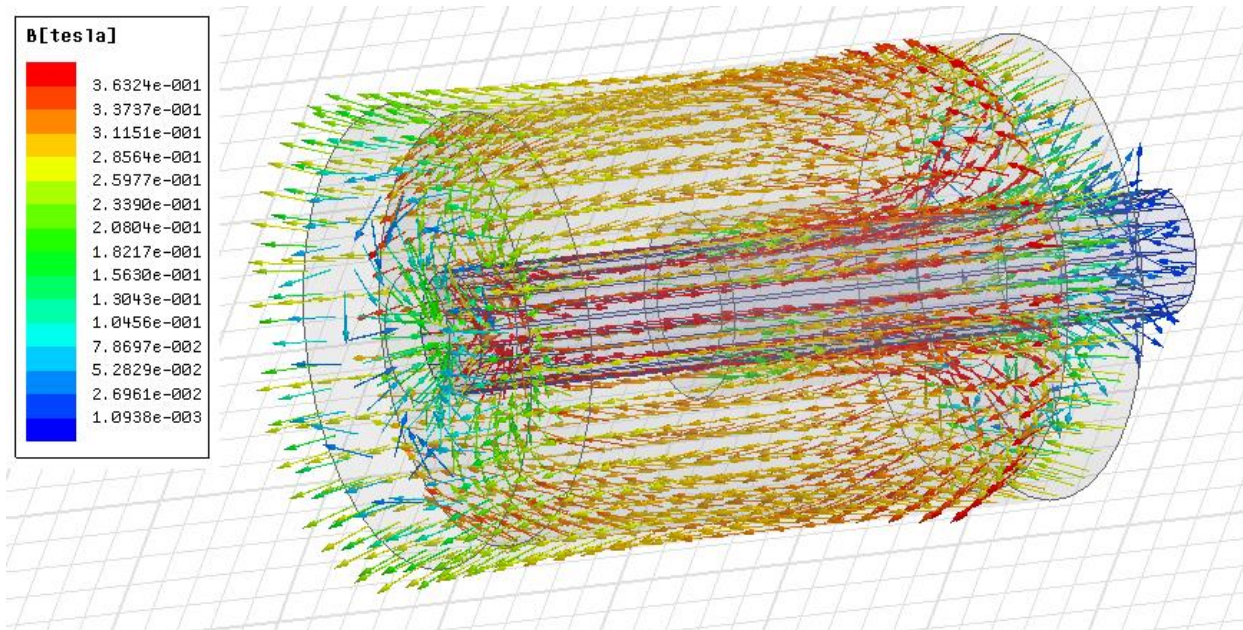
Figure 3.17 – FEM simulated solenoids magnetic flux density vector field
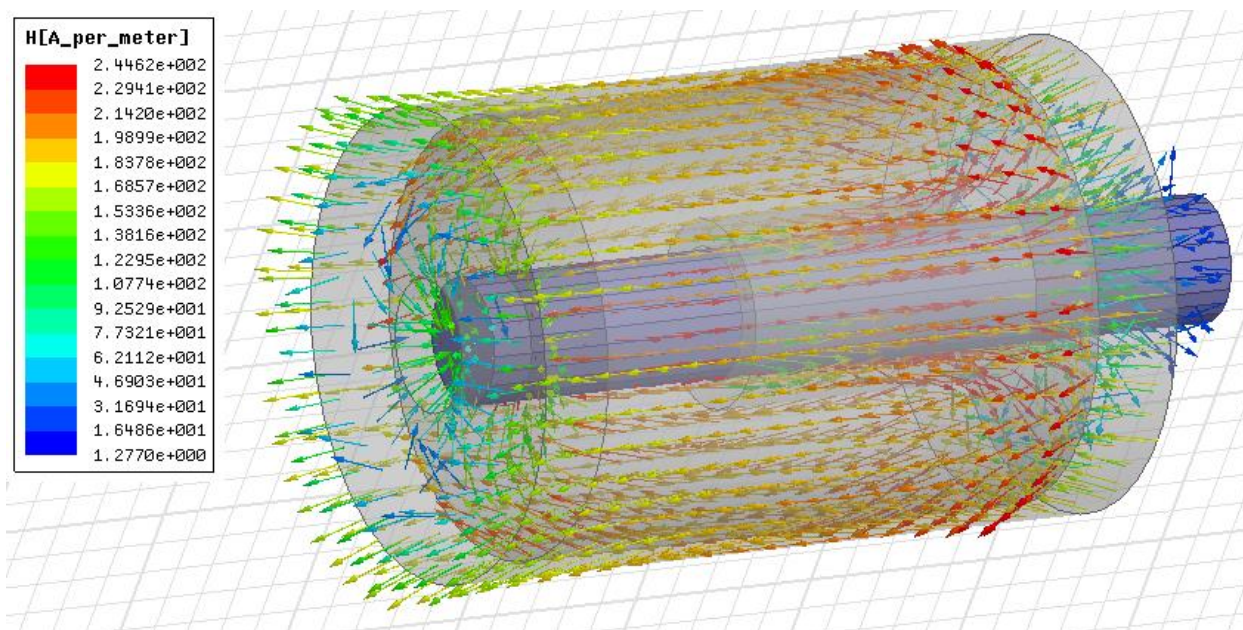
Figure 3.18 – FEM simulated solenoids magnetic field strength vector field

3.3.1 Validation of Reluctance Calculations

Using these parameters, the FEM simulated reluctance values and those predicted by summing together equations (3.44), (3.45) and (3.46) as a function of armature displacement is shown in figure 3.19.
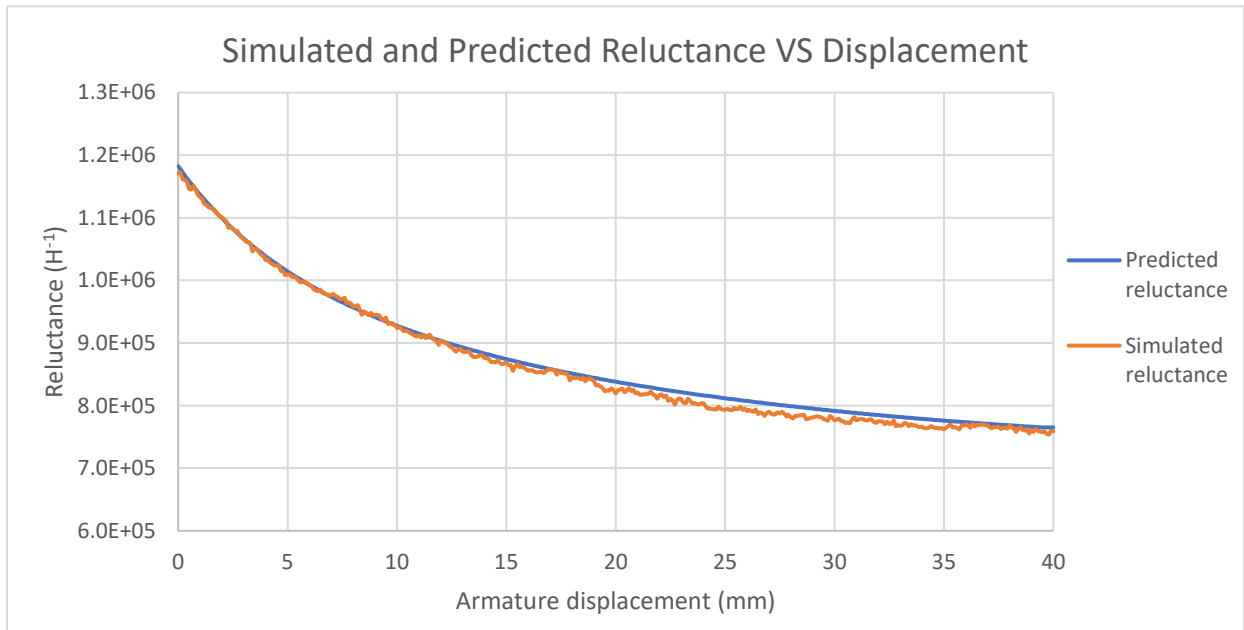
Figure 3.19 – Simulated and predicted reluctance vs displacement of the solenoid

Predicted values using energy based magnetic circuit analysis as shown in figure 3.19 are on average within 0.99% of those predicted using FEM simulation for this solenoid. As the differences between FEM and energy based magnetic circuit analysis are similar to the expected error of FEM for this example, it can be concluded that the derived magnetic circuit reluctances are valid for the analysis of this solenoid.

3.3.2 Validation of Transient waveforms

Both FEM and magnetic circuit analysis can be used to simulate the transient behavior of electromagnetic devices. An advantage of lumped parameter magnetic circuit analysis is its ability to model transient behavior of electromagnetic devices faster than using FEM. A common tradeoff is that FEM is considered to be more accurate than lumped parameter. This difference in accuracy needs to be assessed to determine whether an application is suitable for lumped parameter.

It is possible to assess the compatibility of magnetic circuit analysis with that of FEM by performing a transient analysis of the solenoid modeled in this chapter. For this example, the only losses to be accounted for will be resistive losses in the solenoid windings. The armature will be modeled as travelling at a constant velocity so no energy is converted into kinetic energy.

Therefore, energy supplied to the circuit will either be transferred to the magnetic field or dissipated as thermal energy in the windings due to resistive losses.

A step voltage will be applied to the solenoid windings at time $t = 0$ in the simulation with no initial winding current and an initial armature displacement of $x = 0$. The following transient parameters will be used in addition to those stated for the reluctance calculations.

- Winding voltage $= 12\text{V}$

- Winding resistance $= 20\Omega$

- Armature velocity $= 2\text{ms}^{-1}$

- Number of turns $= 200$

To calculate the winding current and the force experienced by the armature using magnetic circuit analysis it is necessary to solve the conservation of energy equation for the solenoid. Each individual energy transfer that will occur in the solenoid and the equation that describes it are stated below.

$$\text{Power in} = vi \qquad (3.47)$$

$$\text{Mechanical energy in} = F\frac{dx}{dt} \qquad (3.48)$$

$$\text{Winding resistive losses} = i^2R \qquad (3.49)$$

$$\text{Power to magnetic field} = \mathcal{R}\Phi\frac{d\Phi}{dt} \qquad (3.50)$$

$$\text{Power to kinetic energy} = \frac{1}{2}\Phi^2\frac{d\mathcal{R}}{dt} \qquad (3.51)$$

Equating the electrical energy supplied to the solenoid is converted into resistive losses and energy transferred to the magnetic field. Therefore, equating the electrical input power to equal the sum of equations (3.49) and (3.50) allows a differential equation to be derived that describes the magnetic flux as a function of time. As the resulting equation is required to describe magnetic flux, Hopkinson's law will be used to substitute the current term i with the product of flux and reluctance divided by the number of turns n.

$$vi = i^2R + \mathcal{R}\Phi\frac{d\Phi}{dt}$$

$$v\frac{\mathcal{R}\Phi}{n} = \left(\frac{\mathcal{R}\Phi}{n}\right)^2 R + \mathcal{R}\Phi\frac{d\Phi}{dt}$$

$$\frac{d\Phi}{dt} = \frac{v}{n} - \frac{R\mathcal{R}\Phi}{n^2} \tag{3.52}$$

As the armature is moving with a constant velocity, the armature's kinetic energy is constant. Therefore, the energy supplied to the system caused by the force applied to the armature must equal the force term of the magnetic circuit power equation.

$$F\frac{dx}{dt} = \frac{1}{2}\Phi^2\frac{d\mathcal{R}}{dt}$$

$$F = \frac{1}{2}\Phi^2\frac{d\mathcal{R}}{dx} \tag{3.53}$$

Using the parameters stated above, the FEM simulation of the winding current and force applied to the armature was performed. Both equations (3.52) and (3.53) were solved iteratively using discrete time stepping to calculate the armature force and magnetic flux using the reluctance data shown in figure 3.19. Equation (3.52) was used to calculate the magnetic flux which can be converted into current using Hopkinson's law. Based on this data, the winding current predicted using magnetic circuit analysis and the simulated winding current can be compared as shown in figure 3.20.
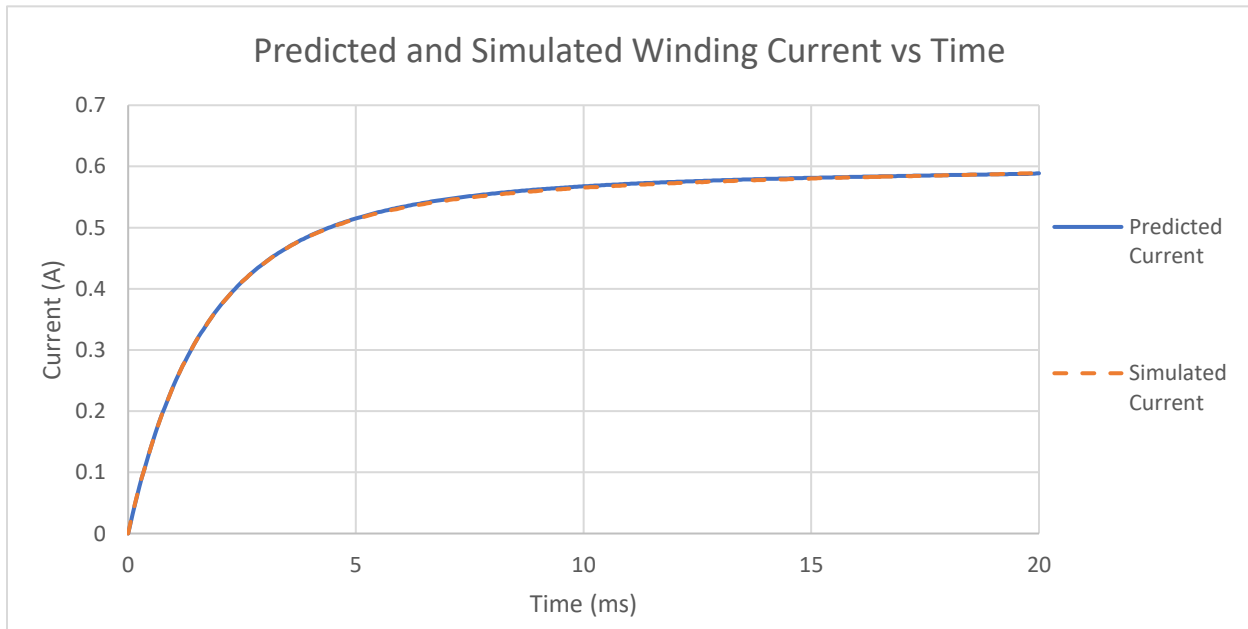
Figure 3.20 – Simulated and predicted winding current vs time

51

The simulated and predicted winding current as shown in figure 3.19 differ by 0.25%. This level of similarity is to be expected as the simulated and predicted reluctances differ on average by less than 1%, and the winding resistance is defined exactly in the simulation.

Force applied to the armature can be calculated using equation (3.53) and compared to the FEM simulation. This comparison is shown in figure 3.21.
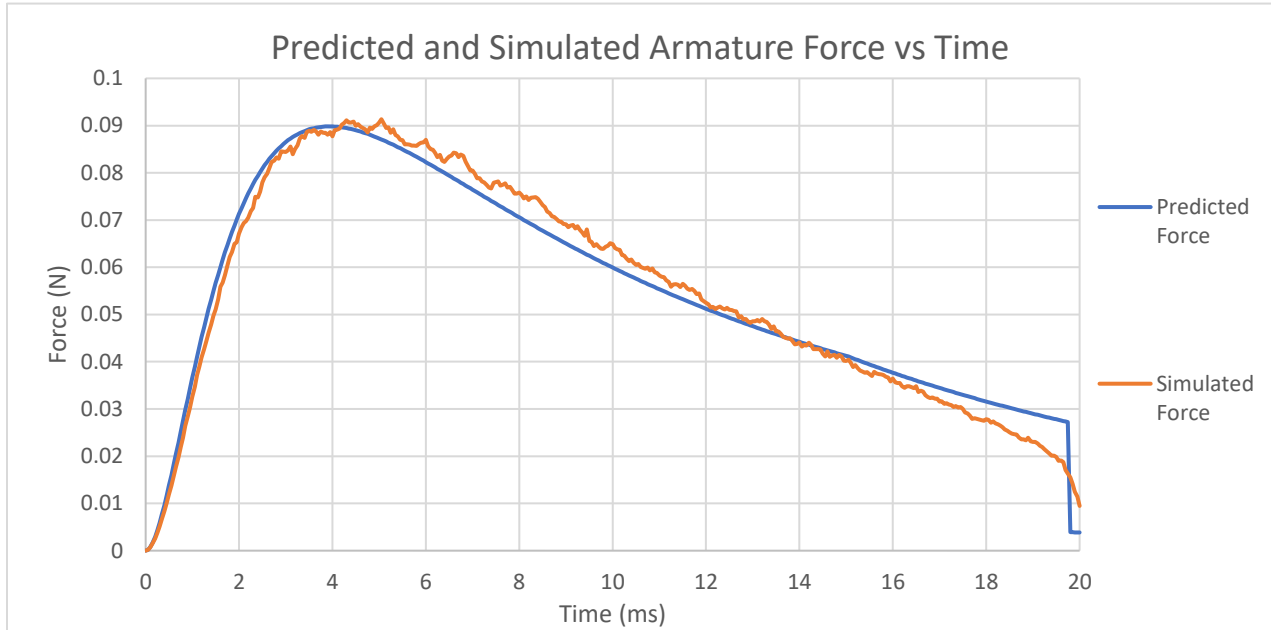
Figure 3.21 – Simulated and predicted armature force vs time

Differences between the predicted and simulated force are more significant than between reluctances and winding current. This is because the force is a function of the reluctance derivative with respect to position. While the simulated and predicted reluctance values are close, any sudden change in reluctance caused by local variations will have a large impact on force due to this derivative term. These local variations are caused by differences in FEM mesh between samples and the complex geometry of the solenoid resulting in small changes in reluctance that are difficult to predict. Increasing the resolution of the FEM simulation and dividing the solenoid into more segments for the magnetic circuit analysis will improve this. Although both options will increase computational complexity.

Another way to compare the simulated and predicted armature force is to integrate the force with respect to distance to calculate energy transfer. This integration reduces the impact of the reluctance derivative term. Performing this integration results in a simulated mechanical energy transfer of 2.214mJ and a predicted energy transfer of 2.216mJ to the armature. These values are within 0.09% which demonstrates that the magnetic circuit model presented is accurate.

An advantage of using closed form equations over numerical methods is they are inherently faster to compute. A mathematical model such as the one used in this chapter can produces results within milliseconds. The FEM solenoid model considered in this chapter consists of approximately 400,000 mesh elements and took 22 hours to compute. The mathematical model also provides insight into the effect of parameter variations on other variables. Therefore, the proposed model provides an advantage to design engineers to rapidly produce results for optimization.

3.4 Conclusion

This thesis chapter has demonstrated how accounting for non-uniform magnetic field distributions and non-aligned B-H field configurations allows magnetic circuit analysis to yield results comparable to those achieved using FEM.

In a solenoid, the magnetic field was always aligned with the central axis. Due to this, the magnetic circuit energy and power transfer equations could be evaluated in scalar form. However, when magnetic fields do not remain aligned to a single axis such as occurs during rotational motion, it is necessary to use vector applications of energy based magnetic circuit theory. Applying magnetic circuit analysis to rotating magnetic fields requires different analytical techniques than what was covered in this chapter. This will be explored further in the next chapter.

Modelling the solenoid in this chapter was sufficient to demonstrate the ability of magnetic circuit equations to model energy transfers caused by changes in magnetic reluctance. However, additional energy transfers can occur due to different sources of MMF being in motion relative to each other. Vector based magnetic circuit analysis can be applied to this situation to calculate energy transfers. This will also be considered in the next chapter by applying magnetic circuit analysis from different frames of reference in an induction motor.

Chapter 4

4 Modelling of Rotating Magnetic Fields Magnetic Circuits with Inhomogeneous Magnetic Field Distribution

In this chapter, vector-based magnetic circuit equations will be used to determine the steady state electrical, magnetic properties of an induction motor. To achieve this, the chapter is divided into the following subsections:

1. **Properties of Rotating Magnetic Flux Vectors**

   This section describes how magnetic flux induced by electric currents in the rotor and stator result in energy being converted into kinetic energy. The relationship between the net magnetic flux and its time derivative are also defined in this section. This establishes the underlying mathematical principals behind the derivation of the proposed induction motor model.

2. **Calculation of rotor and stator flux**

   This section describes and quantifies the induced magnetic flux due to currents in the rotor and stator. A homogenized model of the rotor bar region of the rotor is used to calculate the induced magnetic flux due to the presence of a rotating magnetic field. Magnetic flux vector addition is used to calculate the total stator induced magnetic flux accounting for the motor specific stator winding distribution.

3. **Modelling of the induction motor flux path reluctance**

   The magnetic reluctance of the induction motor is required to transfer electrical quantities such as current and voltage to magnetic circuit quantities such as magnetic flux and its time derivative. Magnetic reluctance is calculated as a function of material properties and the distribution of magnetic flux due to rotor and stator currents.

4. **Evaluation of power transfer in the magnetic circuit**

   In this section, all the derived properties of magnetic flux and reluctance are combined using the vector equations described in the first section. Current induced magnetic flux vectors are used to define one set of equations and voltage dependent magnetic flux derivative vectors define another set of equations. Combining these equations with the vector properties of rotating magnetic fields allows energy transfer equations to be derived.

5. **Finite element model-based validation**

   Results predicted using magnetic circuit analysis will be benchmarked against those derived using FEM based simulations. Confirming that the derived magnetic circuit

analysis predictions are comparable to existing high accuracy models will be used to validate this analytical technique.

By undertaking these steps, magnetic circuit-based model of an induction motor has been developed without the need for numerical methods. The resulting model describes the operation of the induction motor at a fundamental level. In doing so, it is possible to describe how electrical, magnetic and mechanical properties of the induction motor relate to each other.

4.1 Properties of Rotating Magnetic Flux Vectors

To analyze rotating magnetic fields such as those found in induction machines, it is first necessary to define the mathematical relationship between the magnetic flux and its time derivative when observed from a rotating frame of reference. In the previous example involving a solenoid, the magnetic flux was always orientated in the same direction with only its magnitude changing. Therefore, the scalar version of the magnetic circuit power transfer equation was sufficient. The same is not true for rotating magnetic fields. To describe the unique properties of rotating magnetic fields, consider the vector representation of a magnetic field as shown in figure 4.1 shown using <i, j> vector notation.
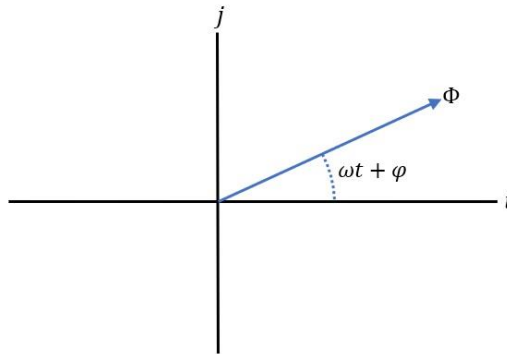
Figure 4.1 – Vector representation of a rotating magnetic field

In figure 4.1, the flux vector can be described mathematically as:

$$\vec{\Phi} = \left|\vec{\Phi}\right| \cos(\omega t + \varphi)\,\hat{\imath} + \left|\vec{\Phi}\right| \sin(\omega t + \varphi)\,\hat{\jmath} \qquad (4.1)$$

Differentiating equation (4.1) with respect to time allows the derivative of the magnetic flux to be expressed in vector form. For the general case, both the magnitude $\left|\vec{\Phi}\right|$ and the phase φ will be considered implicit functions of time and the radian frequency ω will be a constant. Using these definitions, the time derivative of equation (4.1) can be calculated as:

$$\frac{d\vec{\Phi}}{dt} = \left(\frac{d\left|\vec{\Phi}\right|}{dt}\cos(\omega t + \varphi) - \left|\vec{\Phi}\right|\left(\omega + \frac{d\varphi}{dt}\right)\sin(\omega t + \varphi)\right)\hat{\imath} + \left(\frac{d\left|\vec{\Phi}\right|}{dt}\sin(\omega t + \varphi) + \left|\vec{\Phi}\right|\left(\omega + \frac{d\varphi}{dt}\right)\cos(\omega t + \varphi)\right)\hat{\jmath}$$

$$(4.2)$$

Taking the vector cross and dot product of the magnetic flux and its time derivative are given by:

$$\vec{\Phi} \times \frac{d\vec{\Phi}}{dt} = \left|\vec{\Phi}\right|^2 \left(\omega + \frac{d\varphi}{dt}\right) \tag{4.3}$$

$$\vec{\Phi} \cdot \frac{d\vec{\Phi}}{dt} = \left|\vec{\Phi}\right| \frac{d\left|\vec{\Phi}\right|}{dt} \tag{4.4}$$

It is also possible to use the fundamental properties of the dot and cross product to derive an equation that is independent of the angle between the magnetic flux and its time derivative. This involves squaring both sides of equation (4.3) and equation (4.4), then adding them together resulting in equation (4.5).

$$\left|\frac{d\vec{\Phi}}{dt}\right|^2 = \left(\frac{d\left|\vec{\Phi}\right|}{dt}\right)^2 + \left|\vec{\Phi}\right|^2 \left(\omega + \frac{d\varphi}{dt}\right)^2 \tag{4.5}$$

If the magnitude of the magnetic field is constant, the derivative of its magnitude will be zero irrespective of rotational frequency. In this situation, the right-hand side of equation (4.4) will equal zero. As the magnitude of the magnetic flux and its time derivative will be non-zero, the angle between these two vectors must be 90° for their dot product as described by equation (4.4) to equal zero. If the phase variable φ is constant, then solving equation (4.3) for this situation results in a value of the magnitude of the derivative of the magnetic flux to equal the product of the magnetic flux and radian frequency. This relationship between the magnetic flux and its time derivative is shown in figure 4.2 for a constant magnitude magnetic flux.
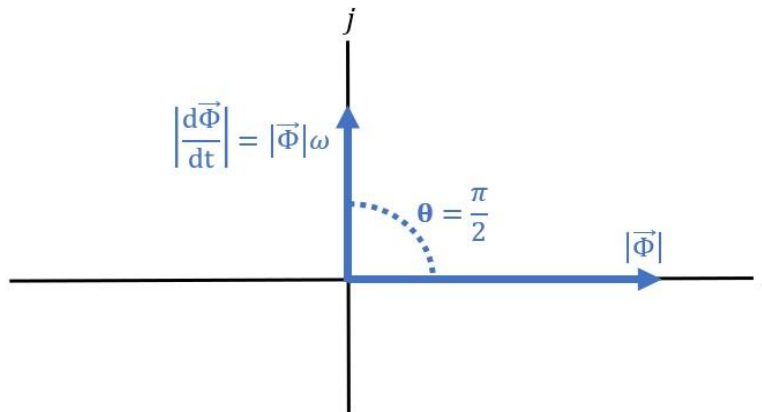
Figure 4.2 – Constant magnitude magnetic flux and its time derivative

Although equations (4.3) to (4.5) can be combined with the vector power transfer equation to describe variable reluctance and magnetic flux magnitude situations, for this analysis, only a constant reluctance and magnetic flux magnitude will be analyzed.

An important observation that can be made from figure 4.2 is that the magnitude of the derivative of the magnetic flux is a function of the rotational frequency. Observing this quantity from a rotating frame of reference will change this value. Computing the magnetic circuit power transfer equation from this rotating frame of reference will result in different value compared to a stationary reference frame. To determine the effect of computing the magnetic circuit power transfer equation from different frames of reference, consider the situation where magnetic flux induced by currents in the rotor of an induction motor are combined with magnetic flux induced by currents in the stator. This is shown in figure 4.3 where $\overrightarrow{\Phi_r}$ is the magnetic flux induced by rotor currents and $\overrightarrow{\Phi_s}$ is magnetic flux induced by stator currents and are separated by an angle of φ.
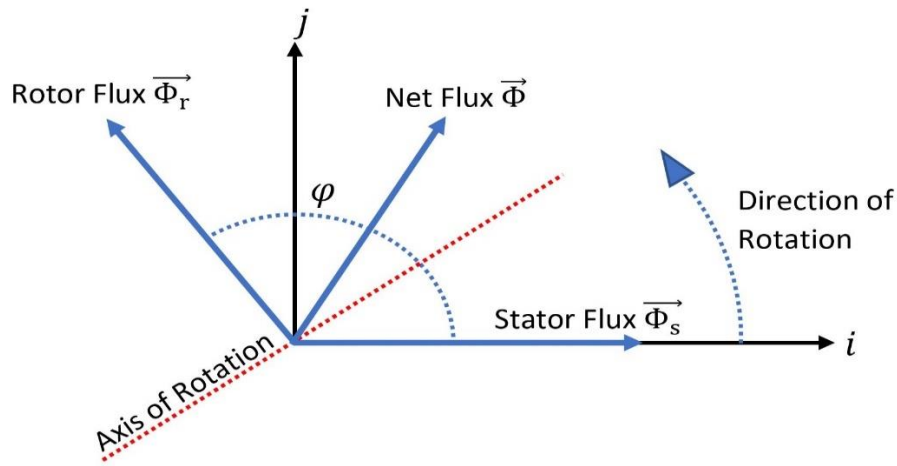
Figure 4.3 – Stator and rotor magnetic flux vectors

Figure 4.3 is a graphical way to represent the magnitude and direction of magnetic flux caused by electric currents in the rotor and stator of the motor. The magnetic flux caused by rotor currents $\overrightarrow{\Phi_r}$ and stator currents $\overrightarrow{\Phi_s}$ can be described in vector form as equation (4.6) and equation (4.7) respectively from the stator's frame of reference where ω_f is the rotational velocity and t is time.

$$\overrightarrow{\Phi_r}\Big|_{stator} = \left|\overrightarrow{\Phi_r}\right| \cos(\omega_f t + \varphi)\,\hat{\imath} + \left|\overrightarrow{\Phi_r}\right| \sin(\omega_f t + \varphi)\,\hat{\jmath} \tag{4.6}$$

$$\overrightarrow{\Phi_s}\Big|_{stator} = \left|\overrightarrow{\Phi_s}\right| \cos(\omega_f t)\,\hat{\imath} + \left|\overrightarrow{\Phi_s}\right| \sin(\omega_f t)\,\hat{\jmath} \tag{4.7}$$

The magnetic flux induced by rotor and stator currents sum together to form the net magnetic flux $\overrightarrow{\Phi}$ as described by equation (4.8).

$$\vec{\Phi}\Big|_{stator} = \left(\left|\vec{\Phi_s}\right|\cos(\omega_f t) + \left|\vec{\Phi_r}\right|\cos(\omega_f t + \varphi)\right)\hat{\imath} + \left(\left|\vec{\Phi_r}\right|\sin(\omega_f t + \varphi) + \left|\vec{\Phi_s}\right|\sin(\omega_f t)\right)\hat{\jmath}$$

<div align="right">(4.8)</div>

The time derivative of the net magnetic flux as observed from the stators frame of reference $\dfrac{\partial\vec{\Phi}}{\partial t}\Big|_{stator}$ can be calculated to as:

$$\frac{\partial\vec{\Phi}}{\partial t}\Big|_{stator} = \omega_f\left(-\left|\vec{\Phi_s}\right|\sin(\omega_f t) - \left|\vec{\Phi_r}\right|\sin(\omega_f t + \varphi)\right)\hat{\imath} + \omega_f\left(\left|\vec{\Phi_s}\right|\cos(\omega_f t) + \left|\vec{\Phi_r}\right|\cos(\omega_f t + \varphi)\right)\hat{\jmath}$$

<div align="right">(4.9)</div>

Equation (4.9) is the derivative of the net magnetic flux as observed from the stator's frame of reference. The magnetic flux power transfer equation can be used to calculate power transferred from the stator, from the stators frame of reference P_{stator_s} using the equation (4.7) value of magnetic flux and the equation (4.9) value of the derivative of the net magnetic flux. As the reluctance is assumed to be constant, only the first product term of the magnetic circuit power transfer equation is required.

$$P_{stator\_s} = \mathcal{R}\vec{\Phi_s}\Big|_{stator} \cdot \frac{\partial\vec{\Phi}}{\partial t}\Big|_{stator}$$

$$P_{stator\_s} = -\omega_f\mathcal{R}\left|\vec{\Phi_s}\right|\left|\vec{\Phi_r}\right|\sin(\varphi) \qquad\qquad (4.10)$$

The same technique can be used to calculate power transferred to the rotor from the stators frame of reference P_{rotor_s}.

$$P_{rotor\_s} = \mathcal{R}\vec{\Phi_r}\Big|_{rotor} \cdot \frac{d\vec{\Phi}}{dt}\Big|_{stator}$$

$$P_{rotor\_s} = \omega_f\mathcal{R}\left|\vec{\Phi_s}\right|\left|\vec{\Phi_r}\right|\sin(\varphi) \qquad\qquad (4.11)$$

Equation (4.11) has the same magnitude as equation (4.10), the only difference is that one value is negative while the other is positive. This is because energy is transferred from the stator to the rotor. Thus, solving the magnetic circuit power transfer equation from the stator's frame of reference for both the rotor and the stator, allows the energy transferred to the rotor to be calculated.

A discrepancy arises when using this analytical technique to calculate the energy transferred to the rotor from the rotor's frame of reference. In the rotor's frame of reference, the magnitude of the net

magnetic flux is the same, however its rotational velocity is different. The rotational velocity of the magnetic flux from the rotor's frame of reference is the slip frequency ω_s which is the difference between the synchronous frequency ω_f and the rotational frequency ω_r. Therefore, evaluating the rotor's magnetic flux vector from the rotor's frame of reference results in equation (4.12).

$$\left.\overrightarrow{\Phi_r}\right|_{rotor} = \left|\overrightarrow{\Phi_r}\right| \cos(\omega_s t + \varphi)\,\hat{\imath} + \left|\overrightarrow{\Phi_r}\right| \sin(\omega_s t + \varphi)\,\hat{\jmath} \qquad (4.12)$$

Evaluating the time derivative of the net magnetic flux from the rotor's frame of reference $\left.\dfrac{\partial \overrightarrow{\Phi}}{\partial t}\right|_{rotor}$ results in:

$$\left.\frac{\partial \overrightarrow{\Phi}}{\partial t}\right|_{rotor} = \omega_s\left(-\left|\overrightarrow{\Phi_s}\right|\sin(\omega_s t) - \left|\overrightarrow{\Phi_r}\right|\sin(\omega_s t + \varphi)\right)\hat{\imath} + \omega_s\left(\left|\overrightarrow{\Phi_s}\right|\cos(\omega_s t) + \left|\overrightarrow{\Phi_r}\right|\cos(\omega_s t + \varphi)\right)\hat{\jmath}$$

$$(4.13)$$

Using these definitions to solve the magnetic circuit power transfer equation from the rotor's rotating frame of reference results in the equation (4.14) value of power transferred to the rotor as represented by the variable P_{rotor_r}.

$$P_{rotor\_r} = \left.\mathcal{R}\overrightarrow{\Phi_r}\right|_{rotor} \cdot \left.\frac{d\overrightarrow{\Phi}}{dt}\right|_{rotor}$$

$$P_{rotor\_r} = \omega_s \mathcal{R}\left|\overrightarrow{\Phi_s}\right|\left|\overrightarrow{\Phi_r}\right| \sin(\varphi) \qquad (4.14)$$

Equation (4.14) states that a stationary observer relative to the rotor's frame of reference, will calculate a different value of energy being transferred to the rotor compared to a stationary observer from the stator's frame of reference. The difference in power transfers evaluated from different frames of references determines the rotor electromechanical power as:

$$P_{rotor\_s} - P_{rotor\_r} = \omega_r \mathcal{R}\left|\overrightarrow{\Phi_s}\right|\left|\overrightarrow{\Phi_r}\right| \sin(\varphi) \qquad (4.15)$$

where ω_r is the difference between the synchronous frequency ω_f and the slip frequency ω_s and is the rotational velocity of the rotor. P_{rotor_r} is therefore the rotor losses incurred at a given slip ω_s. It can be demonstrated that the power transfer referred to in equation (4.15) describes electromechanical power conversion. This can be achieved by calculating the torque required to change the rotor's angular position. To calculate torque, consider the energy stored in the net magnetic field using magnetic circuit analysis from the stator's frame of reference.

$$U = \frac{1}{2}\mathcal{R}\left|\overrightarrow{\Phi}\right|_{stator}^2$$

59

$$U = \frac{1}{2}\mathcal{R}\left[\left(\left|\overrightarrow{\Phi_s}\right|\cos(\omega_f t) + \left|\overrightarrow{\Phi_r}\right|\cos(\omega_f t + \varphi)\right)^2 + \left(\left|\overrightarrow{\Phi_r}\right|\sin(\omega_f t + \varphi) + \left|\overrightarrow{\Phi_s}\right|\sin(\omega_f t)\right)^2\right]$$

<div align="right">(4.16)</div>

Rotor torque T_r can be calculated using the derivative of energy with respect to rotor position.

$$T_r = \frac{dU}{d\varphi}$$

$$T_r = \mathcal{R}\left|\overrightarrow{\Phi_r}\right|\left|\overrightarrow{\Phi_s}\right|\sin(\varphi) \qquad (4.17)$$

Power can be calculated by multiplying torque by the rotational velocity, which in this case is ω_r. Therefore, the power transfer caused by rotor torque P_T in this example can be calculated to be equation (4.18).

$$P_T = \omega_r\mathcal{R}\left|\overrightarrow{\Phi_s}\right|\left|\overrightarrow{\Phi_r}\right|\sin(\varphi) \qquad (4.18)$$

The equation (4.18) is equivalent to equation (4.15) and is therefore referring to electromechanical power conversion.

This theory can be used to derive a magnetic circuit model of an induction motor which can be verified using FEM based simulations. To use magnetic circuit theory to model an induction motor it is necessary to calculate the relationship between stator currents and the magnetic flux they induce in the rotor. Although there are numerous configurations of stator windings that can be implemented, it is possible to derive a generic equation that can be used for all possible configurations. Assuming the current in each AC phase has the same amplitude, and the motor has been sinusoidal wound distributed winding configuration, the magnetic flux induced by stator currents will be proportional to the amplitude of the stator phase current. If the stator phase current amplitude is i_s then the stator currents induced magnetic flux is therefore given by:

$$\left|\overrightarrow{\Phi_s}\right| = K_i i_s \qquad (4.19)$$

where K_i is a motor specific constant.

The voltage induced in the stator windings due to the rotating magnetic field will be proportional to the derivative of the net magnetic flux as per Faraday's law of induction. Therefore, a generic representation of the winding voltage is shown in equation (4.20) where V_s is the stator winding voltage and K_v is a motor specific constant:

$$\left|\frac{d\overrightarrow{\Phi}}{dt}\right| = K_v V_s \qquad (4.20)$$

4.2 Calculation of rotor and stator flux

4.2.1 Calculation of rotor flux

The rotor's magnetic flux is caused by induced currents flowing through the rotor bars. To calculate these currents, it is necessary to know the induced voltages due to a rotating magnetic field and the resistance of the current path. For this analysis, a standard squirrel cage induction motor rotor which consists of a magnetically permeable cylindrical volume with electrically conductive rotor bars running parallel to the axis of rotation has been considered. Currents will be induced in these rotor bars caused by the derivative of the net magnetic flux. These currents will induce magnetic flux that needs to be quantified to calculate the operational characteristics of the motor. To calculate the magnetic flux induced in the rotor caused by the rotating magnetic field, consider the rotor as shown in Figure 4.4.
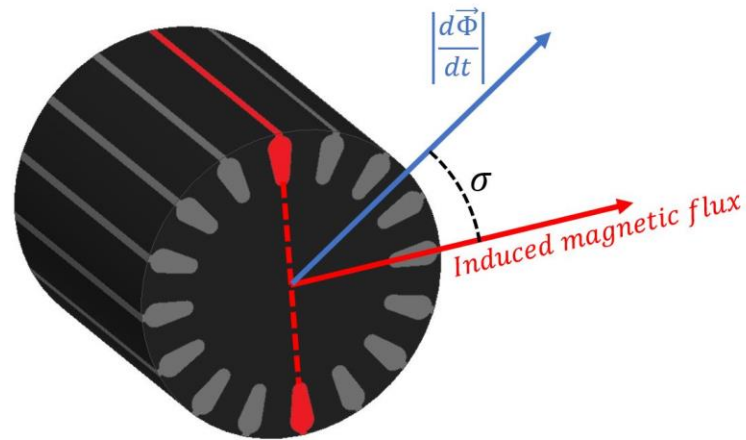
Figure 4.4 – Induction motor rotor with superimposed magnetic flux vector

In figure 4.4 the dark grey area is the magnetically permeable material and the rotor bars are light grey. Electric current flowing through the red rotor bars in figure 4.4 will induce magnetic flux in the direction of the induced magnetic flux vector shown. Faraday's law of induction can be used to determine the voltage around the current path enclosed by the red rotor bars from figure 4.4 by calculating the dot product of the magnetic flux derivative vector and the surface normal vector. Performing this operation results in the equation (4.21) value of voltage around the current loop incorporating the rotor bars shown in red.

$$\text{Induced loop voltage} = \left| \frac{d\vec{\Phi}}{dt} \right| \cos(\sigma) \qquad (4.21)$$

The current flowing through the two rotor bars shown in red can be calculated by dividing the loop voltage by the loop resistance. Defining the loop resistance to be R_{loop} the current can be calculated using ohms law to be equation (4.22).

$$\text{Induced loop current} = \left|\frac{d\vec{\Phi}}{dt}\right|\frac{\cos(\sigma)}{R_{loop}}$$
(4.22)

Dividing equation (4.22) by the magnetic reluctance allows the amount of magnetic flux caused by currents in the red rotor bars to be calculated. However, this process needs to be repeated for each pair of rotor bars in an inhomogeneous magnetic field distribution. This process requires the number of rotor bars to be known and the total induced magnetic flux caused by rotor currents to be then determined by the vector sum of all flux components.

An alternative technique to calculate magnetic flux independent of the number of rotor bars is to express the rotor resistance in terms of ohm radians resulting in a homogenized representation of the cage rotor.

4.2.2 Homogenized representation of the cage-rotor

A homogenized representation of the cage rotor is developed in this section and uses the concept 'Ohm radians' in a way to define the relationship between voltage and current when working in cylindrical coordinates. To understand this concept and why it is useful, consider the figure 4.5 diagram of two opposite rotor bars from an induction motor connected by two end caps.
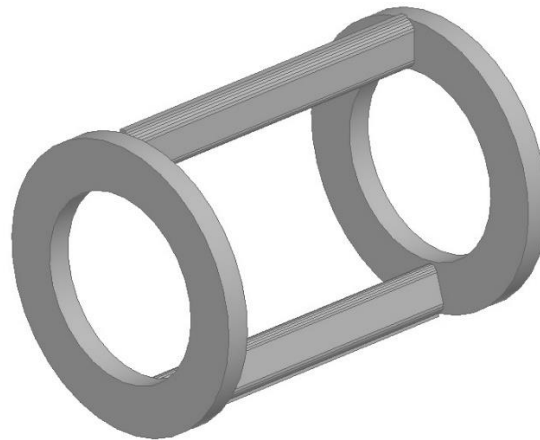
Figure 4.5 – Two induction motor rotor bars with end caps

The induced voltage around the conductive loop can be calculated using Faraday's law of induction. Ohms law can then be used to calculate the induced current based on the loop resistance. Equation (4.22) allows the loop current to be calculated based on induced voltage due to the changing magnetic flux flowing through the loop. However, to solve equation (4.22) it is necessary

to know the number of rotor bars in the rotor. As this number is rotor specific, it would be useful to define a parameter that allows the rotor current and magnetic flux to be calculated independent of the number of rotor bars.

This parameter can be calculated by multiplying the loop resistance of two opposite rotor bars R_{loop} as shown in figure 4.5 by the angular displacement between each rotor bar. As there are 18 rotor bars in this example, their angular displacement will be 2π divided by 18. Therefore, the rotor resistance in ohm radians will be equation (4.23).

$$Rotor\ resistance = \frac{\pi}{9} R_{loop} \qquad (4.23)$$

Now consider the case where the resistance of two pairs of opposite rotor bars is measured. These rotor bar pairs are shown in figure 4.6 where one pair is colored red while the other pair is brown.
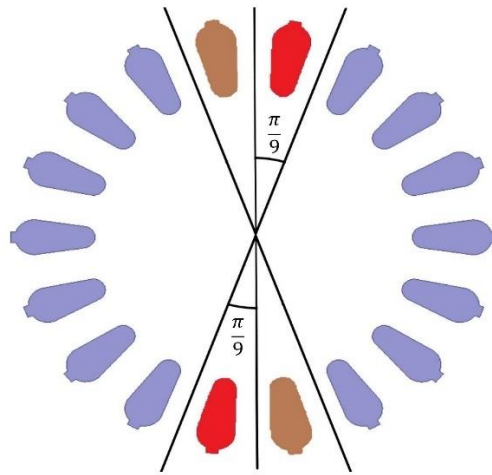
Figure 4.6 – Rotor bar cross section

The parallel connected resistance of two pairs of rotor bars will be half that of a single rotor bar pair defined previously to be R_{loop}. However, the angular displacement of the two pairs of rotor bars will be twice that of a single rotor bar pair. Therefore, the rotor resistance in ohm can be calculated as:

$$Rotor\ resistance = \left(\frac{1}{2} R_{loop}\right) \times \left(\frac{2\pi}{9}\right) = \frac{\pi}{9} R_{loop} \qquad (4.24)$$

Calculating the rotor resistance in ohm radians using two pairs of rotor bars resulted in the same value as using only one pair of rotor bars. This is because measuring the rotor resistance in ohm radians is only a function of the total rotor bar cross sectional area and length. Changing the number of rotor bars while keeping the total rotor bar length and cross-sectional area constant will result

in the same ohm radian resistance value. Therefore, multiplying the total resistance of two rotor bar pairs by their angular displacement results in the same value.

By defining the rotor resistance in terms of ohm radians, it is possible to define equations to calculate induced currents and magnetic flux using terms independent of the number of rotor bars. This allows calculus to be used to derive an expression for the induced magnetic flux. To demonstrate this, consider a segment of the rotor enclosed by a small angular displacement $d\sigma$ at an angle of σ to the time derivative of the magnetic flux vector. Assuming the rotor resistance in ohm radians is R_r, the resistance of this current loop can be calculated by dividing the rotor resistance in ohm radians by the angular displacement $d\sigma$.
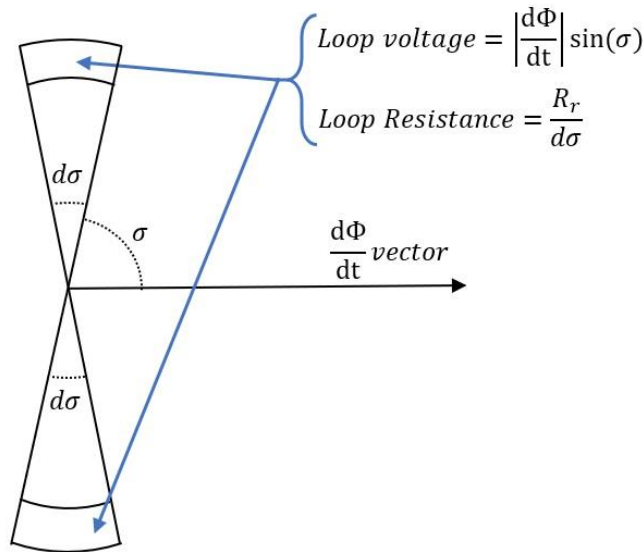
Figure 4.7 – Rotor segment enclosed by a small angular segment $d\sigma$

The current enclosed by this small angular displacement can be calculated using ohms law by dividing the loop voltage by the loop resistance.

$$\text{Induced loop current} = \left|\frac{d\vec{\Phi}}{dt}\right|\frac{\sin(\sigma)}{R_r}\,d\sigma \qquad (4.25)$$

The magnetic flux caused by this current can be calculated using Hopkinson's law by dividing the current by the magnetic path reluctance $\mathcal{R}$.

$$\text{Induced loop magnetic flux} = \left|\frac{d\vec{\Phi}}{dt}\right|\frac{\sin(\sigma)}{R_r\mathcal{R}}\,d\sigma \qquad (4.26)$$

Each angular segment of the rotor will produce magnetic flux that when combined, will constitute the total rotor's induced magnetic flux.

4.2.3 Magnetic Flux Vector Addition

To calculate the total rotor induced magnetic flux consider the magnetic flux caused by a single rotor bar as shown in figure 4.8.
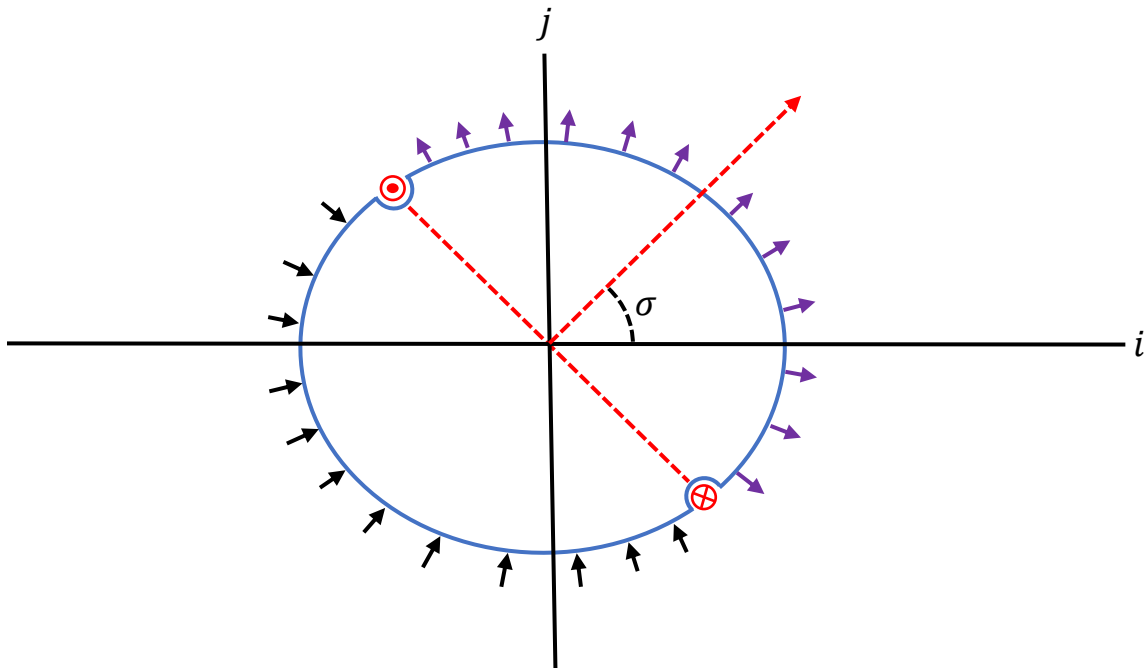
Figure 4.8 – Rotor with superimposed magnetic flux lines

As shown in figure 4.8, the magnetic flux induced by currents in the rotor will be spread approximately evenly across the air gap between the rotor and stator. Magnetic flux directions out of the rotor is shown with purple arrows and magnetic flux returning to the rotor is shown with black arrows. The magnetic flux will form this distribution as it naturally tracks the path of least energy due to the presence of the magnetic flux. However, the rotor is comprised of multiple rotor bars and the magnetic flux induced by some currents will be canceled out by other currents. To illustrate this, consider the magnetic flux induced in the same rotor from figure 4.8 with two rotor bars.
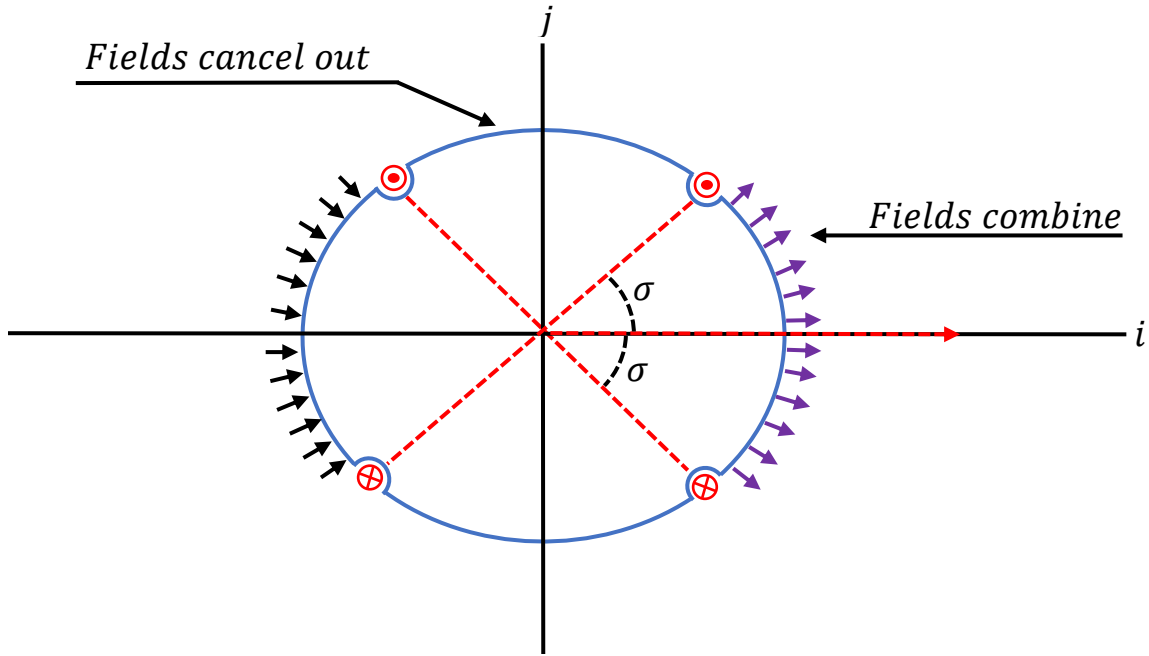
Figure 4.9 – Rotor with superimposed magnetic flux lines

Figure 4.9 depicts rotor bars with equal current and the resulting induced magnetic flux. The resulting magnetic flux will either have twice the magnetic flux density as a single rotor bar or cancel out depending on the location. By limiting the range of the angle variable σ to between 0 and $\frac{\pi}{2}$, the total magnetic flux caused by a differential current pair will be given by:

$$\text{Differential pair magnetic flux} = \frac{4i_{segment}\sigma}{\pi\mathcal{R}} \qquad (4.27)$$

where $i_{segment}$ is the current flowing through each rotor bar shown in figure 4.9.

The current $i_{segment}$ as a function of the angle σ was previously calculated to be equation (4.25). Substituting the equation (4.25) value of current into equation (4.27) and integrating for all induced currents in the rotor allows the total magnetic flux induced by rotor currents Φ_r to be calculated as:

$$\Phi_r = \int_0^{\frac{\pi}{2}} \left|\frac{d\vec{\Phi}}{dt}\right| \frac{4\sigma \sin(\sigma)}{\pi\mathcal{R}R_r} \, d\sigma$$

$$\Phi_r = \frac{4}{\pi\mathcal{R}R_r} \left|\frac{d\vec{\Phi}}{dt}\right| \qquad (4.28)$$

66

As equation (4.27) was calculated using the rotor resistance in ohm radians, it is independent of the number of rotor bars and is therefore valid for all rotors. However, the magnetic flux induced by stator currents is dependent on the winding configuration. The following section studies an example stator with a 2-pole winding configuration.

4.2.4 Calculation Stator Magnetic Flux

For this analysis, the magnetic flux induced by a 2 pole, 3 phase induction motor with 24 rotor slots is considered as a case study. The stator winding configuration is shown in figure 4.10 with phases labeled A, B and C.
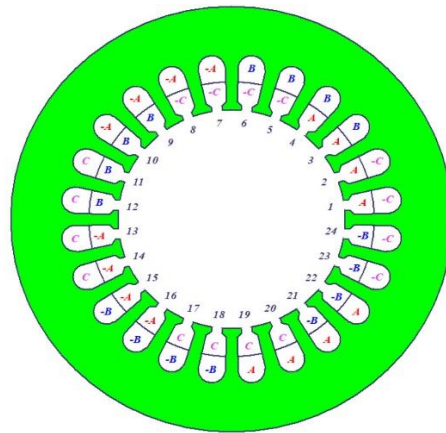
Figure 4.10 – Stator winding configuration

Assuming all three stator phases have the same current amplitude of i_s and have n turns per phase winding per stator slot, the combined current amplitude flowing through each stator slot will be equation (4.29).

$$\text{Stator slot combined current amplitude} = \sqrt{3}i_s n \qquad (4.29)$$

The combined current amplitude flowing into slot 1 and 2 are equivalent as they contain the same number of turns of the same phase windings. Each sequential group of two stator slots will have the same combined amplitude. The phase difference of the combined current amplitude for each group of two stator slots will differ by a phase angle of 30°. Based on this winding configuration, the magnetic flux caused by a differential combined current pair for one quadrant (slots 7-12 and slots 19-24) is shown in figure 3.10 when the net stator magnetic flux is aligned with the i axis.
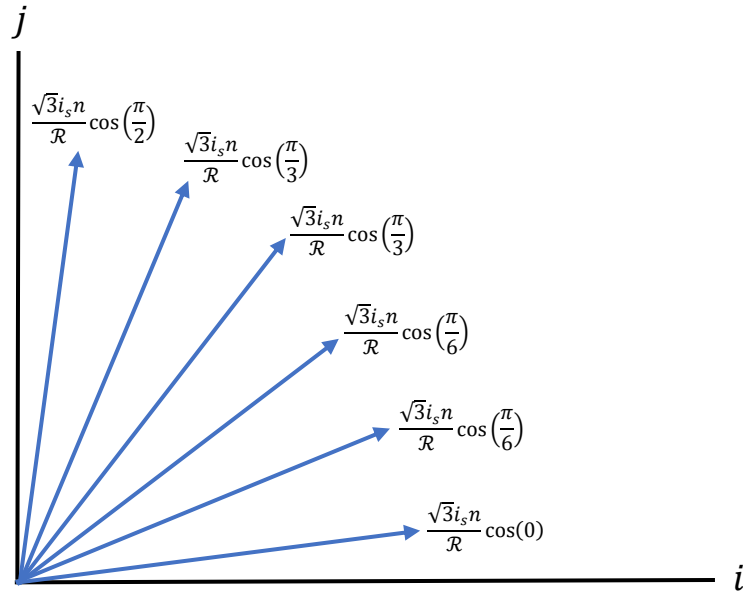
Figure 4.11 – One quadrant of induced magnetic flux vectors

Each quadrant will have the same magnitude of magnetic flux vectors as shown in figure 4.11 when the net stator induced magnetic flux is aligned with the i axis. The vector sum of all the flux components result in the total magnetic flux Φ_s:

$$\Phi_s = \frac{\sqrt{3}i_s n}{\mathcal{R}} \times \left(\frac{11}{6}\cos(0) + \frac{9}{6}\cos\left(\frac{\pi}{6}\right) + \frac{7}{6}\cos\left(\frac{\pi}{6}\right) + \frac{5}{6}\cos\left(\frac{\pi}{6}\right) + \frac{3}{6}\cos\left(\frac{\pi}{3}\right) + \frac{1}{6}\cos\left(\frac{\pi}{2}\right) \right)$$

$$\Phi_s \approx 8.3301 \frac{i_s n}{\mathcal{R}} \tag{4.30}$$

To calculate the value of the rotor and stator current induced magnetic flux it is necessary to calculate the reluctance of the induction motor. This is undertaken in the following section.

4.3 Modelling of the Induction Motor Flux Path Reluctance

Modelling of the induction motor flux path reluctance can be achieved using the same technique as for the solenoid presented in the previous chapter. This involves calculating the amount of magnetic field energy caused by the presence of magnetic flux. To achieve this, the induction motor has been divided into 5 separate cylindrical segments as shown in figure 4.12.
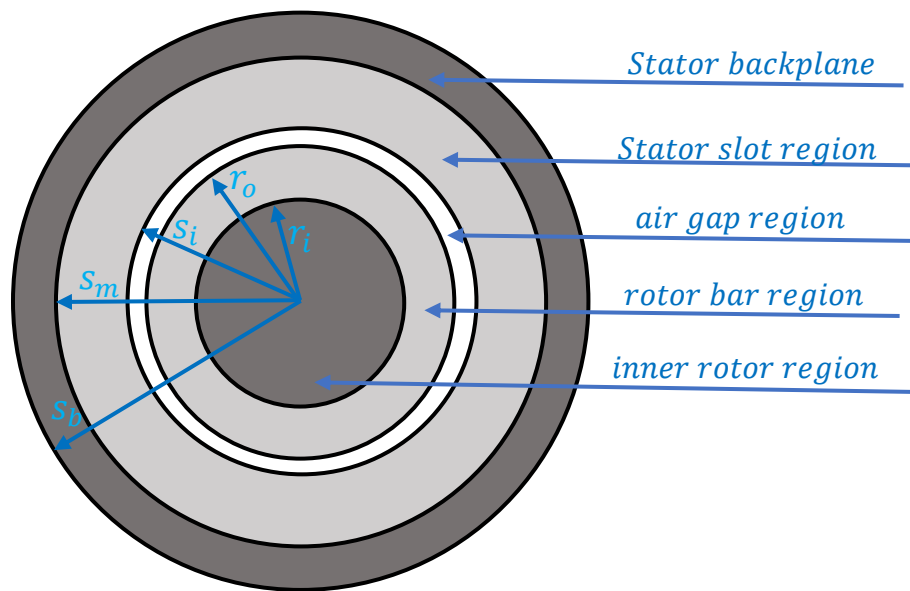
Figure 4.12 – Induction motor segments

Each segment of the induction motor will have a different magnetic field distribution and therefore a different amount of magnetic field energy.

4.3.1 Energy stored in the inner rotor region

The first segment of the induction motor to be analyzed is the inner rotor region. This is the region of the rotor where there are no rotor bars. Although in a practical rotor there will be a shaft made of a low permeability material in this region, for this analysis the region will be assumed to be homogenously filled with a high permeability material. This assumption has a negligible impact on overall accuracy as this region does not contribute much to the total reluctance.

In this region, the magnetic flux will be assumed to be uniformly distributed with all magnetic flux vectors pointing in a single direction. This region is cylindrical in shape with a radius of r_i and a length of l as shown in figure 4.13 with blue superimposed magnetic field lines.
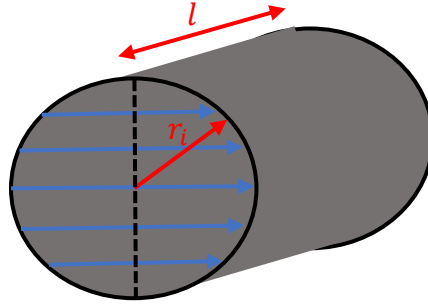
Figure 4.13 – Induction motor inner rotor region

All the net magnetic flux Φ will pass through the black dotted line shown in figure 4.13. Therefore, the magnetic flux density of this region can be calculated by dividing the net magnetic flux by the cross-sectional area of the inner rotor if cut along the black dotted line in figure 4.13.

$$B_{inner\ rotor} = \frac{\Phi}{2r_i l} \qquad (4.31)$$

Multiplying the energy density caused by the equation (4.31) magnetic flux density by the cylindrical volume of the inner rotor allows the inner rotor energy to be calculated.

$$\text{Inner rotor energy} = \frac{\pi \Phi^2}{8\mu_0 \mu_r l} \qquad (4.32)$$

4.3.2 Energy stored in the outer rotor region

The outer rotor area comprises of magnetically permeably material referred to as the rotor tooth area and low electrical resistivity rotor bars referred to as rotor slot area. Magnetic flux will pass through both the rotor slot and tooth area, although most magnetic flux will pass through the tooth area. The ratio of the area of the rotor slot and tooth area of a cross section of the rotor in this region needs to be defined as it will be rotor specific. Therefore, a new variable will be defined C_r which is the cross-sectional area of the rotor slot area in the outer rotor divided by the total cross-sectional area of the outer rotor.

$$C_r = \frac{\text{rotor slot area}}{\text{outer rotor total area}} \qquad (4.33)$$

Using the variable C_r a small angular section $d\sigma$ of the outer rotor at a distance of r from the central axis with a length of dl and an angle of σ from the net magnetic flux direction can be described as shown in figure 4.14.

70

Figure 4.14 – Induction motor outer rotor region segment

In figure 4.14, the area with the rotor slot is colored blue and the rotor tooth area is colored grey. The boundary between the inner rotor and the rotor bar region occurs at a distance of r_i as shown in figure 4.12. At this boundary the magnetic flux enters at an angle of $\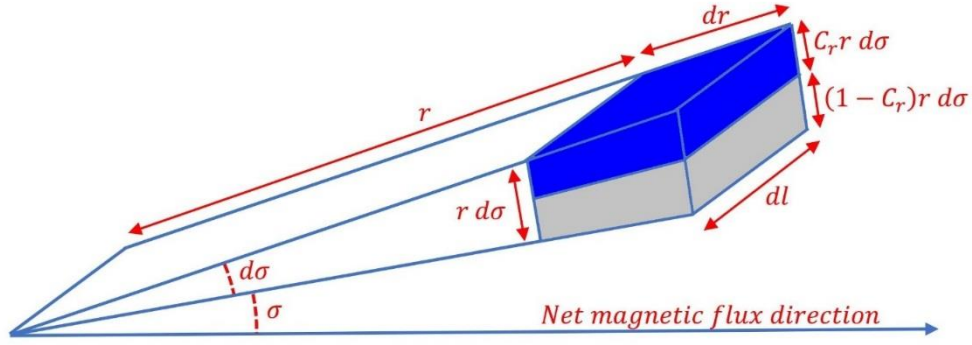cos(\sigma)$. Therefore, the magnetic flux flowing through the rotor bar region as shown in figure 4.12 bounded by the small angle $d\sigma$ can be calculated using equation (4.31) to be equation (4.34).

$$\text{Flux in rotor bar segment} = \frac{\Phi}{2l}\cos(\sigma)\ d\sigma\ dl \tag{4.34}$$

Some of the magnetic flux entering the rotor bar region will travel through the rotor slot area and some will travel through the rotor tooth area. The ratio of the magnetic flux passing through the rotor tooth area compared to the rotor slot area can be determined by calculating the magnetic reluctance of these respective regions. These two reluctance values will be connected in parallel to form the total reluctance of the small angular segment shown in figure 4.14. Using this reluctance model of the rotor bar region, the total magnetic flux passing through the rotor slot and tooth region as shown in figure 4.14 can be calculated to be equation (4.35) and (4.36).

$$\text{Magnetic flux entering rotor slot area} = \left(\frac{\Phi}{2l}\ d\sigma\ dl\right)\frac{C_r\cos(\sigma)}{C_r + \mu_r(1 - C_r)} \tag{4.35}$$

$$\text{Magnetic flux entering rotor tooth area} = \left(\frac{\Phi}{2l}\ d\sigma\ dl\right)\frac{\mu_r(1 - C_r)\cos(\sigma)}{C_r + \mu_r(1 - C_r)} \tag{4.36}$$

As the magnetic flux travels radially outwards in the rotor bar region, the amount of magnetic flux for a given angular displacement remains the same. However, the cross-sectional area of the angular segment increases as distance from the central axis increases, thereby decreasing the magnetic flux density. Therefore, the magnetic flux density within the small rotor bar segment as shown in figure 4.14 can be calculated to be equation (4.37) for the rotor tooth area and 4.38 for the rotor slot area.

$$\text{Rotor slot magnetic flux density} = \frac{\Phi \cos(\sigma)}{2l\, r\left(C_r + \mu_r(1 - C_r)\right)} \tag{4.37}$$

$$\text{Rotor tooth magnetic flux density} = \frac{\Phi \mu_r \cos(\sigma)}{2l\, r\left(C_r + \mu_r(1 - C_r)\right)} \tag{4.38}$$

The magnetic flux density from equation (4.36) can be used to calculate the energy within the electrical conductor of the rotor segment shown in figure 4.14. Integrating this energy over the cylindrical volume of the rotor bar region allows the energy within the electrical conduction area of the rotor bar region to be calculated.

$$\text{Rotor slot energy} = \int_0^l \int_0^{2\pi} \int_{r_i}^{r_o} \frac{\Phi^2 \cos^2(\sigma)\, C_r}{8\mu_0 l^2\, r\left(C_r + \mu_r(1 - C_r)\right)^2}\, dr\, d\sigma\, dl$$

$$\text{Rotor slot energy} = \frac{\pi \Phi^2 C_r}{8\mu_0 l \left(C_r + \mu_r(1 - C_r)\right)^2} \log_e\left(\frac{r_o}{r_i}\right) \tag{4.39}$$

The same process can be utilized to calculate the magnetic field energy within the rotor tooth area of the rotor bar region. Integrating the magnetic field energy within the rotor tooth segment as shown in figure 3.12 over the entire rotor bar region allows the total magnetic conductor energy to be calculated.

$$\text{Magnetic conductor energy} = \int_0^l \int_0^{2\pi} \int_{r_i}^{r_o} \frac{\Phi^2 \cos^2(\sigma)\, \mu_r(1 - C_r)}{8\mu_0 l^2\, r\left(C_r + \mu_r(1 - C_r)\right)^2}\, dr\, d\sigma\, dl$$

$$\text{Magnetic conductor energy} = \frac{\pi \Phi^2 \mu_r(1 - C_r)}{8\mu_0 l \left(C_r + \mu_r(1 - C_r)\right)^2} \log_e\left(\frac{r_o}{r_i}\right) \tag{4.40}$$

Summing together the rotor slot and tooth energy in the rotor bar region allows the total magnetic field energy for the rotor bar region to be calculated as:

$$\text{Rotor bar region energy} = \frac{\pi \Phi^2}{8\mu_0 l \left(C_r + \mu_r(1 - C_r)\right)} \log_e\left(\frac{r_o}{r_i}\right) \tag{4.41}$$

4.3.3 Energy stored in the air gap region

Energy in the air gap region between the stator and rotor can be calculated using a similar technique to that used for the rotor bar region. To calculate the energy in the air gap region, consider the small segment of this region bounded by the small angular displacement of $d\sigma$.
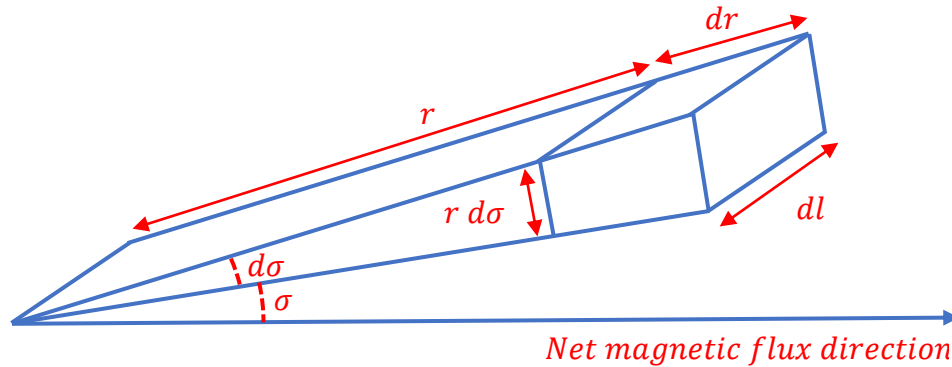
Figure 4.15 – Induction motor air gap region segment

As the magnetic flux is travelling radially outward in this region, the magnetic flux bounded by the angular displacement $d\sigma$ in the air gap region will be the same as that bounded by the same angular displacement in the rotor bar region. Therefore, the magnetic flux entering the segment in the air gap region as shown in figure 4.15 will be the same as that defined by equation (4.34). This allows the magnetic flux density of the segment shown in figure 4.15 at a distance of r from the central axis to be calculated to be equation (4.42).

$$\text{Air gap segment magnetic flux density} = \frac{\Phi}{2lr}\cos(\sigma) \qquad (4.42)$$

Integrating the magnetic field energy over the air gap region as shown in figure 4.15 allows its total energy to be calculated.

$$\text{Air gap region energy} = \int_{r_o}^{s_i}\int_0^l\int_0^{2\pi}\frac{\Phi^2\cos(\sigma)}{8\mu_0 l^2 r}\,d\sigma\,dl\,dr$$

$$\text{Air gap region energy} = \frac{\pi\Phi^2}{8\mu_0 l}\log_e\left(\frac{s_i}{r_o}\right) \qquad (4.43)$$

73

4.3.4 Energy stored in the stator slot region

Energy within the stator slot region can be calculated using the same technique used to calculate magnetic field energy within the rotor bar region. In the stator slot region, the stator slot area is where the stator windings are, and the stator tooth area is where the material with high magnetic permeability is. As the ratio of these areas will differ from that of the rotor, a new variable needs to be defined. This variable is C_s and is defined to be the cross-sectional area of all stator slots where the stator windings are located divided by the total cross-sectional area of the stator slot region as defined in figure 4.12.

$$C_s = \frac{\text{total stator slot area}}{\text{stator slot region total area}} \qquad (4.44)$$

Using the variable C_s, a small segment of the stator bounded by the angular displacement $d\sigma$ is shown in figure 4.16.
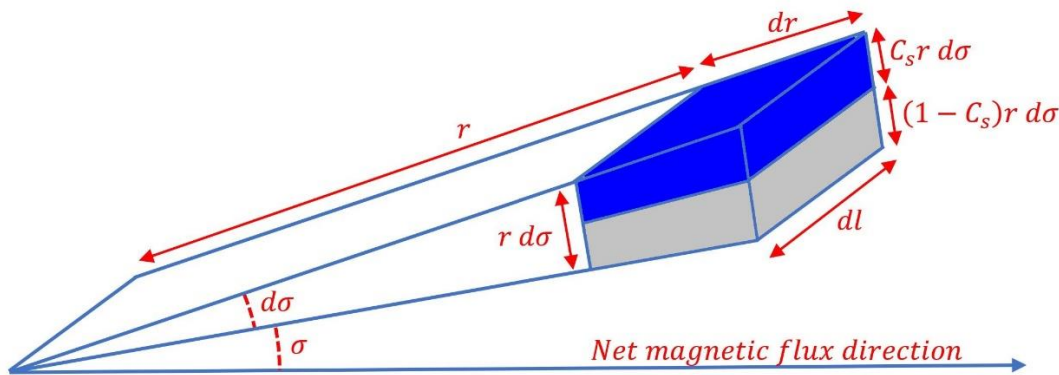
Figure 4.16 – Induction motor stator slot region segment

In figure 4.16, the blue area represents where the stator slot area is, while the grey area represents the area where the stator tooth is. If all the magnetic flux from the rotor bar region travels into the stator slot region, the energy within this region can be calculated with the same method used for the rotor bar region. This is because the magnetic flux from the inner rotor flows radially outwards in the rotor bar, air gap and stator slot region. Therefore, the magnetic flux bounded by any given angular displacement will be the same for all these regions.

Using the same technique used to calculate the rotor bar region energy, the stator slot region energy as defined in figure 4.12 can be calculated to be equation (4.45).

$$\text{Stator slot region energy} = \frac{\pi\Phi^2}{8\mu_0 l\big(C_s + \mu_r(1 - C_s)\big)}\log_e\left(\frac{s_m}{s_i}\right) \qquad (4.45)$$

4.3.5 Energy stored in the stator backplane region

Magnetic flux travelling out of the stator slot region will travel through the stator backplane region before returning to the rotor via the stator slot region. In this region, the magnetic flux will be a function of angular displacement from the direction of the net magnetic flux. For this analysis, it will be assumed that the magnetic flux density in this region is not a function of radial distance from the central axis or displacement parallel to the central axis.

Magnetic flux will enter the stator backplane at a distance of s_m from the central axis as shown by the grey area in figure 4.17 for a small angular displacement of $d\sigma$.
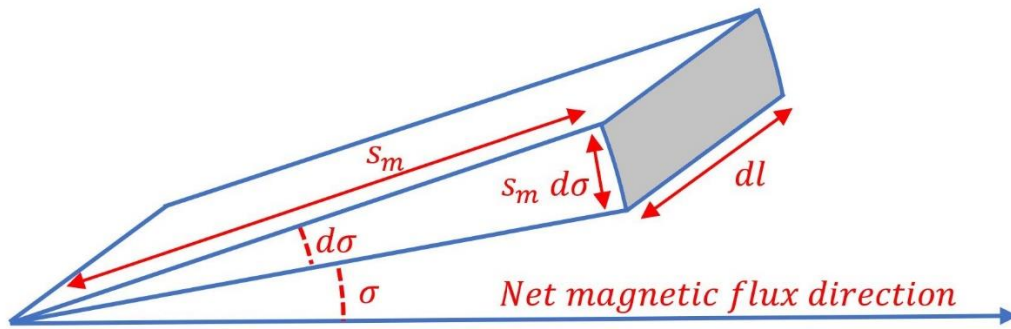
Figure 4.17 – Induction motor stator backplane segment

The magnetic flux entering the stator backplane through this angular displacement of $d\sigma$ will be the same the magnetic flux leaving the inner rotor for the same angular displacement. This was previously calculated to be equation (4.34). Magnetic flux entering the stator backplane through this small angular displacement will add to the magnetic flux that entered the backplane at different angles. Therefore, to calculate the magnetic flux in the stator backplane as a function of the angle σ, it is necessary to integrate the contribution of all angular segments to the total magnetic flux.

$$\text{Stator backplane magnetic flux} = \int_\sigma^0 \frac{\Phi \, dl}{2l} \cos(\sigma) \, d\sigma$$

$$\text{Stator backplane magnetic flux} = \frac{\Phi}{2l} \sin(\sigma) \, dl \qquad (4.46)$$

The magnetic flux density in the stator backplane can be calculate by dividing the magnetic flux by the cross-sectional area of the backplane. This cross-sectional area is shown as the grey area in figure 4.18.
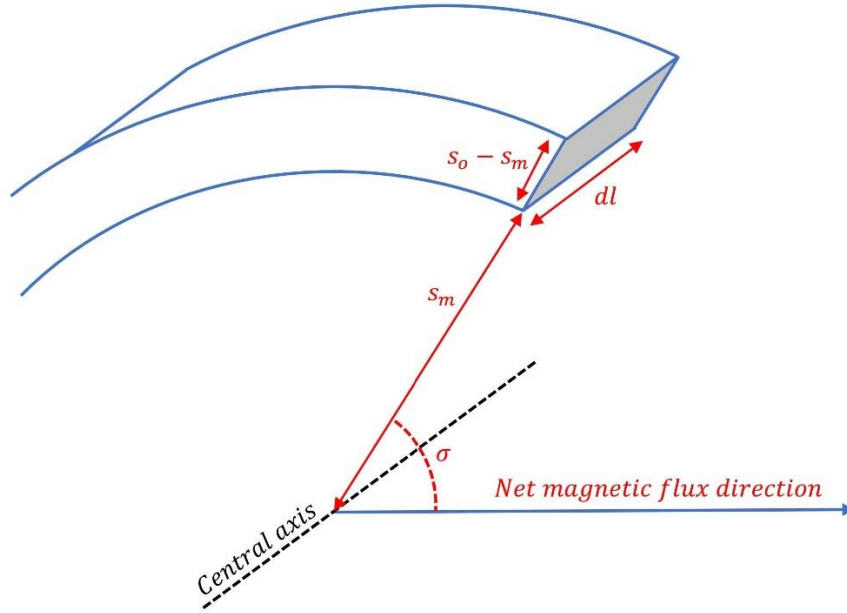
Figure 4.18 – Induction motor stator backplane segment

The magnetic flux density in the grey area shown in figure 4.18 can be calculated to be equation (4.47).

$$\text{Stator backplane magnetic flux density} = \frac{\Phi}{2l(s_o - s_m)}\sin(\sigma) \qquad (4.47)$$

Integrating the energy due to the presence of this magnetic field over the entire stator backplane region using cylindrical coordinates allows the total energy of this region to be calculated.

$$\text{Stator backplane energy} = \int_0^{2\pi} \int_0^l \int_{s_m}^{s_o} \frac{\Phi^2 r}{8\mu_0\mu_r l^2 (s_o - s_m)^2}\sin^2(\sigma)\,dr\,dl\,d\sigma$$

$$\text{Stator backplane energy} = \frac{\pi \Phi^2 (s_o + s_m)}{16\mu_0\mu_r (s_o - s_m)l} \qquad (4.48)$$

The contribution to total induction motor reluctance of each region can be calculated as per the energy equation (1.13) by multiplying the region's energy by 2 and then dividing by the square of the magnetic flux. Performing this operation to the derived energy values for each region allows the following magnetic reluctance values to be calculated.

$$\text{Inner rotor reluctance} = \frac{\pi}{4\mu_0\mu_r l} \qquad (4.49)$$

$$\text{Rotor bar region reluctance} = \frac{\pi}{4\mu_0 l\left(C_r + \mu_r(1 - C_r)\right)} \log_e\left(\frac{r_o}{r_i}\right) \qquad (4.50)$$

$$\text{Air gap region reluctance} = \frac{\pi}{4\mu_0 l} \log_e\left(\frac{s_i}{r_o}\right) \qquad (4.51)$$

$$\text{Stator slot region reluctance} = \frac{\pi}{4\mu_0 l\left(C_s + \mu_r(1 - C_s)\right)} \log_e\left(\frac{s_m}{s_i}\right) \qquad (4.52)$$

$$\text{Stator backplane reluctance} = \frac{\pi(s_o + s_m)}{8\mu_0 \mu_r (s_o - s_m) l} \qquad (4.53)$$

The total induction motor reluctance can be calculated by summing together equations (4.49) to 4.53. These reluctance equations are expressed in terms of geometric and material properties that do not change during motor operation. It is therefore possible to calculate this parameter without knowing any time dependent variables such as the state of the magnetic or electric fields.

4.4   Evaluation of power transfer in the magnetic circuit

As the stator magnetic flux, rotor magnetic flux and motor reluctance have been defined, it is possible to calculate the net magnetic flux. The net magnetic flux will be the sum of the rotor and stator magnetic flux. As these are both vector quantities, their relative phase angle needs to be accounted for when summing these two quantities together. The magnetic flux induced by both the rotor and stator will be approximately sinusoidally distributed in the air gap region thereby allowing vector addition to be used to calculate the net magnetic flux.

It was shown in figure 4.2 that the derivative of the net magnetic flux vector will be at a 90° angle to the net magnetic flux. The rotor's magnetic flux will have the same phase angle to the derivative of the net magnetic flux as it is caused by induced currents. This can be observed from figure 4.7 and equation (4.26) that states the maximum induced magnetic flux will be in the direction of the derivative of the net magnetic flux.

Based on this information, the relationship between the rotor magnetic flux Φ_r, stator magnetic flux Φ_s and net magnetic flux Φ is shown in figure 4.19 where λ is the angle between the net and stator magnetic flux.
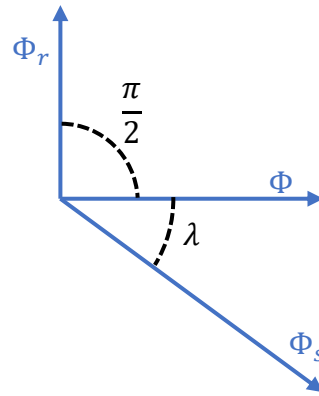
Figure 4.19 – Magnetic flux vectors

The rotor magnetic flux is perpendicular to the net magnetic flux and the sum of the rotor and stator magnetic flux must equal the net magnetic flux. This vector relationship allows the equation (4.54) relationship between the stator magnetic flux and net magnetic flux to be calculated.

$$\Phi = \Phi_S \cos(\lambda) \tag{4.54}$$

Substituting equation (4.19) Φ_S into equation (4.54) allows the equation (4.55) relationship between the stator current amplitude i_s and the net magnetic flux Φ to be expressed as:

$$\Phi = K_i i_s \cos(\lambda) \tag{4.55}$$

It is also possible to represent the externally applied winding voltage in vector form. This stator voltage vector is shown in figure 4.20 where θ is the angle of this vector relative to the direction of the net magnetic flux.
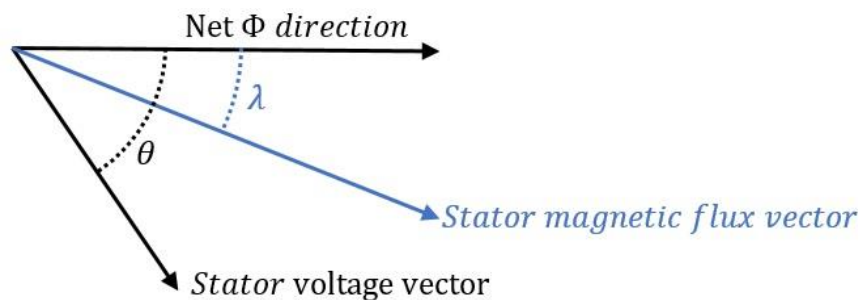
Figure 4.20 – Stator magnetic flux and voltage vectors

The voltage induced in the stator windings caused by the time derivative of the net magnetic flux vector will equal the negative of externally applied voltage minus the current induced voltage as per Faraday's law of induction. This value will equal the stator's voltage vector due to an externally applied voltage minus the current induced voltage vector. The voltage drop in the stator winding

due to electrical resistance can be calculated using ohms law to be $i_s R_s$ where R_s is the stator winding resistance.

In an AC circuit, the phase of the voltage and current are not necessarily aligned. The induced voltage in the stator windings due to resistive losses will be in phase with the current, not the voltage. Therefore, to calculate the derivative of the net magnetic flux due to the stator voltage, a vector addition of the applied voltage and any induced voltages needs to be performed.

To convert voltages from the electrical domain into the magnetic domain requires the voltage to be multiplied by K_v as per equation (4.20). To transfer current from the electrical domain to magnetic flux in the magnetic domain requires current to be multiplied by K_i as per equation (4.19). Therefore, the stator voltage vector as represented in the magnetic domain has an amplitude of $K_v V_s$ where V_s is the stator voltage amplitude and the voltage induced by stator currents has an amplitude of $K_v i_s R_s$. The voltage vectors in the magnetic domain must equal $|\vec{\Phi}|\omega$ as per figure 4.2. This can be represented on a vector diagram shown in figure 4.21 from the stators frame of reference when the rotational frequency is the synchronous frequency ω_f.
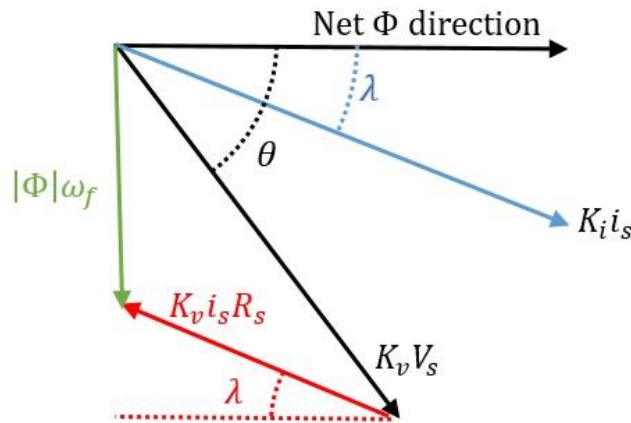
Figure 4.21 – Stator voltage vectors accounting for resistive voltages

Not all the magnetic flux from the stator windings will pass through the rotor as there will be some leakage flux from the stator. These stray fields will act like an inductor placed in series with the mutually coupled section of the stator's windings. To incorporate these effects into the induction motor model, the voltage and phase shift caused by these induced voltages in the stator windings needs to be calculated. Assuming the stator winding current is sinusoidal with a magnitude of i_s and frequency of ω_f, the magnitude of the voltage caused by resistive losses $i_s R_s$ and stray fields inductance can be calculated as:

$$Stator\ winding\ resistive\ and\ inductive\ voltage = i_s\sqrt{R_s{}^2 + (\omega_f L)^2} \qquad (4.56)$$

where L is the stator winding stray inductance. The effect of leakage inductance will also change the phase of the combined voltage caused by the resistive losses and stray fields. This change in phase relative to a resistive only loss is represented by the variable ρ can be calculated to be equation (4.56).

$$\rho = \tan^{-1}\left(\frac{\omega_f L}{R_s}\right) \tag{4.57}$$

Incorporating this information into the vector diagram from figure 4.21 allows the vector diagram shown in figure 4.22 to be derived.
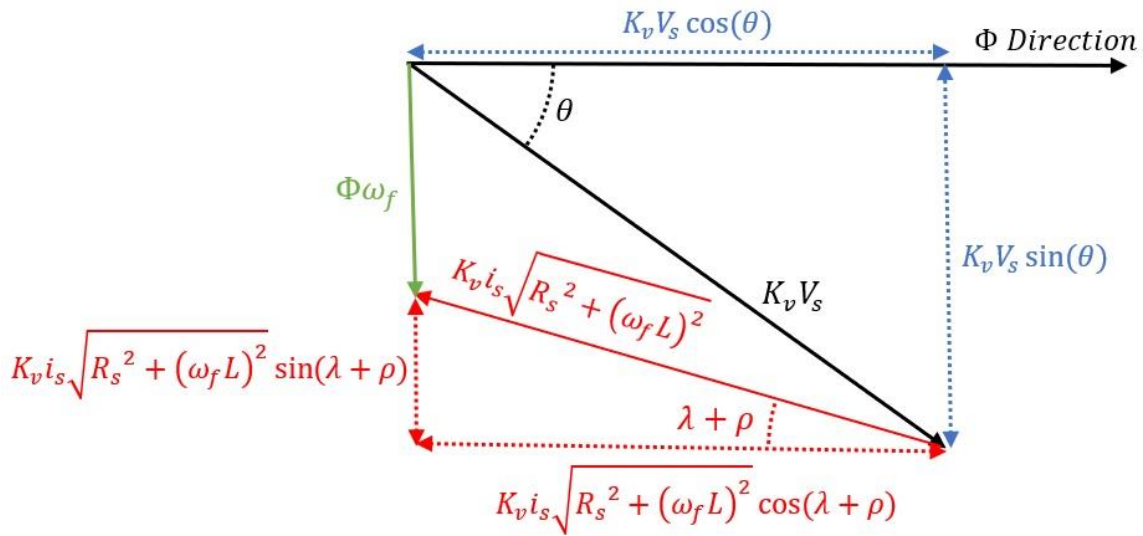
Figure 4.22– Stator voltage vectors accounting for resistive and inductive voltages

The vectors geometry from figure 4.22 allows two important relationships to be calculated.

$$V_s \sin(\theta) = i_s\sqrt{R_s^2 + (\omega_f L)^2}\sin(\lambda + \rho) + \frac{\omega_f}{K_v}\Phi \tag{4.58}$$

$$V_s \cos(\theta) = i_s\sqrt{R_s^2 + (\omega_f L)^2}\cos(\lambda + \rho) \tag{4.59}$$

Using equation (4.58), equation (4.59) and the formula for AC power incorporating displacement power factor, it is possible to calculate the rate of energy transfer from the voltage supply to the motor i.e. P_{supply}. This is because the phase angle between the stator windings AC voltage and current is the same as that between the stator voltage and current vectors as depicted in figure 4.20.

$$P_{supply} = \frac{3}{2}V_s i_s \cos(\theta - \lambda) \tag{4.60}$$

Substituting equations (4.58) and (4.59) into equation (4.60) allows the value of power supplied to the motor P_{supply} to be expressed in terms independent of the angle θ.

$$P_{supply} = \frac{3}{2} i_s{}^2 R_s + \frac{3\omega_f}{2K_v} i_s \Phi \sin(\lambda) \qquad (4.61)$$

The equation (4.55) relationship between the net magnetic flux and stator winding current amplitude i_s can be used to express the second product term of equation (4.61) in terms independent of i_s.

$$P_{supply} = \frac{3}{2} i_s{}^2 R_s + \frac{3\omega_f}{2K_i K_v} \Phi^2 \tan(\lambda) \qquad (4.62)$$

Equation (4.62) contains the product of the scaling factors K_v and K_i. These two scaling factors are not independent of each other and their product can be calculated using the conservation of energy. The magnetic circuit vector power transfer equation is very versatile and can be applied to the vectors shown in figure 4.20. By equating the power supplied to the motor using electrical circuit analysis to the value predicted using magnetic circuit analysis allows for the product of K_v and K_i to be calculated. To equate the magnetic circuit parameters to electrical circuit paramteres, the equation (4.19) value of stator magnetic flux and the equation (4.20) value of the derivitive of the magnetic flux is used.

$$\frac{3}{2} V_s i_s \cos(\theta - \lambda) = \mathcal{R} \overrightarrow{\Phi_s} \cdot \frac{d\overrightarrow{\Phi}}{dt}$$

$$\frac{3}{2} V_s i_s \cos(\theta - \lambda) = \mathcal{R} |\overrightarrow{\Phi_s}| \left| \frac{d\overrightarrow{\Phi}}{dt} \right| \cos(\theta - \lambda)$$

$$\frac{3}{2} V_s i_s = \mathcal{R} K_i i_s K_v V_s$$

$$K_i K_v = \frac{3}{2\mathcal{R}} \qquad (4.63)$$

Substituting equation (4.63) into equation (4.62) allows equation (4.64) to be derived.

$$P_{supply} = \frac{3}{2} i_s{}^2 R_s + \mathcal{R}\omega_f \Phi^2 \tan(\lambda) \qquad (4.64)$$

Equation (4.64) describes the energy transferred to the motor from an external power supply. However, this equation is in terms of the angle between the stator's current induced magnetic flux and the net magnetic flux λ and the net magnetic flux magnitude Φ. These parameters cannot be determined by an observer external to the motor. For an equation to have practical applications it

will need to be expressed in terms of stator voltage amplitude V_s and frequency ω_f and the rotor slip frequency ω_s as these are externally observable quantities. The value of λ can be expressed in terms of known values by equating equation (4.64) with the total power transfers within the motor. The first product term of equation (4.64) is the energy lost due to resistive losses in the stator's windings. Therefore, the second product term of equation (4.64) must equal inductive energy transfers.

4.4.1 Consideration on magnetic losses

One component of inductive energy transfers are magnetic losses. The dominant component of magnetic losses is eddy current losses. Eddy current losses can be modelled using the Steinmetz's equation as being proportional to the square of both the magnetic flux and frequency. Using these magnetic loss approximations, the stator magnetic losses P_{sm} can be calculated to be equation (3.65) where M_{se} is the coefficient of stator eddy current losses.

$$P_{sm} = M_{se}\omega_f{}^2\Phi^2 \qquad (4.65)$$

The rotor magnetic losses P_{rm} can be calculated using this same technique. The only difference is that the observed rotational speed of the magnetic field will be proportional to the slip frequency ω_s from the rotor's frame of reference. This allows equation rotor magnetic losses to be derived as:

$$P_{rm} = M_{re}\omega_s{}^2\Phi^2 \qquad (4.66)$$

where M_{re} is the coefficient of rotor eddy current losses.

4.4.2 Consideration on rotor resistive losses

Rotor resistive losses can be determined by calculating the magnetic flux induced by electric currents in the rotor bars. This can be determined by substituting the magnitude of the derivative of the net magnetic flux as observed from the from the rotor's frame of reference into equation (4.28).

$$\Phi_r = \frac{4\omega_s\Phi}{\pi\mathcal{R}R_r} \qquad (4.67)$$

The magnetic circuit vector power transfer equation can be used to calculate the power loss due to rotor currents P_{re} by substituting in the equation (4.67) value of magnetic flux and the derivative of the net magnetic flux as observed from the rotor's frame of reference. As the rotor's magnetic flux has the same phase angle as the derivative of the net magnetic flux, the dot product can be replaced with magnitude multiplication operation as:

$$P_{re} = \mathcal{R}\Phi_r \cdot \left.\frac{d\vec{\Phi}}{dt}\right|_{rotor}$$

$$P_{re} = \frac{4}{\pi R_r}\omega_s{}^2\Phi^2 \qquad (4.68)$$

The equation (4.66) and equation (4.68) rotor power loss equations have both been evaluated from the rotor's frame of reference. From this frame of reference, the magnetic flux rotational speed is the slip frequency ω_s. However, to calculate inductive power transfer from the stator, the magnetic circuit vector power transfer equation must be evaluated from the stator's frame of reference. This can be achieved by substituting the equation (4.66) and (4.68) power loss equations into the magnetic circuit vector power transfer equation to calculate the impact these losses have on magnetic flux. The resulting magnetic flux vector can then be substituted into the magnetic flux vector power transfer equation and evaluated from the stator's frame of reference.

Converting a power loss from the rotors frame of reference to the stator's using the afore mentioned technique results in the rotor losses being scaled by the synchronous frequency ω_f divided by the slip frequency ω_s. Converting energy transferred to the rotor from the stator's frame of reference to the rotor's can be achieved by multiplying by the slip frequency ω_s divided by the synchronous frequency ω_f. This process is shown graphically in figure 4.23.

$$\times \frac{\omega_f}{\omega_s}$$

Rotor reference frame power loss   Stator reference frame power transfer
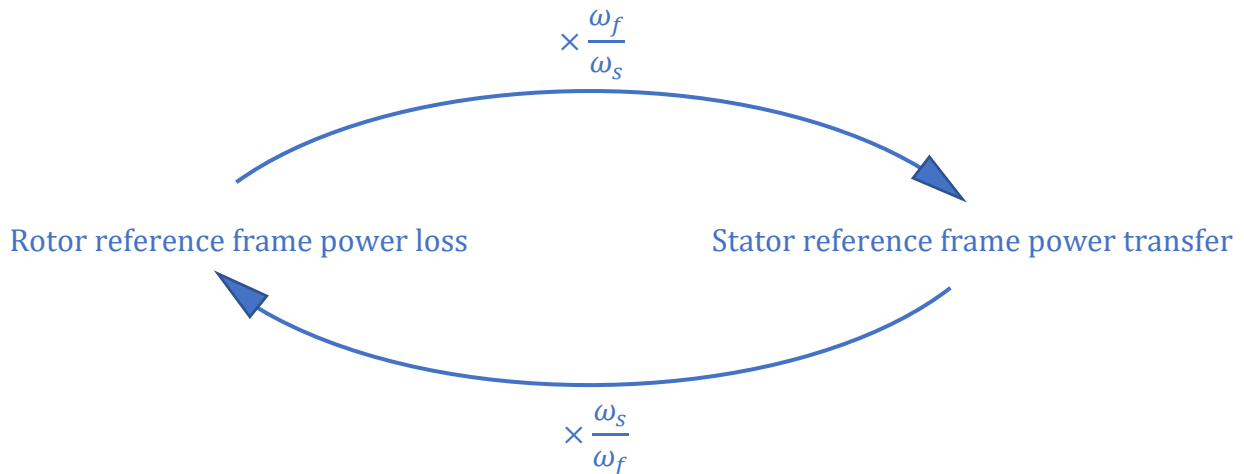
$$\times \frac{\omega_s}{\omega_f}$$

Figure 4.23 – Converting power transfers between rotating reference frames

Applying this process to the total rotor power loss from equation (4.66) and (4.68) can be calculated to be equation (4.69) from the rotor's frame of reference and equation (4.70) from the stator's frame of reference.

$$P_r|_{rotor} = \omega_s{}^2 \Phi^2 \left(\frac{4}{\pi R_r} + M_{re} \right) \tag{4.69}$$

$$P_r|_{stator} = \omega_s \omega_f \Phi^2 \left(\frac{4}{\pi R_r} + M_{re} \right) \tag{4.70}$$

The difference between the rates of energy transfer from the stator to the rotor minus the rotor losses is the electromechanical power developed in the cage rotor. This power transfer due to rotor torque P_τ can be calculated to be equation (4.71) where ω_r is the rotational speed of the rotor and the difference between the synchronous and slip frequencies.

$$P_\tau = \omega_s \omega_r \Phi^2 \left(\frac{4}{\pi R_r} + M_{re} \right) \tag{4.71}$$

4.4.3 Complete power transfer equation

Equation (4.70) describes the inductive energy transfer to the rotor and equation (4.65) describes the inductive losses in the stator. Equating these power transfers to the second product term of equation (4.64) allows the angle between the stator's current induced magnetic flux and the net magnetic flux λ to be calculated.

$$\mathcal{R}\omega_f \Phi^2 \tan(\lambda) = \omega_s \omega_f \Phi^2 \left(\frac{4}{\pi R_r} + M_{re} \right) + M_{se} \omega_f{}^2 \Phi^2$$

$$\tan(\lambda) = \frac{\omega_s}{\mathcal{R}} \left(\frac{4}{\pi R_r} + M_{re} \right) + \frac{M_{se} \omega_f}{\mathcal{R}} \tag{4.72}$$

It is also necessary to express the net magnetic flux Φ in terms of the stator voltage amplitude V_s. This involves squaring both sides of equations (4.58) and (4.59) and summing them together to eliminate their dependency on the angle θ.

$$V_s{}^2 = i_s{}^2 \left(R_s{}^2 + (\omega_f L)^2 \right) + \frac{\omega_f{}^2}{K_v{}^2} \Phi^2 + 2 i_s \sqrt{R_s{}^2 + (\omega_f L)^2} \sin(\lambda + \rho) \frac{\omega_f}{K_v} \tag{4.73}$$

Substituting equations (4.55), (4.57) and (4.63) into equation (4.73) allows the stator current amplitude term i_s, the phase angle ρ and the voltage scaling factor K_v to be eliminated.

$$\frac{V_s{}^2}{\Phi^2} = \frac{\left(R_s{}^2 + (\omega_f L)^2 \right)}{K_i{}^2} (\tan^2(\lambda) + 1) + \left(\frac{2 \mathcal{R} K_i \omega_f}{3} \right)^2 + \frac{4 \mathcal{R}}{3} \omega_f \left(R_s \tan(\lambda) + \omega_f L \right) \tag{4.74}$$

Substituting the equation (4.72) value of $\tan(\lambda)$ into equation (4.74) allows the net magnetic flux Φ to be expressed in terms of known and observable variables.

$$\Phi^2 = \frac{V_s{}^2}{\left(\left(\frac{R_s}{K_i}\right)^2 + \left(\frac{\omega_f L}{K_i}\right)^2\right)\left(\left(\frac{\omega_s}{\mathcal{R}}\left(\frac{4}{\pi R_r} + M_{re}\right) + \frac{M_{se}}{\mathcal{R}}\omega_f\right)^2 + 1\right) + \frac{4}{3}\omega_f{}^2\left(R_s\left(\frac{\omega_s}{\omega_f}\left(\frac{4}{\pi R_r} + M_{re}\right) + M_{se}\right) + L\mathcal{R} + \frac{(\mathcal{R}K_i)^2}{3}\right)}$$

(4.75)

Substituting the equation (4.75) value of net magnetic flux into the equation (4.71) rate energy is converted into kinetic energy and dividing by the rotor rotational speed ω_r allows the rotor torque T_r to be calculated.

$$T_r = \frac{\omega_s\left(\frac{4}{\pi R_r} + M_{re}\right)}{\left(\left(\frac{R_s}{K_i}\right)^2 + \left(\frac{\omega_f L}{K_i}\right)^2\right)\left(\left(\frac{\omega_s}{\mathcal{R}}\left(\frac{4}{\pi R_r} + M_{re}\right) + \frac{M_{se}}{\mathcal{R}}\omega_f\right)^2 + 1\right) + \frac{4}{3}\omega_f{}^2\left(R_s\left(\frac{\omega_s}{\omega_f}\left(\frac{4}{\pi R_r} + M_{re}\right) + M_{se}\right) + L\mathcal{R} + \frac{(\mathcal{R}K_i)^2}{3}\right)}$$

(4.76)

The equation (4.75) value of the net magnetic flux and the equation (4.72) value of $\tan(\lambda)$ can be used to determine parameters such as stator winding current amplitude and efficiency.

4.5 Finite element model based validation

4.5.1 Case study induction motor description

The equations and parameters derived in this chapter can be simulated using FEM to establish a benchmark against which the accuracy of these equations can be compared. A computer rendering of the induction motor simulated using FEM used to assess the accuracy of these equations is shown in figure 4.24.
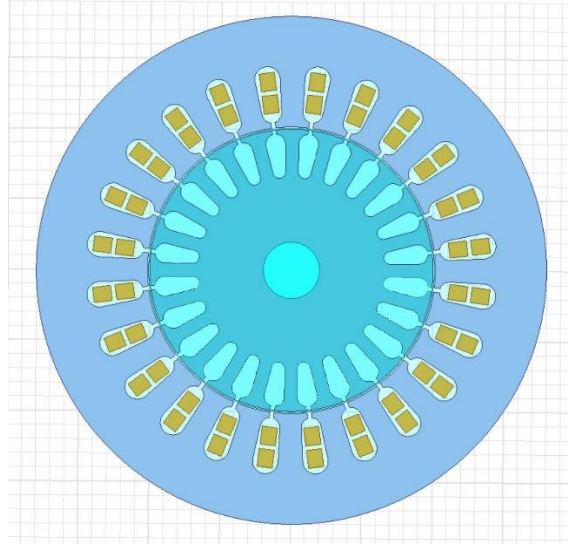
Figure 4.24 – FEM simulation rendering of induction motor

Radius variables from figure 4.12 and 4.13 used in this simulation are listed below in meters. The ratio of the rotor slot area to total area in the outer rotor region C_r and the ratio of the stator slot area to total inner stator region area C_s are also listed.

- $r_i = 0.038m$
- $r_o = 0.05m$
- $s_i = 0.0508m$
- $s_m = 0.075m$
- $s_b = 0.09m$
- $l = 0.12m$
- $C_r = 0.55$
- $C_s = 0.45$

Using these dimensions, the motor reluctance from equations (4.49) to (4.53) is as follows.

- Inner rotor reluctance $= 1302 \text{ H}^{-1}$
- Rotor bar region reluctance $= 794 \text{ vH}^{-1}$
- Air gap region reluctance $= 82,674 \text{ H}^{-1}$
- Stator slot region reluctance $= 922 \text{ H}^{-1}$
- Stator backplane reluctance $= 7,161 \text{ H}^{-1}$

Summing these reluctance values together results in a total motor reluctance of $92,853H^{-1}$.

The simulated induction motor has the same winding configuration as shown in figure 4.10 with 50 turns per slot per phase. This allows the value of K_i with units of Henry to be calculated as defined in equation (4.19) by substituting the calculated motor reluctance and $n = 50$ into equation (4.30).

$$K_i = 4.485628 \times 10^{-3} H \qquad (4.77)$$

4.5.2 Leakage inductance calculation

The only remaining parameter that needs to be calculated is the value of the stator leakage inductance L. Calculating this value requires the magnetic flux induced by stator currents that does not mutually couple with the rotor to be determined. This can be achieved using a lumped parameter approximation of the stator slot and air gap region. To illustrate how the parameters of this leakage model are determined, consider the magnetic path of the leakage flux from stator currents as shown in figure 4.25.
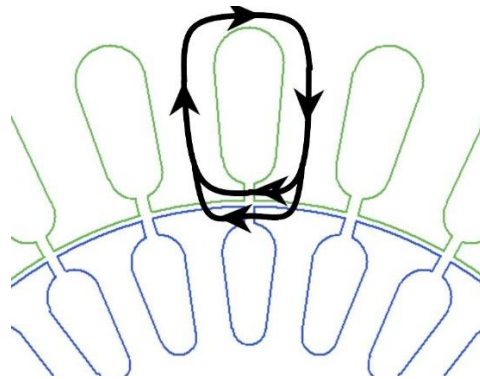
Figure 4.25 – Stator leakage magnetic flux

To calculate the reluctance the leakage magnetic flux encounters, the region around the air gap is divided into 9 segments as shown in figure 4.26.
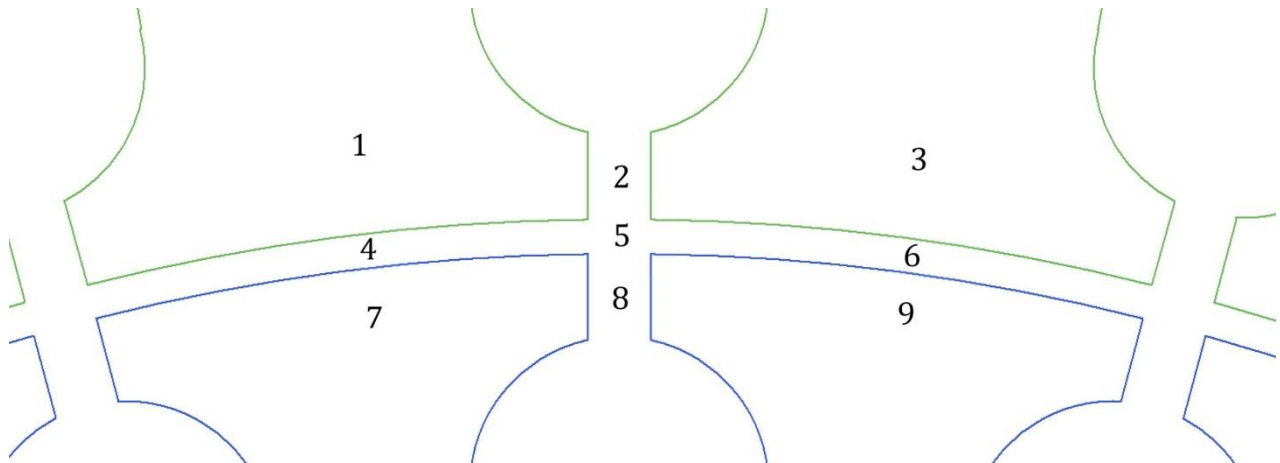

Figure 4.26 – Air gap and surrounding region labels

Each labeled region in figure 4.26 represents an area of magnetic reluctance through which leakage magnetic flux can flow. The reluctance of the stator backplane and the inner rotor are considered

too small to impact this model and will therefore be assumed to be zero. Using the region labels as shown in figure 4.26, a reluctance mesh can be derived as shown in figure 4.27.
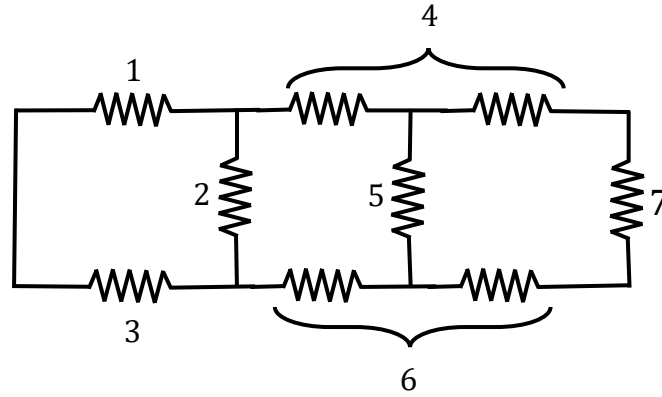

Figure 4.27 – Reluctance mesh for leakage induction calculation

Reluctance values 1 and 3 from figure 4.27 can be calculated using the conventional reluctance formula, assuming the stator tooth has a width of 7.5mm, a height of 14mm, a length of 120mm and relative permeability of 4000.

$$\text{Reluctance 1 and 3} = \frac{\text{length}}{\mu_0 \mu_r \times \text{Area}}$$

$$\text{Reluctance 1 and 3} = \frac{0.014}{4000\mu_0 \times 0.0075 \times 0.12}$$

$$\text{Reluctance 1 and 3} = 3094.7 \text{H}^{-1} \tag{4.78}$$

Region 2 and 7 from figure 4.27 have a width of 1.5mm, a height of 2.1mm and length of 120mm resulting in the equation (4.78) value of reluctance.

$$\text{Reluctance 2 and 7} = \frac{0.0015}{\mu_0 \times 0.0021 \times 0.12}$$

$$\text{Reluctance 2 and 7} = 4.737 \times 10^6 \tag{4.79}$$

Region 5 from figure 4.26 has a width of 1.5mm, a height of 0.8mm and length of 120mm resulting in the equation (4.80) value of reluctance.

$$\text{Reluctance 5} = \frac{0.0015}{\mu_0 \times 0.0008 \times 0.12}$$

$$\text{Reluctance 5} = 1.243 \times 10^7 \tag{4.80}$$

Region 4 and 6 from figure 4.26 have a width of 11.59mm, a height of 0.8mm and length of 120mm resulting in the equation (4.81) value of reluctance.

$$\text{Reluctance 4 and 6} = \frac{0.0008}{\mu_0 \times 0.0115 \times 0.12}$$

$$\text{Reluctance 4 and 6} = 4.577 \times 10^5 \qquad\qquad (4.81)$$

The reluctance value for areas 4 and 6 as calculated to be equation (4.81) is total reluctance of their respective air gap region. This reluctance is divided into two equal values for the reluctance mesh as shown in figure 4.27.

As shown in figure 4.10, each pole phase winding is spread over 8 stator slots. Four slots for the current in one direction and four slots for the current in the opposite direction. This configuration will result in the stray magnetic flux being canceled out in the stator teeth between windings of the same phase and polarity. Only the magnetic flux flowing through the stator teeth adjacent to the first and last winding of the same phase and polarity will not cancel out. This can be modeled by inserting the MMF source into the reluctance mesh from figure 4.27 in series with reluctance element 1 and 3 for the total value of the MMF per phase per pole. In this situation, there are four stator slots with 50 turns each per phase resulting in an MMF of 200At.

The total leakage inductance as seen by the current flowing through 4 stator slots can be calculated using the reluctance mesh shown in figure 4.27 with the reluctance values of equations (4.78) to (4.81). This reluctance as seen by the source of MMF is $2.583 \times 10^6 H^{-1}$ and the number of turns is 200. Inductance can be calculated by dividing the square of the number of turns by the reluctance.

$$\text{Stray inductance for 4 stator slots} = \frac{200^2}{2.583 \times 10^6}$$

$$\text{Stray inductance for 4 stator slots} = 15.48mH \qquad\qquad (4.82)$$

Each phase winding for the two-pole motor being analyzed has four groups of four windings as shown in figure 4.10 that result in stray magnetic fields. Summing the total of these inductances together allows the equation (4.83) value of inductance caused by magnetic flux from the stator not coupled to the rotor to be calculated.

$$L = 61.93mH \qquad\qquad (4.83)$$

4.5.3 Rotor resistance calculation

Another parameter that needs to be calculated in the rotor resistance. Each rotor bar has a cross sectional area of $7 \times 10^{-5} m^2$ and a length of $0.12m$. Therefore, each aluminum rotor bar will have a resistance of $4.543 \times 10^{-5} \Omega$. The rotor end ring has an average radius of $40mm$ and a cross sectional area as seen by electric current to be $1 \times 10^{-4} m^2$. Current flowing out of a rotor bar into the end ring will flow via two paths to the opposite rotor bar. Therefore, the resistance of the rotor end ring is half the resistance of a $180°$ segment of the rotor ring. In this situation, the rotor end ring resistance will be $1.666 \times 10^{-5} \Omega$.

The electrical circuit for this current path is shown in figure 4.28.
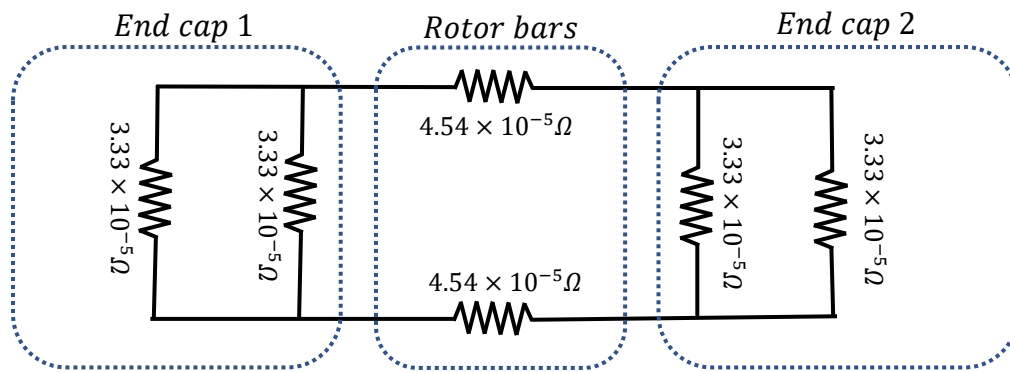

Figure 4.28 – Electrical circuit for current flowing through the rotor bars

The total resistance of this path will be $1.242 \times 10^{-4} \Omega$. Multiplying this resistance value by the angular displacement between rotor bars, which in this case is $\frac{\pi}{12}$ radians allows the rotor resistance R_r to be calculated.

$$R_r = 3.2515 \times 10^{-5} \Omega rad \qquad (4.84)$$

The remaining parameters needing to be calculated are listed below based on the simulation settings and geometry.

- Stator winding resistance $R_s = 2.54\Omega$
- Line to neutral voltage amplitude $V_s = 325V$
- Sychronous frequency $\omega_f = 100\pi$ rad s^{-1}

4.5.4 Finite element simulation results

A FEM simulation was undertaken to simulate the electrical, mechanical and magnetic characteristics of the induction motor to be compared to those predicted using magnetic circuit analysis. The simulated and predicted mechanical characteristics of the induction motor can be

compared by simulating the output power of the induction motor as a function of rotor's rotational speed. This comparison is shown in figure 4.29 where the predicted values were obtained by multiplying the equation (4.76) value of torque by rotational speed.
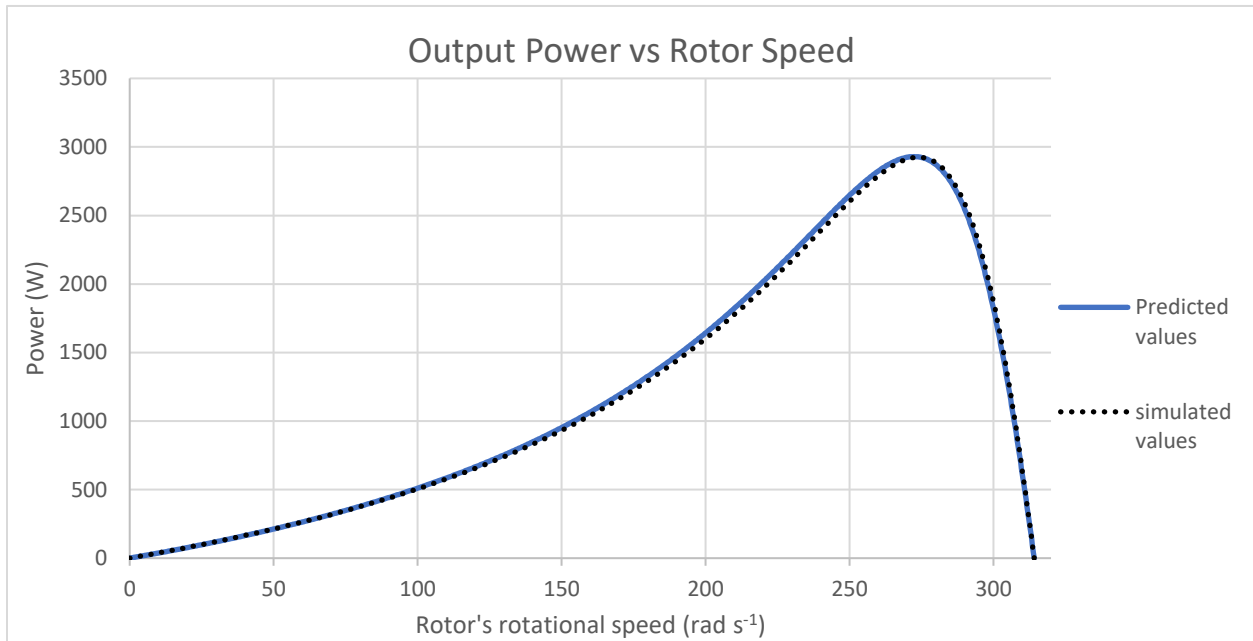

Figure 4.29 – Simulated and predicted induction motor output power

Figure 4.29 demonstrates that magnetic circuit analysis does result in values that are comparable to those obtained using FEM simulations. The average difference between the FEM simulated and predicted output power is 28.4W which is 0.97% of the maximum output power. Most of this discrepancy between the FEM simulation and predicted values occurs for rotational speeds between 150 $rad\ s^{-1}$ and 250 $rad\ s^{-1}$ with an average difference of 39.7W in this region. For rotational speeds above $300 rad\ s^{-1}$ where the motor will most likely be operating in, FEM and magnetic circuit analysis yield almost identical results.

To compare the electrical characteristics of the induction motor as predicted by FEM and magnetic circuit analysis, the RMS stator phase current was simulated using FEM. This was then compared to magnetic circuit analysis by solving equation (4.72) to calculate the angle between the stator magnetic flux and the net magnetic flux λ. This value was then substituted into equation (4.74) to calculate the magnitude of the net magnetic flux and equation (4.55) to calculate the stator current amplitude i_s. Figure 4.30 shows the comparison between the FEM simulated stator current and that predicted using magnetic circuit analysis.
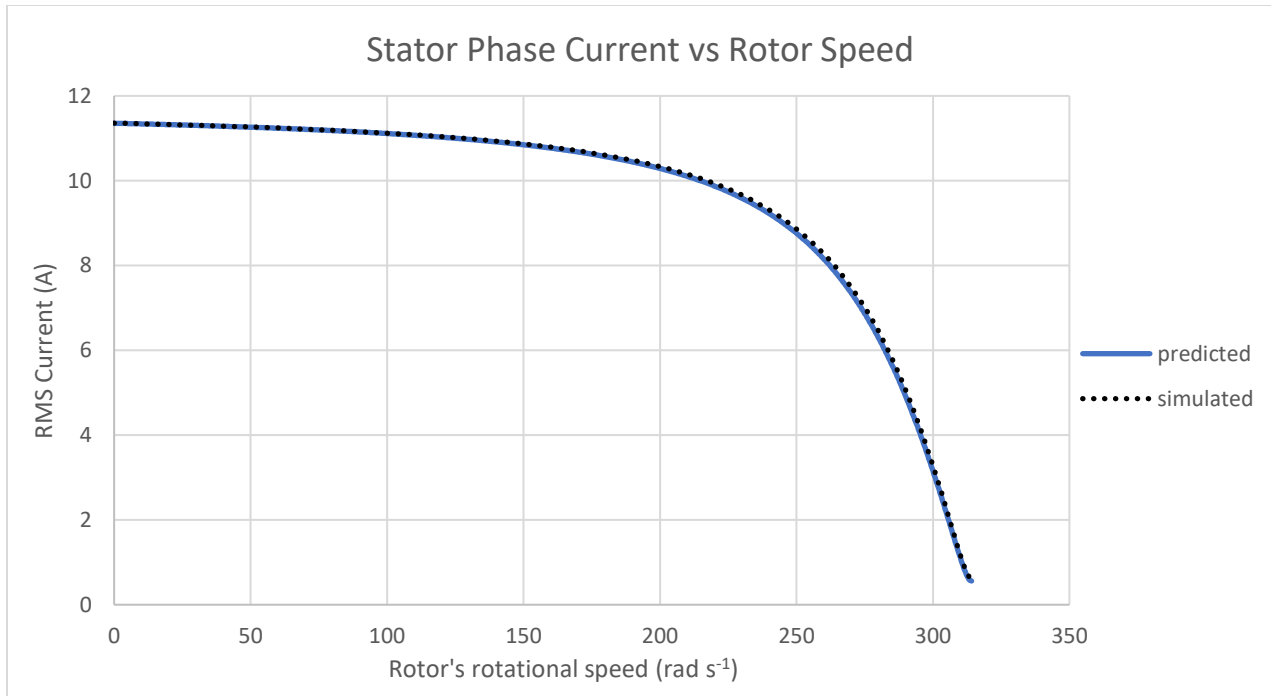
Figure 4.30– Simulated and predicted induction motor phase current

There is an average difference between the FEM simulated and predicted current of 0.054A over the range of speeds simulated. The most significant observable difference occurs for rotational speeds between $200\ rad\ s^{-1}$ and $270\ rad\ s^{-1}$ with and average difference of 0.080A in this region. As was the case for output power, rotational speeds above $300\ rad\ s^{-1}$ FEM and magnetic circuit analysis yield almost identical results.

Comparisons between both electrical and mechanical operational characteristics of the induction motor can be observed when analyzing efficiency. This is achieved by dividing the output power as shown in figure 4.29 by the predicted electrical input power from equation (4.64). Figure 4.31 shows the comparison between efficiency predicted by magnetic circuit analysis and that which was derived using FEM simulation.
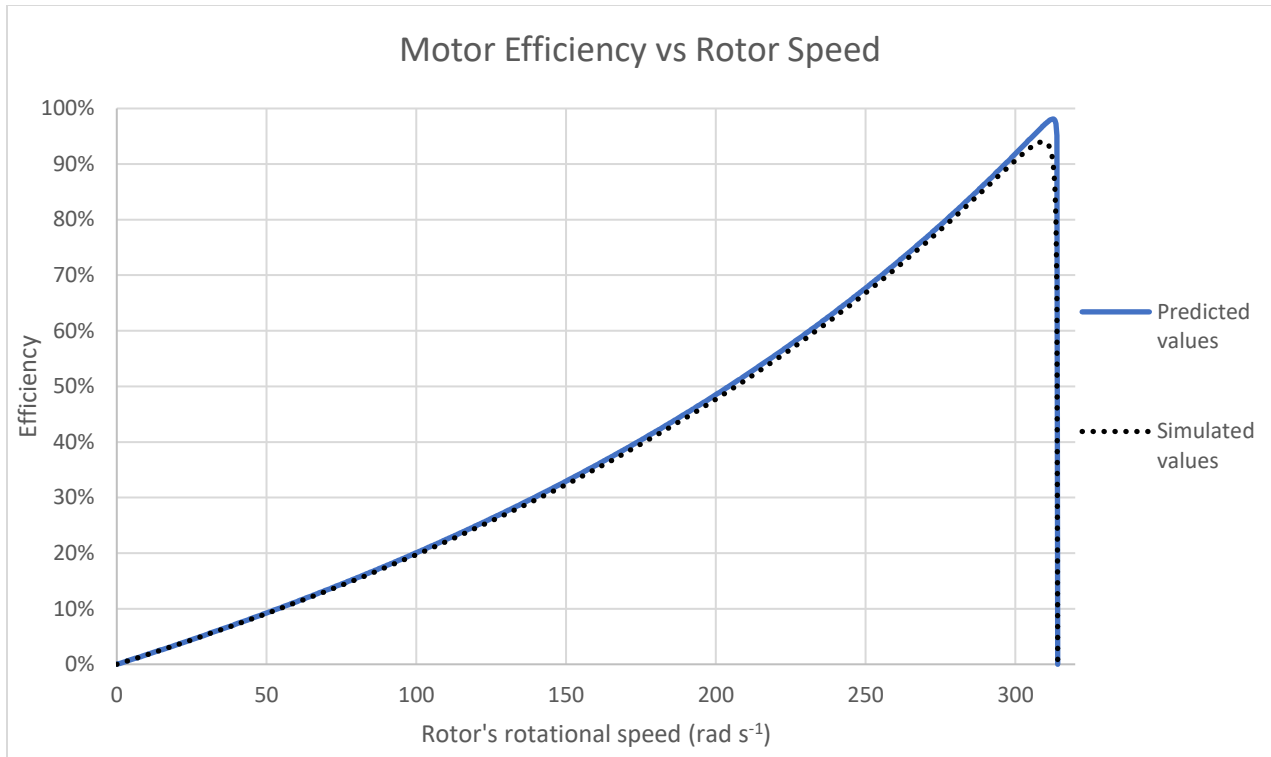
Figure 4.31 – Simulated and predicted induction motor efficiency

The magnetic circuit predicted efficiency is slightly greater than that predicted by FEM for most rotational speeds with the discrepancy being greatest for rotational speeds above $300 \, rad \, s^{-1}$. Average difference between the FEM simulated and predicted efficiency was 0.82% with a difference of up to 9.8% at $313 \, rad \, s^{-1}$. This was unexpected as both output power and stator phase current calculated using magnetic circuit analysis was closest to FEM simulated values for rotational speeds above $300 \, rad \, s^{-1}$. Despite this discrepancy, the overall difference between both the FEM simulated and magnetic circuit results was only minimal with no significant diverging trend.

In addition to electrical and mechanical motor operational characteristics, magnetic parameters such as the angle between the stator and net magnetic flux. As this is not a commonly used parameter for induction motor design, it's value as a function of rotor speed cannot be readily obtained using commonly used FEM design software. This value is however a critical component of the magnetic circuit induction motor model presented in this thesis. It is also an important parameter to quantify to understand the relationship between stator currents and torque. This angle between the stator's current induced magnetic flux and the net magnetic flux as represented by the angle λ and defined in figure 4.19 is shown in figure 4.32.
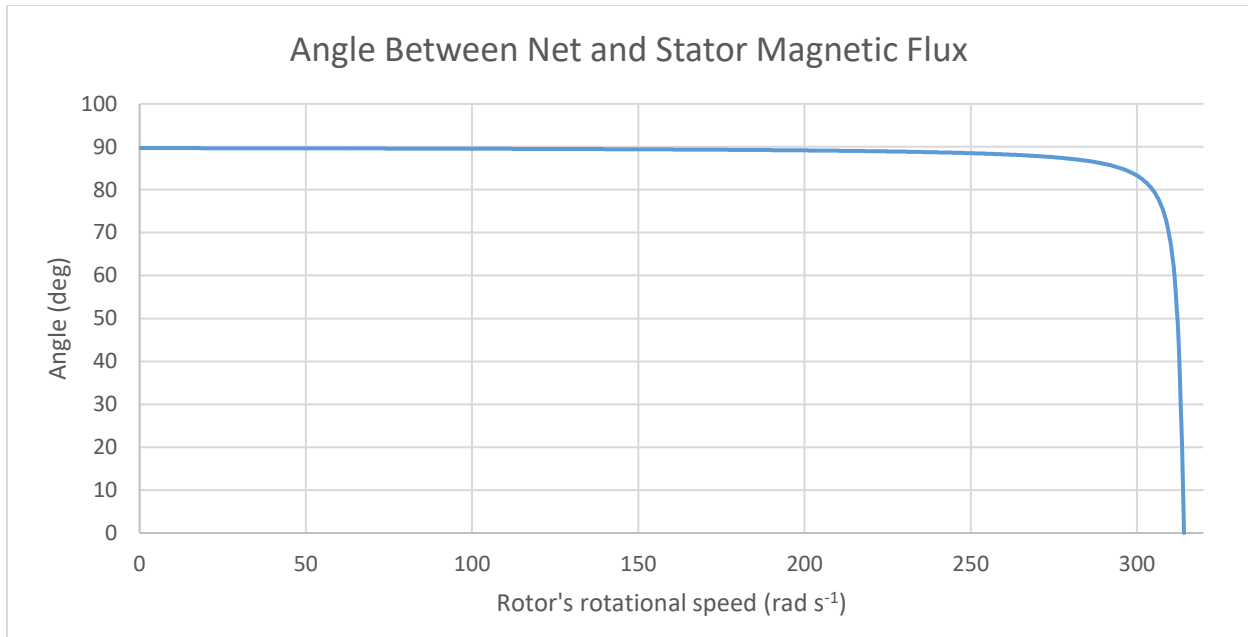
Figure 4.32 – Magnetic circuit predicted angle between the stator's and the net magnetic flux

Figure 4.32 shows that the angle between the stator's current induced magnetic flux and the net magnetic flux starts at close to 90° and reduces to 0° when the rotor's rotational speed reaches the synchronous speed. As the rotor's current induced magnetic flux as shown in figure 4.32 is at a 90° angle to the net magnetic flux, the stator's magnetic flux will be close to 180° out of phase with the rotor's magnetic flux for low rotational speeds. This means that the net magnetic flux will be much less than the stator's magnetic flux as much of the stators magnetic flux will be cancelled out by to rotor's magnetic flux.

Therefore, despite a large amount of stator winding current at low rotational speeds as depicted in figure 4.30, the net magnetic flux will be at a minimum in this operating area. This can be verified by plotting the net magnetic flux as a function of rotational speed as shown in figure 4.33.
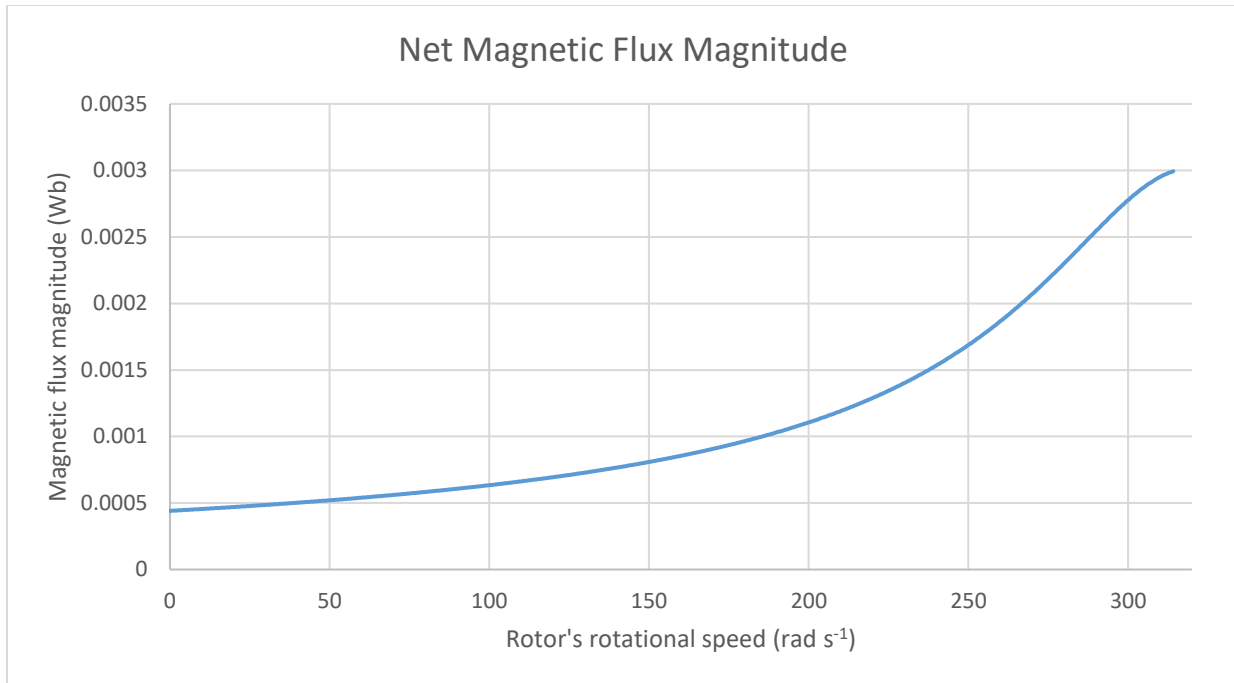
Figure 4.33 – Magnetic circuit predicted net magnetic flux magnitude

Figure 4.33 demonstrates that the net magnetic flux increases with rotational speed between stationary and the synchronous rotational speed. However, it was demonstrated in figure 4.30 that stator current which is directly proportional to the stators current induced magnetic flux decreases as a function of rotational speed over the same range. This difference can be explained using the figure 4.32 value of the angle between the stator's current induced magnetic flux and the net magnetic flux. As this angle decreases, less stator flux is canceled out by the rotor magnetic flux resulting in a greater value of net magnetic flux.

4.6 Conclusion

This chapter of the thesis has demonstrated how it is possible to apply magnetic circuit analysis to describe the operation of the induction motor without the need for empirically derived parameters. By modelling the magnetic flux and the time derivative of the magnetic flux in vector form it is possible to calculate both electrical and magnetic parameters. Combining this with the magnetic circuit energy transfer equation results in a magnetic flux based induction motor model with comparable accuracy to that obtained using FEM based simulations.

Modelling the rotor, stator and net magnetic flux as separate vectors, differentiates this magnetic flux model from other magnetic flux models such as the D-Q model. The D-Q model states that there should be two relevant magnetic flux quantities at right angles to each other without justifying why this would be the case for an AC motor. This research demonstrates that the rotor magnetic flux will be at right angles to the net magnetic flux under steady state operating

95

conditions. This provides some justification to the underlying assumptions of the D-Q model, although it is worth noting that this only occurs during steady state conditions. Another advantage to this approach is that induction motor operational characteristics can be described using closed form equations. As closed form equations can be solved in less time than numerical method techniques, it is possible to use models based on this magnetic circuit analysis for both design optimization and real time control.

Therefore, based on this research, the advantages of using vector applications of magnetic circuit analysis can be summarized in the following points.

- It can be derived from the geometry and material properties of the induction motor as opposed to equivalent circuits where parameters need to be matched with empirical data.
- It has been derived at a lower level of abstraction relative to other magnetic flux models such as the D-Q model.
- As closed form equations have an inherent computational speed advantage compared to numerical methods giving this model and advantage relative to FEM and LPM
- The vector based magnetic circuit equations could match FEM predictions without the need for additional empirical correction factors as is sometimes required for LPM induction motor models.

Chapter 5

5 Conclusion

This thesis has demonstrated how it is possible to use magnetic circuit analysis to model complex magnetic path problems without the need for numerical methods. The presented analytical technique allows for closed form equations to be derived directly from the electromagnetic device's geometry and material properties. This approach can expand the applications of magnetic circuit analysis thereby reducing the need for computationally intensive modelling techniques in some situations.

The magnetic circuit modelling was achieved in this thesis using an energy-based approach. This allowed the contribution that individual components of an electromagnetic device to the total magnetic reluctance to be calculated in the presence of non-homogeneous magnetic fields. As energy based magnetic circuit analysis only required the magnitude of the magnetic flux to be known, the direction of the magnetic flux in most situation was not required to be known.

It was demonstrated in this thesis that when the B and H fields do not align in an electromagnetic device, the underlying assumptions need to be accurate or otherwise will result in significant errors. By accounting for the difference in magnetic field energy in these situations, it was demonstrated that magnetic circuit analysis can calculate results with high accuracy.

The energy based magnetic circuit equations presented in this thesis were calculated in vector form. Combining these vector-based energy transfer equations with vector equations relating the magnetic flux and its time derivative when experiencing rotation allowed an advanced model of the induction motor to be derived. This model was derived without the need for high level assumptions on the relative angles between magnetic flux vectors. In doing so it was possible to define the relative angle between magnetic flux vectors as a function of the rotor's rotational speed and stator winding voltage.

To summarize the findings of this research, it was demonstrated that,

- Energy based analysis of magnetic field can be used to model inhomogeneous magnetic field distribution and is compatible with existing magnetic circuit theory.
- Accounting for non-uniform magnetic field distributions and non-aligned B-H field configurations allows magnetic circuit analysis to yield results comparable to those achieved using FEM.
- Modelling the magnetic flux and the time derivative of the magnetic flux in vector enabled electrical and magnetic parameters to be calculated with comparable accuracy to that obtained using FEM based simulations.

Overall, the energy based magnetic circuit modelling presented in this thesis offers a compromise between computational intensity and accuracy relative to existing techniques. The application of this theory requires the use of more complex equations compared to simple linear models derived from traditional magnetic circuit analysis. However, these equations can model inhomogeneous fields in complex geometries that would typically require the use of more computationally intensive numerical methods. This research also presented an alternative way to calculate magnetic reluctance based on the total amount of energy due to the presence of electric current. In so doing, it was possible to use an alternative approach to calculate dynamic energy transfers due to changes in magnetic reluctance and circular motion.

The magnetic flux model of the induction motor derived in chapter 4 of this thesis demonstrates how to apply magnetic circuit analysis to inductive energy transfers due to rotating fields. Therefore, only eddy current losses were included in the calculations. Future research could improve on the magnetic loss section of the model to include non-linear losses such as hysteresis losses. This research could also be used to derive the coefficients of eddy current losses directly from the motor geometry.

Future research can also be conducted on transient behavior of the induction motor. The magnetic flux vector equations were only used to derive the steady state solution in this thesis, although they are versatile enough to be used for transient analysis. A transient analysis could result in improvements to magnetic flux modelling compared to the D-Q model. This is because the rotor magnetic flux and net magnetic flux will not necessarily be at a 90° angle to each other as is assumed in the D-Q model.

In this thesis an induction motor model was derived to describe the characteristics of the induction motor. However, this model has not yet been applied to deriving control algorithms for induction motor operations. As this is a magnetic flux-based model, it would be possible to use it to implement a flux vector control system or equivalent. This future research could be used to determine any advantages this model possesses relative to existing models used for real time control of rotating machines that operate on the principle of electromagnetic induction.

6 References

[1]   S. AG, "Sinamics function manual," p. 560, 07/2007 2007.

[2]   T. I. Incorporated, "Scalar V/F control of 3 phase induction motors," p. 25, 07/2013 2013.

[3]   C. P. Steinmetz, "Theory and Calculation of Alternating Current Phenomena," 1897.

[4]   B. Mirafzal, G. L. Skibinski, and R. M. Tallam, "Determination of parameters in the universal induction motor model," *IEEE Transactions on Industry Applications,* vol. 45, pp. 142-151, 2009.

[5]   D. Jee, "V/f control of induction motor drive," National Institute of Technology Rourkela, 2013.

[6]   M. Fan, J. Chai, and X. Sun, "Induction motor parameter identification based on T-model equivalent circuit," in *Electrical Machines and Systems (ICEMS), 2014 17th International Conference on*, 2014, pp. 2535-2539.

[7]   D. Hochfelder, "Joseph Henry: Inventor of the Telegraph?," *Smithsonian Institution Archives,* 2007, 2007.

[8]   J. Hopkinson, "Origional papers volume 1 technical papers of John Hopkinson," *Cambridge university press,* vol. 1, 2014 1901.

[9]   O. Heaviside, *Electrical papers* vol. 2: Cambridge University Press, 2011.

[10]   A. V. Radun, "Development of dynamic magnetic circuit models including iron saturation and losses," *IEEE Transactions on Magnetics,* vol. 50, no. 5, pp. 1-10, 2014.

[11]   J. G. Niesten and O. T. Tan, "The induction machine operation demonstrated by Arago's disc," *IEEE Transactions on Education,* vol. 32, pp. 160-162, 1989.

[12]   B. Walter, "A Mode of producing Arago's Rotation," *Proceedings of the Physical Society of London,* vol. 3, p. 115, 1879.

[13]   G. Neidhofer, "Early three-phase power [History]," *IEEE Power and Energy Magazine,* vol. 5, pp. 88-100, 2007.

[14]   M. J. Seifer, *Wizard: the life and times of Nikola Tesla: biography of a genius*: Citadel Press, 1996.

[15]   R. H. Park, "Two-reaction theory of synchronous machines generalized method of analysis-part I," *Transactions of the American Institute of Electrical Engineers,* vol. 48, pp. 716-727, 1929.

[16]   M. Popescu, *Induction motor modelling for vector control purposes*: Helsinki University of Technology, 2000.

[17]   S. Shah, A. Rashid, and M. Bhatti, "Direct quadrate (dq) modeling of 3-phase induction motor using matlab/simulink," *Canadian Journal on Electrical and Electronics Engineering,* vol. 3, pp. 237-243, 2012.

[18]   K. Bradley and A. Tami, "Reluctance mesh modelling of induction motors with healthy and faulty rotors," in *Industry Applications Conference, 1996. Thirty-First IAS Annual Meeting, IAS'96., Conference Record of the 1996 IEEE*, 1996, pp. 625-632.

[19]   M. Amrhein and P. T. Krein, "Induction machine modeling approach based on 3-D magnetic equivalent circuit framework," *IEEE Transactions on Energy Conversion,* vol. 25, pp. 339-347, 2010.

[20]   C. Gerada, K. Bradley, M. Sumner, P. Wheeler, S. Picker, J. Clare*, et al.*, "The results do mesh," *IEEE Industry Applications Magazine,* vol. 13, pp. 62-72, 2007.

[21]   H. Kapeller, D. Dvorak, J. V. Gragger, F. Müllner, and H. Neudorfer, "Modeling of iron losses in an induction machine based on a magnetic equivalent circuit in Modelica," in *Electric Machines and Drives Conference (IEMDC), 2017 IEEE International*, 2017, pp. 1-8: IEEE.

[22]   R. Courant, "Variational methods for the solution of problems of equilibrium and vibrations," *Lecture Notes in Pure and Applied Mathematics,* pp. 1-1, 1994.

[23]   A. M. Winslow, "Magnetic field calculations in an irregular triangle mesh," Lawrence Radiation Lab., Univ. of California, Livermore1965.

[24]   M. Chari and P. Silvester, "Analysis of turboalternator magnetic fields by finite elements," *IEEE Transactions on Power Apparatus and Systems,* pp. 454-464, 1971.

[25]   C. Gerada, K. Bradley, M. Sumner, and P. Sewell, "Evaluation of a vector controlled induction motor drive using the dynamic magnetic circuit model," in *Industry Applications Conference, 2003. 38th IAS Annual Meeting. Conference Record of the*, 2003, pp. 862-869.

[26]   F. Lftisi, G. H. George, and M. A. Rahman, "An application of a finite element controller map for speed control for saturated induction motors," in *IECON 2017 - 43rd Annual Conference of the IEEE Industrial Electronics Society*, 2017, pp. 8756-8762.